Fat sensory cues in early life program central response to food and obesity

Laura Casanueva Reimon[1,2,10], Ayden Gouveia[1,2,10], André Carvalho[1,2], Joscha N. Schmehr[1,2], Mouna El Mehdi[1,2], Rolando D. Moreira-Soto[3,4], Carlos G. Ardanaz [1,2], Janice Bulk[1,2], Lionel Rigoux[2,5], Paul Klemm [6], Anna Lena Cremer[7], Frederik Dethloff[8], Yvonne Hinze[8], Heiko Backes[7], Patrick Giavalisco [8] & Sophie M. Steculorum [1,2,9] ✉

Maternal obesity predisposes offspring to metabolic diseases. Here, we show that non-nutritive sensory components of a high-fat diet (HFD), beyond its hypercaloric, obesogenic effects, are sufficient to alter metabolic health in the offspring. To dissociate the caloric and sensory components of HFD, we fed dams a bacon-flavoured diet, isonutritional to a normal chow diet but enriched with fat-related odours. Offspring exposed to these fat-related odours during development display metabolic inflexibility and increased adiposity when fed HFD in adulthood independently of maternal metabolic health. Developmental exposure to fat-related odours shifts mesolimbic dopaminergic circuits and Agouti-related peptide (AgRP) hunger neurons' responses to phenocopy those of obese mice, including a desensitization of AgRP neurons to dietary fat. While neither neonatal optogenetic activation of sensory circuits nor passive exposure to fat-related odours is sufficient to alter metabolic responses to HFD, coupling optogenetic stimulation of sensory circuits with caloric intake exacerbates obesity. Collectively, we report that fat-related sensory cues during development act as signals that can prime central responses to food cues and whole-body metabolism regulation.

Exposure to a maternal hypercaloric, hyperlipidaemic diet during development is a major risk factor for life-long obesity and metabolic syndrome[1–5]. Maternal obesity and consumption of calorie-rich high-fat foods predispose offspring to a wide array of metabolic and behavioural impairments, including adiposity and insulin resistance, and shift food preference towards increased intake of highly palatable foods[1–5]. Extensive research has shown that the metabolic consequences of maternal high-fat diet (HFD) consumption, such as excess gestational weight gain, adiposity and insulin resistance, are considered key contributors to the metabolic programming of the offspring[1–5]. However, outcomes of metabolic programming can occur in lean HFD-fed dams independent of maternal adiposity or insulin resistance[1–3,6–8], suggesting that the heightened risk of obesity development in the offspring is not solely triggered by maternal obesity or nutritive components of HFD per se. It is unknown which components of HFD, aside from its nutritive effects, can trigger metabolic programming.

[1]Max Planck Institute for Metabolism Research, Max Planck Research Group Neurocircuit Wiring and Function, Cologne, Germany. [2]Excellence Cluster on Cellular Stress Responses in Aging-Associated Diseases (CECAD), University of Cologne, Cologne, Germany. [3]Max Planck Institute for Chemical Ecology, Department of Evolutionary Neuroethology, Jena, Germany. [4]Universidad de Costa Rica, Centro de Investigación en Enfermedades Tropicales, Facultad de Microbiología, San José, Costa Rica. [5]Max Planck Institute for Metabolism Research, Translational Neurocircuitry Group, Cologne, Germany. [6]Max Planck Institute for Metabolism Research, Neuronal Control of Metabolism Group, Cologne, Germany. [7]Max Planck Institute for Metabolism Research, Multimodal Imaging Group, Cologne, Germany. [8]Max Planck Institute for Biology of Ageing, Metabolomics Core Facility, Cologne, Germany. [9]German Center of Diabetes Research (DZD), Neuherberg, Germany. [10]These authors contributed equally: Laura Casanueva Reimon, Ayden Gouveia. ✉e-mail: sophie.steculorum@sf.mpg.de

Food is not only composed of nutrients, but also contains non-nutritive sensory components such as volatile odours. Although the hypercaloric component of HFD has been a major focus of interest, HFD carries a distinct chemosensory signature. During development, fetuses and newborns are exposed to both nutritive and non-nutritive sensory food signals where volatile odours from the mother's diet are directly transferred to the amniotic fluid and milk[9–14]. Perinatal olfactory experiences foster sensory memories upon which the organism relies throughout life to make food choices and dictate feeding habits until adulthood towards a preference for the odours encountered during development[12,13,15–19]. To date, the consequences of developmental exposure to non-nutritive sensory food cues of HFD on life-long regulation of the central representation, preference, intake and metabolic response to HFD remain elusive.

While the role of the sensory environment during development is yet to be defined, food sensory perception has emerged as a regulator of key neural circuits that control feeding behaviour and whole-body metabolism in adulthood[20–29]. Here, we explored the influence of fat-related sensory cues during development, independent of the nutritive content, on the regulation of the central responses to food cues, metabolic health and obesity susceptibility during adulthood.

A model for developmental exposure to fat-related sensory cues

To dissociate the nutritive caloric components from the non-nutritive sensory components of HFD, we designed a diet that is isonutritional to commonly used normal chow diet (NCD) but flavoured with fat-related odours. To selectively mimic the commonly used lard-based HFD (HFD$_{lard}$), we enriched NCD with bacon odours to create an isonutritional bacon-flavoured diet (BFD) (Fig. 1a). We first aimed to characterize the diet's odour profile by performing a thermal-desorption gas chromatography–time-of-flight mass spectrometry (TD-GC–ToFMS)-based analysis of volatile organic compounds (VOCs) emitted by these diets. To investigate whether the BFD sensory profile resembles that of HFD$_{lard}$ particularly, we also included a non-pork-based HFD: a butter fat-based HFD (HFD$_{butter}$). These analyses revealed that the complex odour profiles of the diets comprised 155 volatiles, predominantly alcohols, aldehydes and ketones (Fig. 1b and Extended Data Fig. 1a,b). According to hierarchical cluster analysis, BFD and HFD$_{lard}$ share high sensory

similarities and their volatile profiles differ from those of HFD$_{butter}$ and NCD (Fig. 1b and Extended Data Fig. 1a,b). To fully characterize BFD, we also performed an untargeted liquid chromatography-mass spectrometry (LC–MS)-based analysis of the hydrophobic (lipids) and polar fractions (metabolites) of BFD, NCD and the two HFDs (Fig. 1c,d, Extended Data Fig. 2a,b and Supplementary Tables 1 and 2). Principal-component analysis of the diets' lipid (Fig. 1c) and polar profiles (Fig. 1d) unveiled that NCD and BFD overlap and are clearly distinct from HFD$_{lard}$ and HFD$_{butter}$. Hence, the sensory profile of BFD resembles more that of HFD$_{lard}$, whereas its nutritional components are more similar to NCD. Consistent with the BFD's low caloric and fat contents, mice subjected to a feeding preference test consumed almost exclusively palatable hypercaloric HFD$_{lard}$ over BFD (Extended Data Fig. 2c). To ascertain that the low BFD consumption did not stem from any aversive or unpalatable properties, we also performed a feeding preference test between BFD and a novel NCD (control diet; CD) (Extended Data Fig. 2d). Although mice displayed a slight preference for CD over BFD the first day of exposure, no preference between the two diets was noticeable over time, hence, revealing that BFD feeding is not aversive to mice (Extended Data Fig. 2d).

To further corroborate the sensory similarities between BFD and HFD, we compared their ability to activate common olfactory receptors (Olfrs). We performed in vivo molecular profiling of olfactory receptors activated by NCD, BFD or HFD$_{lard}$ odours using phosphorylated S6 ribosomal subunit capture (pS6-ribotrap)[30,31] coupled to RNA sequencing (RNA-seq) in lean adult mice (Extended Data Fig. 2e). We confirmed that food odours induce phosphorylation of S6 in olfactory sensory neurons (OSNs) residing in the main olfactory epithelium (Extended Data Fig. 2f). NCD, BFD and HFD$_{lard}$ odours activated 36, 41 and 45 olfactory receptors above the statistical threshold, respectively (Fig. 1e). Among the activated olfactory receptor repertoires of each diet, olfactory receptors activated by BFD showed a greater exclusive overlap with HFD$_{lard}$ (eight common Olfrs) than NCD (three common Olfrs) (Fig. 1e and Extended Data Fig. 2g,h), suggesting that BFD shares an increased subjective olfactive similarity to HFD$_{lard}$ compared with NCD.

After thoroughly characterizing the BFD, we next used this diet to generate a model of developmental exposure to fat-related sensory cues. At gestational day 4.5, dams were either maintained on NCD or

Fig. 1 | Developmental exposure to fat-related sensory cues is sufficient to exacerbate obesogenic responses to HFD$_{lard}$. a, Paradigm of developmental exposure to fat-related sensory cues induced by feeding dams NCD (control group) or BFD. **b**, Hierarchical clustering of volatile profiles of NCD, BFD, butter-based HFD (HFD$_{butter}$) and lard-based HFD (HFD$_{lard}$). The colour scale represents the concentration of each volatile in per cent. Volatiles with a concentration >5% are depicted, volatiles <5% are shown in Extended Data Fig. 1. **c,d**, Principal-component analysis plots of the diets' hydrophobic (lipids) (**c**) and diets' polar (metabolites) components (**d**). **e**, In vivo identification of olfactory receptor repertoire of NCD, BFD and HFD$_{lard}$ in adult mice. Volcano plot of olfactory receptor genes, fold change of odour-exposed (NCD, BFD and HFD$_{lard}$) over no odour exposure using phospho-S6 ribosomal protein immunoprecipitation ($n = 5$–6 per diet containing four main olfactory epithelia each; $P < 0.001$ considered significant following multiplicity adjustment). **f**, Interscapular brown adipose tissue (iBAT) temperature upon HFD$_{lard}$ odour presentation in adult mice developmentally exposed to NCD (NCD$_{dev}$) or BFD (BFD$_{dev}$) naive to HFD$_{lard}$ (two-way ANOVA; uncorrected Fisher's LSD post hoc; $n = 14, 7$; P diet = 0.0361, P BFD$_{dev}$ NoOdour versus HFDodour = 0.0421). **g**, HFD$_{lard}$ odour-induced changes in hepatic p-mTOR in fasted mice naive to HFD$_{lard}$ (two-way ANOVA; Tukey's post hoc; $n = 5, 5$; $P = 0.0003$). **h–m**, Metabolic phenotyping of dams fed either NCD or BFD. Maternal body weight across gestation and lactation (two-way repeated-measures ANOVA; $n = 8, 9$) (**h**). Maternal body composition and representative micro-CT image (two-tailed Wilcoxon rank-sum test; $n = 5, 5$) (**i**). Maternal fasted blood glucose (unpaired two-tailed t-test; $n = 5, 5$) (**j**). Maternal fasted insulin levels (unpaired two-tailed t-test; $n = 5, 5$) (**k**). Maternal insulin resistance

defined by HOMA-IR (unpaired two-tailed t-test; $n = 5, 5$) (**l**). Maternal leptin levels (unpaired two-tailed t-test; $n = 5, 4$) (**m**). **n–u**, Metabolic phenotyping of NCD$_{dev}$ or BFD$_{dev}$ offspring fed HFD$_{lard}$ during adulthood. Body weight gain of male offspring on HFD$_{lard}$ (mixed-effects model; Tukey's post hoc; $n = 21, 20$; P group = 0.006, P interaction = 0.022) (**n**). Body composition and representative micro-CT image of males (two-tailed Wilcoxon rank-sum test; $n = 17, 13$; $P = 0.002$) (**o**). Insulin tolerance test (ITT) and associated area under the curve (AUC) in males (time curve: two-way repeated-measures ANOVA; Tukey's post hoc; $n = 13, 8$; P group = 0.0029, P interaction = 0.0003) (AUC: unpaired two-tailed t-test; $n = 13, 8$; $P = 0.0032$) (**p**). Male ad libitum resting blood glucose (unpaired two-tailed t-test; $n = 11, 9$; $P = 0.0409$) (**q**). Body weight gain of female offspring on HFD$_{lard}$ (mixed-effects model; Tukey's post hoc; $n = 25, 29$; P group = 0.0060, P interaction < 0.0001) (**r**). Body composition and representative micro-CT image of females (two-tailed Wilcoxon rank-sum test; $n = 10, 16$; $P = 0.029$) (**s**). ITT and associated AUC in females (time curve: two-way repeated-measures ANOVA; Tukey's post hoc; $n = 17, 14$; P group < 0.0001) (AUC: unpaired two-tailed t-test; $n = 17, 14$; $P < 0.0001$) (**t**). Female ad libitum resting blood glucose (unpaired two-tailed t-test; $n = 17, 14$; $P = 0.0303$) (**u**). **v**, Paradigm of adult exposure to NCD (NCD$_{adult}$) or BFD (BFD$_{adult}$) followed by HFD$_{lard}$ feeding. **w**, Body weight curve (two-way repeated-measures ANOVA; $n = 10, 10$). **x**, Body composition (two-tailed Wilcoxon rank-sum test; $n = 5, 5$). **y**, ITT (time curve: two-way repeated-measures ANOVA; $n = 10, 10$). **z**, Resting ad libitum blood glucose (unpaired two-tailed t-test; $n = 10, 10$) of NCD$_{adult}$ and BFD$_{adult}$. Statistics are depicted as for two-way repeated-measures ANOVA or mixed-effects model, group comparison and time × group interaction; Wilcoxon rank-sum test and t-test. Bars represent mean value. Error bars represent s.e.m. *$P \leq 0.05$, **$P \leq 0.01$, ***$P \leq 0.001$.

switched to BFD until weaning of the pups to mimic sensory experiences associated with HFD$_{lard}$ feeding during development without its nutritive consequences (Fig. 1a and Extended Data Fig. 3a). To characterize our model, we aimed to validate that exposure to BFD could

indeed mimic the exposure to HFD$_{lard}$. Under normal conditions, mice naive to a palatable diet (such as HFDs) show minimal responses to its sensory signals at the first encounter, and the sensory response is contingent and tuned by its consumption[20]. Therefore, we sought to
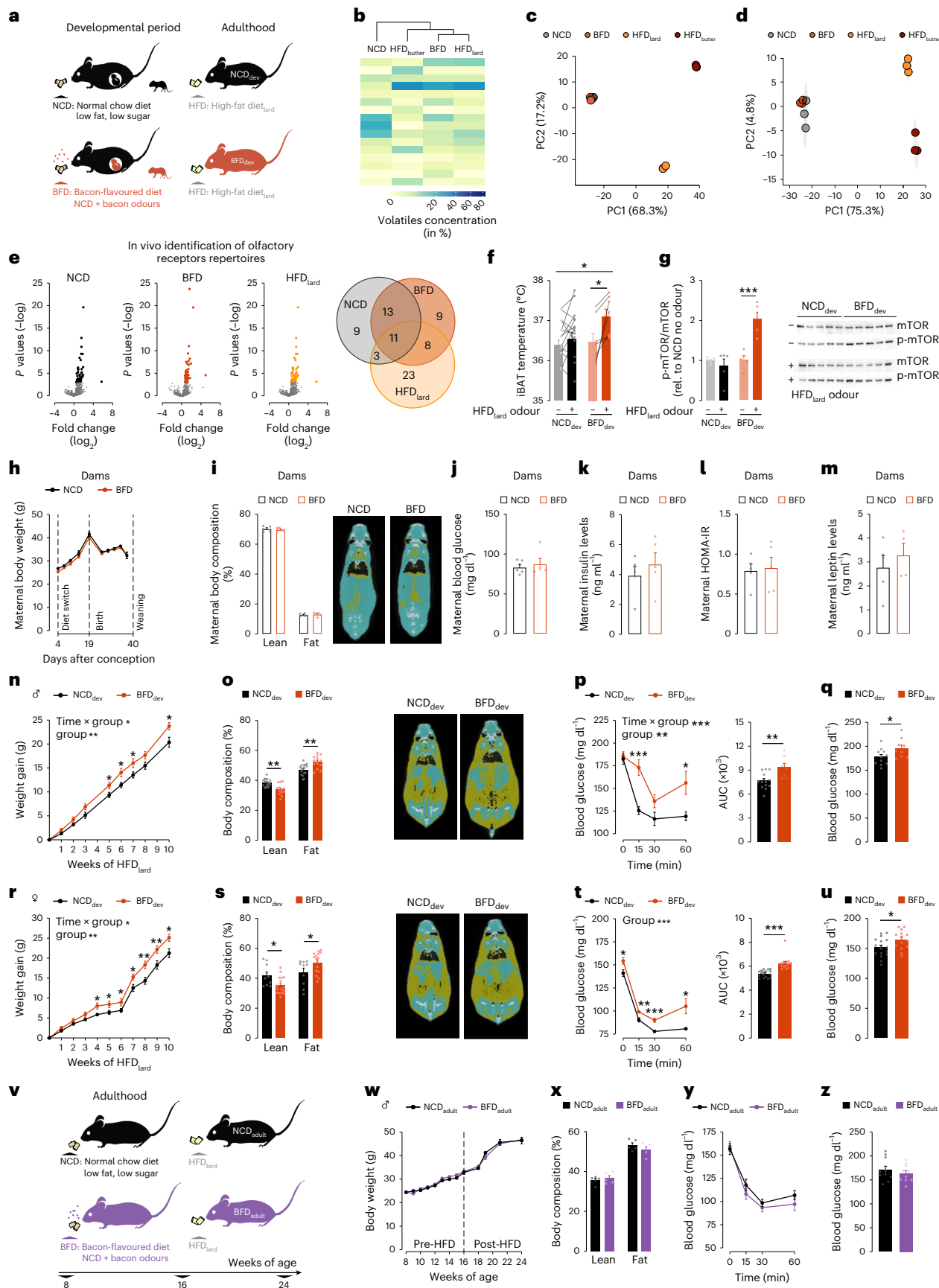
test whether developmental exposure to BFD is sufficient to prime a differential response to HFD_{lard} odour in adult offspring naive to HFD_{lard}. We measured two sensory-evoked metabolic readouts: (1) HFD_{lard} odour-induced increase in interscapular brown adipose tissue (iBAT) temperature[21] (Fig. 1f) and (2) priming of hepatic post-prandial responses, for example mTOR phosphorylation (p-mTOR)[22] (Fig. 1g). In control mice exposed to NCD during development (NCD_{dev}) and naive to HFD_{lard}, we found that HFD_{lard} odour exposure did not induce changes in iBAT temperature or hepatic p-mTOR responses (Fig. 1f,g). In contrast, iBAT temperature and hepatic p-mTOR increased upon HFD_{lard} odour exposure in mice developmentally exposed to BFD (BFD_{dev}) but naive to HFD_{lard} (Fig. 1f,g). Thus, developmental exposure to BFD is sufficient to emulate sensory exposure to HFD_{lard} and to prime metabolic responses to HFD_{lard} before its first encounter.

To further characterize our mouse model of developmental exposure to fat-related sensory cues, we conducted a thorough analysis of the dams' metabolism and behaviour. BFD feeding did not alter maternal body weight (Fig. 1h), weight gain per pup (Extended Data Fig. 3b) or body composition (Fig. 1i). Additionally, fasting (Fig. 1j) and ad libitum-fed glycaemia (Extended Data Fig. 3c), circulating insulin levels (Fig. 1k) and insulin resistance (Fig. 1l) were comparable between BFD-fed and control dams. Circulating levels of the hunger and satiety hormones leptin (Fig. 1m), CCK (Extended Data Fig. 3d) and PYY (Extended Data Fig. 3e) were also similar between the two groups. Furthermore, BFD feeding had no impact on the expression of key hypothalamic peptides involved in regulating feeding and energy balance (Extended Data Fig. 3f). Hypothalamic-pituitary-adrenal and hypothalamic-pituitary-thyroid axes were also unaffected (Extended Data Fig. 3f). Maternal behaviour remained unchanged between BFD- and NCD-fed dams as illustrated by similar expression of pivotal hormones governing parental behaviour (prolactin, oxytocin and galanin; Extended Data Fig. 3g) and similar performance in a pup retrieval test (Extended Data Fig. 3h–k). Moreover, BFD feeding did not alter fetal and placental weights (Extended Data Fig. 3l,m), further demonstrating that maternal health and fetal development were unaffected.

As maternal lipid profiles are well-known contributors to metabolic programming[32,33], we also performed untargeted LC–MS analyses of extracted lipid fractions on blood and milk of dams fed NCD or BFD (Extended Data Fig. 3n). These analyses revealed that BFD feeding in dams did not significantly alter blood or milk lipid composition (Extended Data Fig. 3o–r). Hence, we successfully developed a model for developmental exposure to fat-related sensory cues independent of maternal insulin resistance, weight gain, adiposity and changes in maternal lipid components.

Exacerbated obesogenic response in sensory programmed offspring

To test whether exposure to HFD_{lard}-related sensory cues during development alters the response to HFD_{lard} feeding in adulthood, we next assessed whether early exposure to fat-related sensory cues impacts the onset of diet-induced obesity and associated metabolic alterations. Before the switch to HFD_{lard}, body length (Extended Data Fig. 4a,b), body composition (Extended Data Fig. 4c,d), and insulin sensitivity (Extended Data Fig. 4e,f) were identical between BFD_{dev} and control NCD_{dev} animals. To determine the long-term influence of developmental exposure to BFD on metabolic health, NCD_{dev} and BFD_{dev} offspring were switched to HFD_{lard} at 8 weeks of age (Extended Data Fig. 4g,h). HFD_{lard} feeding induced an aggravated body weight gain (Fig. 1n and Extended Data Fig. 4i) and adiposity (Fig. 1o and Extended Data Fig. 4j) in male BFD_{dev} animals compared with control NCD_{dev}. Similarly, insulin resistance (Fig. 1p and Extended Data Fig. 4k) and higher resting glycaemia (Fig. 1q) induced by HFD_{lard} feeding were increased in BFD_{dev} mice compared with NCD_{dev}. Female BFD_{dev} mice also displayed exacerbated HFD-induced weight gain (Fig. 1r and Extended Data Fig. 4l), adiposity (Fig. 1s), insulin resistance (Fig. 1t and Extended Data Fig. 4m) and hyperglycaemia (Fig. 1u). Hence, developmental exposure to BFD exacerbates the obesogenic responses to HFD_{lard} to a comparable extent in both sexes, demonstrating that fat-related sensory cues during early life exert potent and generalized metabolic defects in adulthood.

To assess whether the adverse metabolic outcomes triggered by BFD are selectively associated with the exposure during development, we exposed animals to BFD exclusively during adulthood. Adult male mice were fed BFD (BFD_{adult}) or NCD (NCD_{adult}) for 8 weeks and then fed HFD_{lard} to assess the influence of BFD feeding on obesity development (Fig. 1v and Extended Data Fig. 5a–f). BFD feeding exclusively during adulthood (BFD_{adult}) had no consequences on HFD_{lard}-induced weight gain (Fig. 1w), adiposity (Fig. 1x and Extended Data Fig. 5c), insulin resistance (Fig. 1y and Extended Data Fig. 5d,e), or hyperglycaemia (Fig. 1z). The exacerbated obesogenic responses in BFD_{dev} animals are, therefore, triggered only by exposure to BFD during development. Thus, early life is a critical period of vulnerability for the metabolic programming induced by fat-related sensory cues, and developmental exposure to fat-related sensory cues is sufficient to exacerbate HFD_{lard}-induced obesity, independent of maternal obesity or insulin resistance.

To investigate whether the sensory programming of metabolism is triggered by a specific developmental period, we selectively fed dams with BFD during gestation (Extended Data Fig. 5g–k) or lactation (Extended Data Fig. 5l–p). Exposure to BFD during gestation (BFD_{ges}) alone did not alter HFD_{lard}-induced obesity in either males

---

**Fig. 2 | Developmental exposure to a single fat-related volatile is sufficient to prime obesity. a**, Paradigm of developmental exposure to fat-related sensory cues induced by NCD or BFD feeding. Adult mice developmentally exposed to NCD (NCD_{dev}) or BFD (BFD_{dev}) are fed butter-based HFD (HFD_{butter}) during adulthood. **b–g**, Metabolic phenotyping of NCD_{dev} and BFD_{dev} offspring on HFD_{butter}. Body weight gain of male offspring on HFD_{butter} (mixed-effects model; Tukey's post hoc; $n = 11, 22$; P interaction = 0.0006) (**b**). Body composition and representative micro-CT image of males (two-tailed Wilcoxon rank-sum test; $n = 11, 22$; $P = 0.021$) (**c**). ITT in males (two-way repeated-measures ANOVA; Tukey's post hoc; $n = 11, 22$; P interaction < 0.0001) (**d**). Body weight gain of female offspring on HFD_{butter} (mixed-effects model; $n = 12, 17$) (**e**). Body composition and representative micro-CT image of females (two-tailed Wilcoxon rank-sum test; $n = 12, 17$; $P = 0.028$) (**f**). ITT in females (two-way repeated-measures ANOVA; Tukey's post hoc; $n = 12,17$; P group = 0.0162) (**g**). **h**, Paradigm of developmental exposure to fat-related sensory cues induced by NCD or isonutritional PB-FD feeding in dams followed by either HFD_{lard} (**i,j**) or peanut butter-based HFD ($HFD_{peanut-butter}$) (**k,l**) feeding in adulthood. **i**, Body weight gain of male offspring on HFD_{lard} (two-way repeated-measures ANOVA; $n = 21, 13$). **j**, Body composition of males on HFD_{lard} (two-tailed Wilcoxon rank-sum test; $n = 17, 11$). **k**, Body weight gain of male offspring on $HFD_{peanut-butter}$ (mixed-effects model; Tukey's post hoc; $n = 16, 18$; P group = 0.0397). **l**, Body composition of males on $HFD_{peanut-butter}$

(two-tailed Wilcoxon rank-sum test; $n = 14, 18$; $P = 0.042$). **m**, Volatile profiles of NCD, BFD and HFD_{lard}. The colour scale represents the concentration of each volatile in per cent. Volatiles with a concentration >5% are depicted, volatiles <5% are shown in Extended Data Fig. 1. **n**, Paradigm of developmental exposure induced by AFD feeding followed by acetophenone-flavoured HFD ($HFD_{acetophenone}$) feeding in adulthood. **o–q**, Metabolic phenotyping of dams fed either NCD or AFD. Maternal body composition (two-tailed Wilcoxon rank-sum test; $n = 20, 5$) (**o**). Maternal blood fasting glycaemia (unpaired two-tailed t-test; $n = 20, 6$) (**p**). Maternal insulin resistance defined by HOMA-IR (unpaired two-tailed t-test; $n = 6, 6$) (**q**). **r–u**, Metabolic phenotyping of NCD_{dev} or AFD_{dev} mice fed $HFD_{acetophenone}$ during adulthood. Body weight gain of male offspring on $HFD_{acetophenone}$ (mixed-effects model; $n = 19,19$) (**r**). Body composition and representative micro-CT image of males (two-tailed Wilcoxon rank-sum test; $n = 18,15$) (**s**). Body weight gain of female offspring on $HFD_{acetophenone}$ (mixed-effects model; Tukey's post hoc; $n = 22,17$; P group = 0.0168; P interaction = 0.0126) (**t**). Body composition and representative micro-CT image of females (two-tailed Wilcoxon rank-sum test; $n = 21,20$; $P = 0.046$) (**u**). Statistics are depicted as for two-way repeated-measures ANOVA or mixed-effects model, group comparison and time × group interaction; Wilcoxon rank-sum test and t-test. Bars represent mean value. Error bars represent s.e.m. *$P \leq 0.05$, **$P \leq 0.01$, ***$P \leq 0.001$.

(Extended Data Fig. 5h,i) or females (Extended Data Fig. 5j,k). However, while BFD exposure during lactation (BFD_{lac}) did not have a clear effect on obesity development in males (Extended Data Fig. 5m,n), it significantly increased weight gain (Extended Data Fig. 5o) and decreased insulin sensitivity (Extended Data Fig. 5p) in females. Collectively these data suggest that lactation might be a period of highest sensitivity to fat sensory cues in females, while exposure to BFD throughout the entire developmental period is required for the exacerbated responses to HFD_{lard} in males.

The sensory programming of metabolism generalizes to non-pork-based HFD and other fat-related odours

Having established that developmental exposure to BFD exacerbates obesity in response to HFD_{lard}, we next aimed to determine whether these metabolic responses were specific to the pork-based HFD that shares high sensory similarities with the BFD. We therefore exposed 8-week-old BFD_{dev} and control NCD_{dev} animals to a butter fat-based
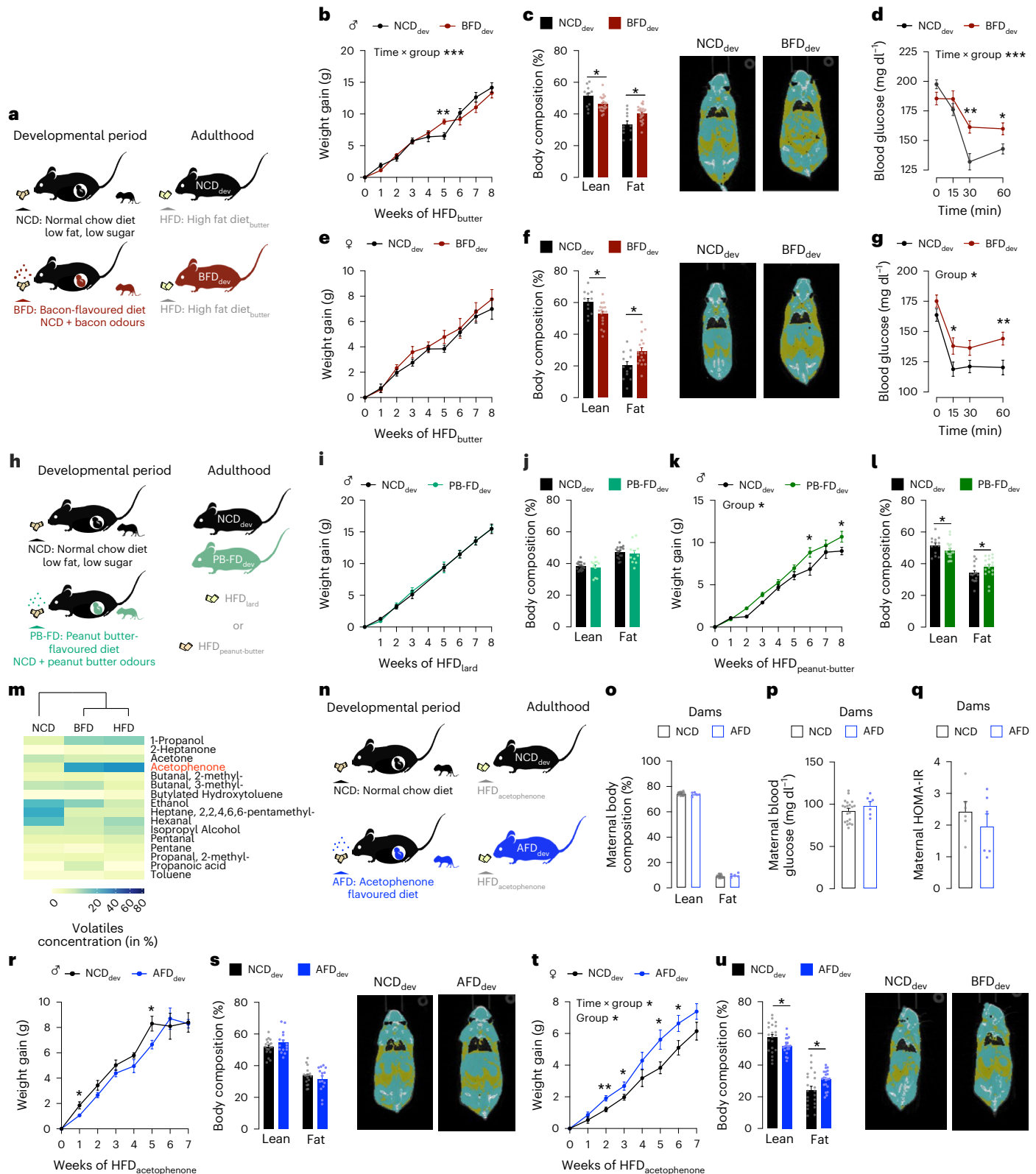
HFD (HFD$_{butter}$) (Fig. 2a). While HFD$_{butter}$ only had a minor influence on body weight gain (Fig. 2b) in male BFD$_{dev}$ animals compared with control NCD$_{dev}$ animals, it increased their adiposity (Fig. 2c), a primary determinant of metabolic and cardiovascular risks[34,35]. HFD$_{butter}$ also decreased insulin sensitivity in BFD$_{dev}$ males (Fig. 2d). A similar phenotype was observed in female BFD$_{dev}$ mice with unchanged body weight gain (Fig. 2e), increased adiposity (Fig. 2f) and insulin resistance (Fig. 2g). Altogether, these results uncover that exposure to fat sensory cues mimicking HFD$_{lard}$ also primes obesity in response to other HFDs, revealing that the sensory programming of metabolism can generalize to other hypercaloric diets.

After demonstrating that the heightened obesogenic responses induced by developmental exposure to bacon sensory cues apply to other HFDs, we next investigated whether non-nutritive sensory programming can be generalized to other fat-related sensory cues. Therefore, we performed an identical developmental paradigm using a peanut butter-flavoured diet (PB-FD) as a separate fat-related odour (Fig. 2h). PB-FD feeding did not alter maternal body weight (Extended Data Fig. 5q,r), weight gain per pup (Extended Data Fig. 5s) nor insulin sensitivity (Extended Data Fig. 5t). We first tested the responses of PB-FD$_{dev}$ and NCD$_{dev}$ animals to HFD$_{lard}$. Animals developmentally exposed to PB-FD (PB-FD$_{dev}$) showed similar obesogenic responses to HFD$_{lard}$ feeding compared with NCD$_{dev}$ with indistinguishable weight gain (Fig. 2i) and adiposity (Fig. 2j and Extended Data Fig. 5u) in males and females (Extended Data Fig. 5v,w). Hence, developmental exposure to PB-related odours does not exacerbate the obesogenic responses to HFD$_{lard}$. Of note, these results further demonstrate that the metabolic phenotype observed in BFD$_{dev}$ animals is not triggered by a generalized effect of increased sensory enrichment or potential maternal stress[36,37].

To explore whether the absence of exacerbated obesogenic responses could originate from the type of HFD used (lard versus peanut butter), we assessed the responses of PB-FD$_{dev}$ and NCD$_{dev}$ control animals to a peanut butter-based HFD (HFD$_{peanut-butter}$) (Extended Data Fig. 5x). HFD$_{peanut-butter}$ feeding increased weight gain (Fig. 2k) and adiposity (Fig. 2l and Extended Data Fig. 5y) in PB-FD$_{dev}$ mice compared with NCD$_{dev}$ controls. Overall, these experiments demonstrate that the sensory programming of metabolism by fat-related sensory cues extends to other diets. Moreover, these findings suggest that, although identical sensory profiles between the developmental diet and the obesogenic diets encountered in adulthood are not required for metabolic effects, a certain degree of similarity may be necessary.

Developmental exposure to a single HFD-enriched volatile is sufficient to prime obesity

To further confirm the influence of HFD sensory cues on long-term metabolic health, we investigated whether early exposure to a single fat-related volatile could affect metabolic health. Volatile analyses revealed several molecules enriched in BFD and HFD, including acetophenone, 1-propanol, benzaldehyde, heptanal, 2-pentanone and ethyl acetate, which are known to contribute to the specific odour of bacon[38] (Fig. 2m and Extended Data Fig. 1). Given that volatile compounds present in the maternal diet can be transferred to the amniotic fluid and milk, we also compared the volatile profiling of those fluids between BFD and NCD dams (Extended Data Fig. 6a,b), revealing clear differences between the two groups. Specifically, these analyses revealed an increase in BFD- and HFD-enriched volatiles, such as benzaldehyde and 1-propanol (in milk), and volatiles potentially derived from degradation of food-derived volatiles, such as acetone, one of the degradation products of acetophenone (Extended Data Fig. 6a,b). Collectively, these results highlight that BFD feeding influences the volatile profile of amniotic fluid and milk and subsequently modifies the in utero and neonatal offspring's food sensory experiences.

We then tested whether developmental exposure to a single HFD-related volatile could influence obesity susceptibility. Among

the several volatiles enriched in BFD and HFD$_{lard}$, we focused on acetophenone as a proof of principle, as it is the most abundant volatile in both diets (Fig. 2m). To model developmental exposure to acetophenone odours, dams were fed NCD flavoured with acetophenone (acetophenone-flavoured diet; AFD) during gestation and lactation (Fig. 2n). AFD feeding did not affect maternal weight gain (Extended Data Fig. 6c,d), adiposity (Fig. 2o and Extended Data Fig. 6e), glycaemia (Fig. 2p), insulin resistance (Fig. 2q) nor insulin levels (Extended Data Fig. 6f). At 8 weeks of age, offspring of AFD-fed (AFD$_{dev}$) and control (NCD$_{dev}$) dams were switched to HFD$_{lard}$ flavoured with acetophenone (HFD$_{acetophenone}$) (Fig. 2n). Weight gain (Fig. 2r) and adiposity (Fig. 2s) induced by HFD$_{acetophenone}$ were similar in AFD$_{dev}$ and NCD$_{dev}$ males. In contrast, AFD$_{dev}$ females exhibited increased weight gain (Fig. 2t) and adiposity (Fig. 2u) in response to HFD$_{acetophenone}$ compared with NCD$_{dev}$ controls (interaction sex × developmental diet × time: $P = 0.005$). These findings further underscore the critical role of food sensory cues in the developmental origin of obesity, demonstrating that exposure to a single fat-related sensory volatile during development is sufficient to exacerbate obesogenic responses in a sexually dimorphic manner.

Developmental exposure to fat-related odours alters dopamine response to food cues and primes feeding preference

Developmental exposure to HFD leads to broad structural changes in the brain and alters hypothalamic homeostatic and mesolimbic reward-related circuits, thereby predisposing the offspring to maladaptive metabolic responses and hyperphagia[1,2,6,39–42]. To determine whether developmental exposure to fat-related sensory cues also alters central responses to food cues, we assessed alterations in brain activity in adult NCD$_{dev}$ and BFD$_{dev}$ mice. We measured glucose metabolism using fluorodeoxyglucose (^{18}FDG) positron emission tomography imaging as a proxy for neuronal activity in response to HFD (Extended Data Fig. 7a). Upon acute HFD$_{lard}$ odour exposure in mice naive to HFD$_{lard}$, BFD$_{dev}$ mice exhibited overall increased neuronal activity in several brain regions (Extended Data Fig. 7a). HFD$_{lard}$ odour activated olfactory relevant regions such as the olfactory bulb, olfactory tubercle and piriform cortex in both groups, with greater responses observed in BFD$_{dev}$ mice (Extended Data Fig. 7b–d). Additionally, HFD$_{lard}$ odour exposure increased neuronal activity in dopaminergic reward-associated regions of the lateral nucleus accumbens shell (LAcbSh) (Fig. 3a) and the ventral tegmental area (VTA) (Fig. 3b) in BFD$_{dev}$ mice, but not in NCD$_{dev}$ mice.

Because dopamine release in the LAcbSh encodes preference for and intake of dietary fat[43–45], we wanted to investigate the effects of developmental exposure to fat odours on adult dopamine responses to food. We performed fibre photometry using the extracellular optical dopamine sensor dLight1.1 (ref. 46) in the LAcbSh (Fig. 3c and Extended Data Fig. 8a). We recorded dopamine release in the LAcbSh in fasted NCD$_{dev}$ and BFD$_{dev}$ adult mice in response to NCD, BFD or HFD$_{lard}$ pellets. All dopamine fibre photometry experiments were performed in NCD$_{dev}$ and BFD$_{dev}$ mice on NCD acclimated to each diet, hence before the onset of any metabolic alterations. These experiments revealed that dopamine release in response to NCD was largely blunted in BFD$_{dev}$ mice compared with NCD$_{dev}$ (Fig. 3d). Furthermore, dopamine release upon BFD (Fig. 3e) or HFD$_{lard}$ presentation (Fig. 3f) was similar between NCD$_{dev}$ and BFD$_{dev}$. Therefore, pre-HFD$_{lard}$ (before the onset of metabolic alterations), BFD$_{dev}$ mice show functional alterations in their central dopamine response to food characterized by a primed devaluation of dopaminergic response to NCD.

Given that dopamine responses to NCD are reduced in BFD$_{dev}$ mice and that dopamine in the LAcbSh dictates preference and fat intake[43–45], we next assessed whether the altered dopamine response translates into behavioural consequences. We performed a two-choice food preference test in adult NCD$_{dev}$ and BFD$_{dev}$ mice by exposing them to HFD$_{lard}$ and a low-fat control diet (Fig. 3g). Compared with NCD$_{dev}$, BFD$_{dev}$ mice

consumed a significantly higher percentage of calories from HFD_{lard} relative to a less palatable low-fat control diet during the first 24 h (Fig. 3g and Extended Data Fig. 8b,c). Of note, the enhanced HFD_{lard} preference observed in BFD_{dev} mice did not correlate with changes in the expression of the key fat taste receptors *Cd36* and *Gpr120* (*Ffar4*) nor *Plcb2*, an intracellular signalling pathway component critical for fat sensing (Extended Data Fig. 8d). Food intake was subsequently assessed under conditions in which mice were exclusively provided with HFD_{lard}, replicating the experimental parameters utilized during metabolic phenotyping (Fig. 1n–u). Pre-HFD_{lard}, both groups of mice consumed similar amounts of food (Fig. 3h). Similarly, total daily food intake of HFD_{lard} did not differ between NCD_{dev} and BFD_{dev} mice, either acutely (the first 2 weeks on HFD_{lard}; Fig. 3i) or after long-term exposure (4–10 weeks on HFD_{lard}; Fig. 3i). Collectively, these results reveal that developmental exposure to fat-related sensory cues influences first encounter feeding by shifting preferences towards HFD_{lard}, while it does not alter total HFD_{lard} intake under exclusive HFD_{lard} feeding.

Developmental exposure to fat-related odours impairs metabolic flexibility towards HFD

Our results suggest that the increased weight gain and adiposity in BFD_{dev} mice under HFD_{lard} is not triggered by increased food intake. Hence, we sought to further characterize the homeostatic responses to HFD feeding in adult BFD_{dev} mice using energy expenditure (EE) as a read-out of homeostatic control of energy metabolism. Before switching to HFD_{lard}, EE was comparable between NCD_{dev} and BFD_{dev} groups, in both males (Fig. 3j) and females (Fig. 3k). In response to HFD_{lard} feeding, while EE increased in NCD_{dev} male mice (Fig. 3j), it decreased in BFD_{dev} male mice (Fig. 3j). EE also decreased in BFD_{dev} females compared with NCD_{dev} females after the switch to HFD_{lard} (Fig. 3k). Unlike EE, locomotion and respiratory exchange ratio were identical between the two groups after the switch to HFD_{lard} (Extended Data Fig. 8e–l). Notably, exposure to BFD exclusively during adulthood did not alter EE upon the switch to HFD_{lard} (Fig. 3l and Extended Data Fig. 8m–r), indicating that the decreased EE observed in BFD_{dev} is contingent on the sensory detection of fat-related cues during early life. As iBAT thermogenesis plays a central role in the regulation of EE in mice, we measured iBAT thermogenesis longitudinally in response to HFD_{lard} feeding (Fig. 3m). Pre-HFD_{lard}, iBAT thermogenesis was similar between BFD_{dev} and NCD_{dev} mice. After switching to HFD_{lard}, iBAT thermogenesis increased in both NCD_{dev} and BFD_{dev} mice (Fig. 3m). However, iBAT thermogenesis was lower in BFD_{dev} compared with NCD_{dev}. This reduction in iBAT temperature was also accompanied by decreased expression of iBAT

thermogenesis-related genes such as *Cidea* or *Pparg* (Fig. 3n). Therefore, we found that developmental exposure to HFD-related sensory signals alters metabolic flexibility and homeostatic responses to HFD in adult mice.

Developmental exposure to fat-related sensory cues alters life-long AgRP neuronal activity dynamics

We next determined whether the exacerbated obesogenic responses and altered homeostatic responses induced by developmental exposure to fat-related sensory cues correlate with functional alterations in key homeostatic circuits. Based on their pivotal metabolic regulatory functions and their known implications in obesity-associated metabolic outcomes, we focused on Agouti-related peptide (AgRP) expressing neurons in the arcuate nucleus of the hypothalamus (ARH)[47–49]. AgRP neurons are highly active upon fasting and are pivotal homeostatic regulators of food intake, insulin sensitivity, EE and iBAT thermogenesis. To probe for the long-lasting influence of early life exposure to fat-related sensory cues on AgRP neurons, we monitored AgRP calcium dynamics in vivo in response to nutritionally relevant stimuli, including food as well as hunger and satiety hormones. To measure AgRP neuronal activity, fibre photometry was performed in adult NCD_{dev} and BFD_{dev} mice expressing the genetically encoded calcium indicator GCaMP6s in AgRP neurons (Fig. 4a).

Sensory detection of food-related cues rapidly and sharply decreases AgRP neuronal activity, and food ingestion sustains their inhibition[20,23–25,27]. In addition, studies have shown that obesity strongly impinges on AgRP neuronal activity dynamics[50,51]. In particular, the responsiveness of AgRP neurons to HFD is reduced in diet-induced obese mice[50,51]. To study the activity dynamics of AgRP neurons in our model, we first studied the AgRP calcium dynamics in fasted mice in response to food presentation. As AgRP neuronal inhibition in response to food is proportional to caloric content, we recorded AgRP calcium dynamics in adult NCD_{dev} and BFD_{dev} in response to both NCD and HFD_{lard} exposure. Of note, these photometry recordings have been performed in lean animals before chronic HFD_{lard} feeding but non-naive to HFD_{lard} to control for behavioural changes upon the first encounter with HFD_{lard} (Extended Data Fig. 9a). These experiments revealed that, as previously described, NCD presentation rapidly inhibited AgRP neurons (Fig. 4b). The AgRP neuronal response upon NCD presentation was identical in both groups (Fig. 4b). In striking contrast, AgRP neuronal inhibition upon HFD_{lard} presentation was largely blunted in BFD_{dev} compared with NCD_{dev} mice (Fig. 4c). In NCD_{dev} mice, the

---

Fig. 3 | Developmental exposure to fat-related odours alters dopaminergic response, gates preference towards HFD_{lard} and decreases energy expenditure. a,b, Lard-based HFD (HFD_{lard}) odour-induced differential glucose transport based on fluorodeoxyglucose (^{18}FDG) PET kinetics in adult mice exposed to NCD (NCD_{dev}) or BFD (BFD_{dev}) during development pre-HFD_{lard} in the lateral nucleus accumbens shell (LAcbSh) (paired two-tailed *t*-test; $n = 7, 8$; $P = 0.0073$) (**a**) and ventral tegmental area (VTA) (paired two-tailed *t*-test; $n = 7$, 8; $P = 0.0213$) (**b**). The colour code on the representative PET images depicts the paired *t*-test value for each voxel. Relative increases in glucose metabolism upon HFD_{lard} odour exposure are colour-coded in yellow to orange, whereas decreases are colour-coded in blue. **c,** Schematic of unilateral viral delivery of the dopamine optical sensor dLight1.1 in the LAcbSh, cannula implantation for fibre photometry analysis of dopamine release, and food exposure paradigm used for dLight1.1 recordings. **d–f,** Dopamine response to food in adult NCD_{dev} and BFD_{dev} mice pre-HFD_{lard}. Dopamine sensor fluorescence depicted as *z*-score and 5-s binned average upon approach to a NCD pellet (two-way ANOVA; $n = 8$, 9; uncorrected Fisher's LSD post hoc; P group < 0.0001; P time$_{0–5} = 0.0055$; P time$_{5–10} = 0.0003$) (**d**), a BFD pellet (two-way ANOVA; $n = 8, 9$) (**e**) or a HFD_{lard} pellet (two-way ANOVA; $n = 8, 7$) (**f**). **g,** Percentage of calories from HFD_{lard} during the first day of a two-choice diet preference test (unpaired two-tailed *t*-test; $n = 13$, 10; $P = 0.0206$). **h,** Cumulative food intake of NCD_{dev} and BFD_{dev} mice before the switch to HFD_{lard} (two-way repeated-measures ANOVA; $n = 8, 8$). **i,** Cumulative

food intake of HFD_{lard} during 10 weeks on HFD_{lard} (two-way repeated-measures ANOVA; $n = 8, 8$). **j,k,** Energy expenditure of NCD_{dev} and BFD_{dev} mice pre-and post-HFD_{lard} feeding and total EE in: males (time curve: two-way repeated-measures ANOVA; $n = 11, 5$; P group $= 0.0054$; P interaction $= 0.0023$) (total EE, linear mixed-effects models; Holm–Bonferroni post hoc; $n = 11, 5$; P interaction $= 0.061$; P post-HFD NCD_{dev} versus post-HFD $BFD_{dev} = 0.004$, P pre-HFD versus post-HFD $NCD_{dev} = 0.049$) (**j**), females (time curve: two-way repeated-measures ANOVA; $n = 13, 8$; P interaction < 0.0001) (total EE, linear mixed-effects models; Holm–Bonferroni post hoc; $n = 13, 8$; P interaction < 0.001; P post-HFD NCD_{dev} post-HFD $BFD_{dev} = 0.048$; P pre-HFD post-HFD $BFD_{dev} = 0.009$; P pre-HFD post-HFD $NCD_{dev} = 0.08$) (**k**). NS, not significant. **l,** Energy expenditure of mice exposed in adulthood to NCD (NCD_{adult}) or BFD (BFD_{adult}) pre-and post-HFD_{lard} feeding (two-way repeated-measures ANOVA; $n = 7, 8$). **m,** Interscapular brown adipose tissue (iBAT) temperature recordings in NCD_{dev} and BFD_{dev} mice pre-and post-HFD_{lard} feeding (two-way repeated-measures ANOVA; Tukey's post hoc; $n = 10,8$; P group $= 0.0047$). **n,** Gene expression of thermogenesis-related genes in iBAT in NCD_{dev} and BFD_{dev} mice fed HFD_{lard} for 1 week (multiple unpaired two-tailed *t*-test; $n = 9,10$; P *Cidea* $= 0.034$; P *Pparg* $= 0.022$). Statistics are depicted as: for two-way repeated-measures ANOVA or mixed-effects model, group comparison and time × group interaction; for multiple unpaired *t*-test and *t*-test. Bars represent mean value. Error bars represent s.e.m. *$P \le 0.05$, **$P \le 0.01$, ***$P \le 0.001$.
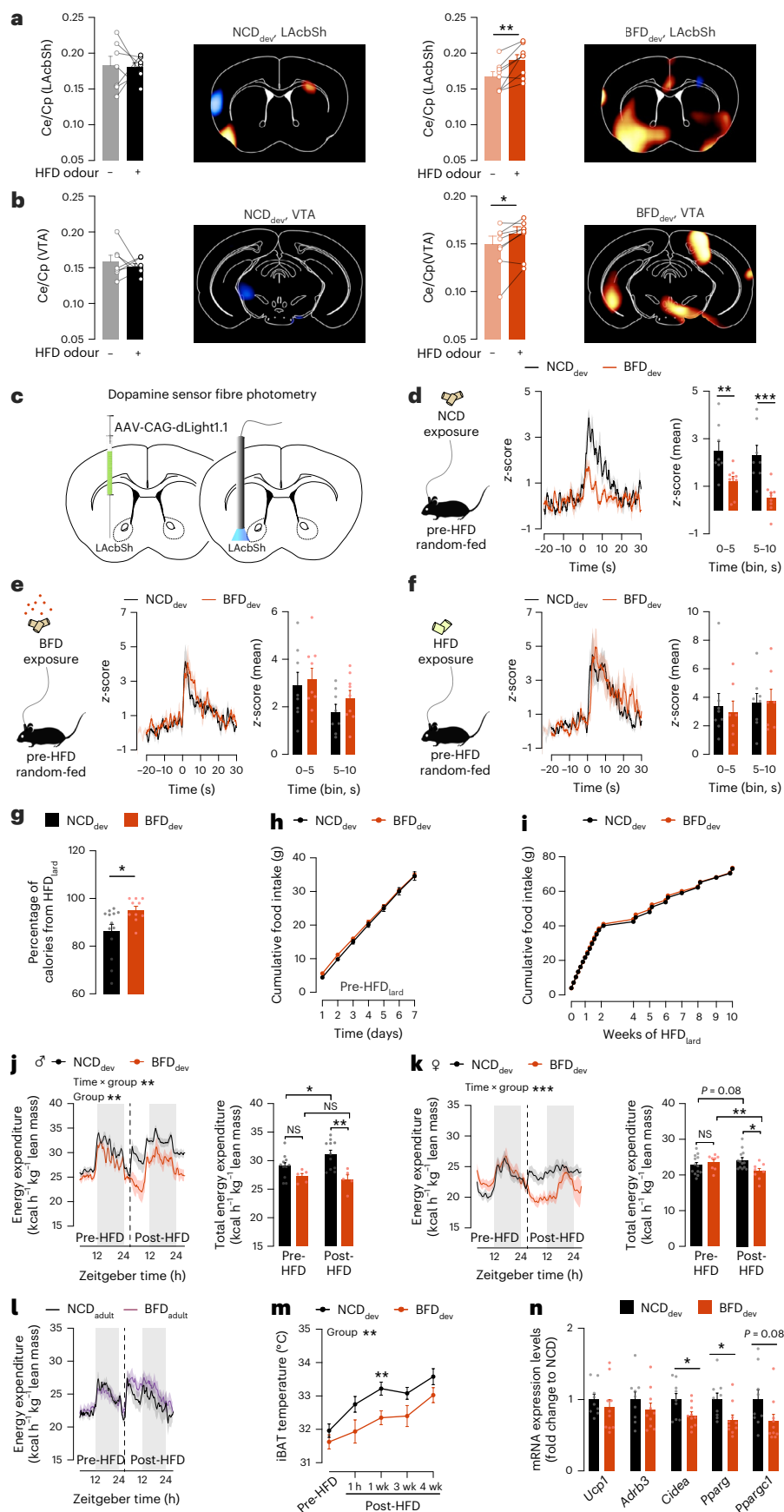
magnitude and dynamics of AgRP neuronal inhibition in response to food is proportional to the nutritional value, with HFD_{lard} presentation resulting in greater AgRP neuronal inhibition than NCD (Fig. 4d). In contrast, AgRP neuronal activity is identical in response to NCD and HFD_{lard} presentation in BFD_{dev} mice (Fig. 4d). Hence, developmental exposure to fat-related sensory cues impairs AgRP neuronal responses to dietary fat and outweighs the learnt responses to the food's nutritional value. Collectively, these results revealed that adult mice developmentally exposed to fat-related sensory cues display functional dysregulations of AgRP neuronal responses that phenocopy those of adult HFD_{lard}-fed obese mice while still lean and maintained on chow diet.

We then sought to investigate whether the 'obese-like' AgRP calcium dynamics in BFD_{dev} mice will be further affected by HFD_{lard}-induced obesity. Hence, mice were switched to HFD_{lard} for 4 weeks and we repeated the fibre photometry recordings (post-HFD_{lard}) (Extended Data Fig. 9a). These analyses revealed that, in line with previous reports, in NCD_{dev} animals, the inhibition of AgRP neuronal activity in response to HFD_{lard} is largely reduced in obese HFD_{lard}-fed mice compared with lean mice (pre-HFD_{lard}) (Fig. 4e and Extended Data Fig. 9b,c). In contrast, in BFD_{dev} mice, chronic HFD_{lard} feeding has no additional effects on AgRP neuronal inhibition in response to HFD_{lard} presentation (Fig. 4e and Extended Data Fig. 9b,c). Notably, the AgRP responses to HFD_{lard} in BFD_{dev} mice pre- and post-HFD_{lard} feeding are indistinguishable (Fig. 4e). Thus, early life exposure to fat-related sensory cues primes AgRP neuronal desensitization to dietary fat in ways that mirror that of diet-induced obese animals and that forego the onset of diet-induced metabolic alterations.

AgRP neuronal activity is modulated not only by food cues but also by hunger and satiety hormones[20,23,24,27,50,51]. Consequently, we next investigated whether the dampened AgRP neuronal response to HFD_{lard} could originate from changes in circulating levels of satiety hormones and/or altered AgRP neuronal responses to these hormones pre-HFD_{lard}. Circulating levels of leptin, cholecystokinin (CCK) and peptide YY (PYY) after HFD_{lard} ingestion were similar between NCD_{dev} and BFD_{dev} mice (Extended Data Fig. 9d–f). We then assessed AgRP neuronal activity of NCD_{dev} and BFD_{dev} mice in response to the hunger-related hormone ghrelin and to key post-prandial AgRP neurons' regulators (CCK, serotonin (5-HT), glucagon and PYY) (Extended Data Fig. 9g). AgRP neuronal activity did not differ between NCD_{dev} and BFD_{dev} mice in response to intraperitoneally (i.p.) administered ghrelin (Fig. 4f and Extended Data Fig. 9h), CCK (Fig. 4g and Extended Data Fig. 9i), 5-HT (Fig. 4h and Extended Data Fig. 9j), glucagon (Fig. 4i and Extended Data Fig. 9k) and PYY (Fig. 4j and Extended Data Fig. 9l). Therefore, developmental exposure to fat-related sensory cues led to a selective impairment in AgRP neuronal responses to dietary fat without affecting responses to key hormonal signals.

Sensory programming of metabolism is dependent on sensory/caloric association

As in our model the bacon sensory cues are associated with the nutritive components of the ingested (flavoured) NCD, we sought to investigate if the sensory programming of obesity is contingent on the coupling with calorie ingestion. To unravel whether sensory stimulation alone

is sufficient to prime long-term metabolic health, we repeated the developmental exposure to BFD in dams fed NCD but exposed to non-accessible BFD (Extended Data Fig. 10a). More precisely, we created a model of passive BFD exposure in NCD-fed dams by placing BFD in a metal mesh in the cage to expose the mice to its sensory signals uncoupled from its intake. Passive exposure to BFD (BFD_{caged}) did not alter maternal weight gain or weight gain per pup (Extended Data Fig. 10b,c). Furthermore, passive exposure to BFD during development ($BFD_{dev;caged}$) did not influence HFD_{lard}-induced weight gain (Extended Data Fig. 10d). Altogether, these experiments suggest that the coupling of both sensory and nutritive food components is a prerequisite for the sensory programming of metabolism.

To substantiate the importance of sensory/caloric associations for the long-term susceptibility to obesity, we designed another model of developmental activation of sensory circuits independent of dietary manipulation. In mice, the neonatal period is critical for the experience-dependent regulation of sensory circuit development and responses later in life[16,17,52]. In particular, developmental acquisition of odour preference is dependent upon the activity of OSNs which reside in the main olfactory epithelium[16,17,52]. Accordingly, we developed a non-invasive optogenetic-based model of neonatal activation of a defined olfactory circuit to assess the subsequent consequences on odour-evoked behaviours, food preference and obesity development. Having identified acetophenone as a volatile highly enriched in BFD and HFDs (Fig. 2m), we selectively activated OSNs expressing olfactory receptor 151 (Olfr151, also known as M71), a primary olfactory receptor for acetophenone[53]. We targeted the red-shifted variant of channelrhodopsin (ReaChR), which allows non-invasive light stimulation[54] of M71-expressing OSNs in pups. This experimental design enables to investigate the role of neonatal activation of an acetophenone-responsive circuit on long-term behavioural and obesogenic outcomes, independent of maternal diet or direct acetophenone exposure. By selectively activating this sensory circuit during early postnatal development, we aimed to establish a proof-of-concept experiment to isolate the effects of early sensory circuit activation on lasting behavioural and metabolic trajectories.

To first validate that optogenetic activation of M71 can resemble exposure to acetophenone in the absence of sensory experience, we conducted experiments in adult mice expressing ReaChR in M71-expressing neurons ($M71^{ReaChR}_{adult}$) (Fig. 5a–e and Extended Data Fig. 10e–h). To determine if optogenetic stimulation of M71 can guide future olfactory behaviour in response to acetophenone, we paired photostimulation of M71 glomeruli in the olfactory bulb (where OSN-expressing M71 axons converge) with a food reward in the form of a sucrose-coated HFD_{lard} pellet (Fig. 5a,b). We then subjected the mice to a two-chamber odour preference test, exposing them to acetophenone and isoamyl acetate as control odour (Fig. 5b). In the absence of experimental intervention, mice typically showed no preference between the two odours (Fig. 5c and Extended Data Fig. 10e). In contrast, pairing M71 stimulation with a food reward triggered a preference for the acetophenone side in $M71^{ReaChR}_{adult}$, while $M71^{WT}_{adult}$ control mice showed no preference between the two odours (Fig. 5d,e and Extended Data Fig. 10f–h).

Fig. 4 | Developmental exposure to fat-related sensory cues primes an obese-like AgRP neuronal response before HFD_{lard}-induced obesity. a, Schematic of viral injection of the calcium sensor GCaMP6s in the ARH and cannula implantation in AgRP-IRES-Cre mice for GCaMP6s-based fibre photometry. **b,c,** AgRP calcium dynamics and average z-score in response to NCD presentation pre-HFD_{lard} (unpaired two-tailed t-test; $n = 6, 5$) (**b**), non-naive HFD_{lard} presentation in NCD_{dev} and BFD_{dev} mice pre-HFD_{lard} (unpaired two-tailed t-test; $n = 6, 6$; $P = 0.0071$) (**c**). **d,** Comparison of the AgRP neuronal dynamics and average z-score in response to NCD and HFD_{lard} presentation in lean mice non-naive to HFD_{lard} in NCD_{dev} and BFD_{dev} (two-way ANOVA; uncorrected Fisher's LSD post hoc; $n = 6, 6$; $n = 5, 6$, respectively; P group = 0.025; P interaction = 0.0417) (AUC_{NCDdev}: unpaired two-tailed t-test; $n = 6, 6$; $P = 0.0085$). **e,** Comparison

of the AgRP neuronal dynamics and average z-score in response to HFD_{lard} presentation following 4 weeks of HFD_{lard} feeding in NCD_{dev} and BFD_{dev} mice with average z-score (two-way ANOVA; uncorrected Fisher's LSD post hoc test; $n = 6, 5$; $n = 6, 5$; P interaction = 0.0292) (AUC_{NCDdev}: unpaired two-tailed t-test; $n = 6, 5$; $P = 0.007$). **f–j,** AgRP calcium dynamics pre-HFD_{lard} in response to intraperitoneal (i.p.) administration of ghrelin ($n = 5, 7$) (**f**), cholecystokinin (CCK) ($n = 5,5$) (**g**), serotonin (5-HT) ($n = 5, 7$) (**h**), glucagon ($n = 4,7$) (**i**) and peptide YY (PYY) ($n = 5, 7$) (**j**). Unpaired two-tailed t-test on the AUC (Extended Data Fig. 9h–l) (**f–j**). Statistics are depicted as for two-way repeated-measures ANOVA group comparison; unpaired t-test. Bars represent mean value. Error bars represent s.e.m. *$P \le 0.05$, **$P \le 0.01$.

These experiments confirm that M71 photostimulation effectively mimics activation of acetophenone-sensitive circuits in the absence of real odour experience.

To activate M71-expressing OSNs during neonatal life, the snouts of pups expressing ReaChR in M71 neurons (M71^ReaChR) and their control

Cre-negative littermates (M71^WT) were light-stimulated from post-natal day 1 to 7 (Fig. 5f), which covers the olfactory critical period pivotal for developmental acquisition of odour preference[16,17,52]. To validate this approach in pups, a red light was placed over the snout of pups expressing ReaChR in all OSNs (OSN^ReaChR) at postnatal day
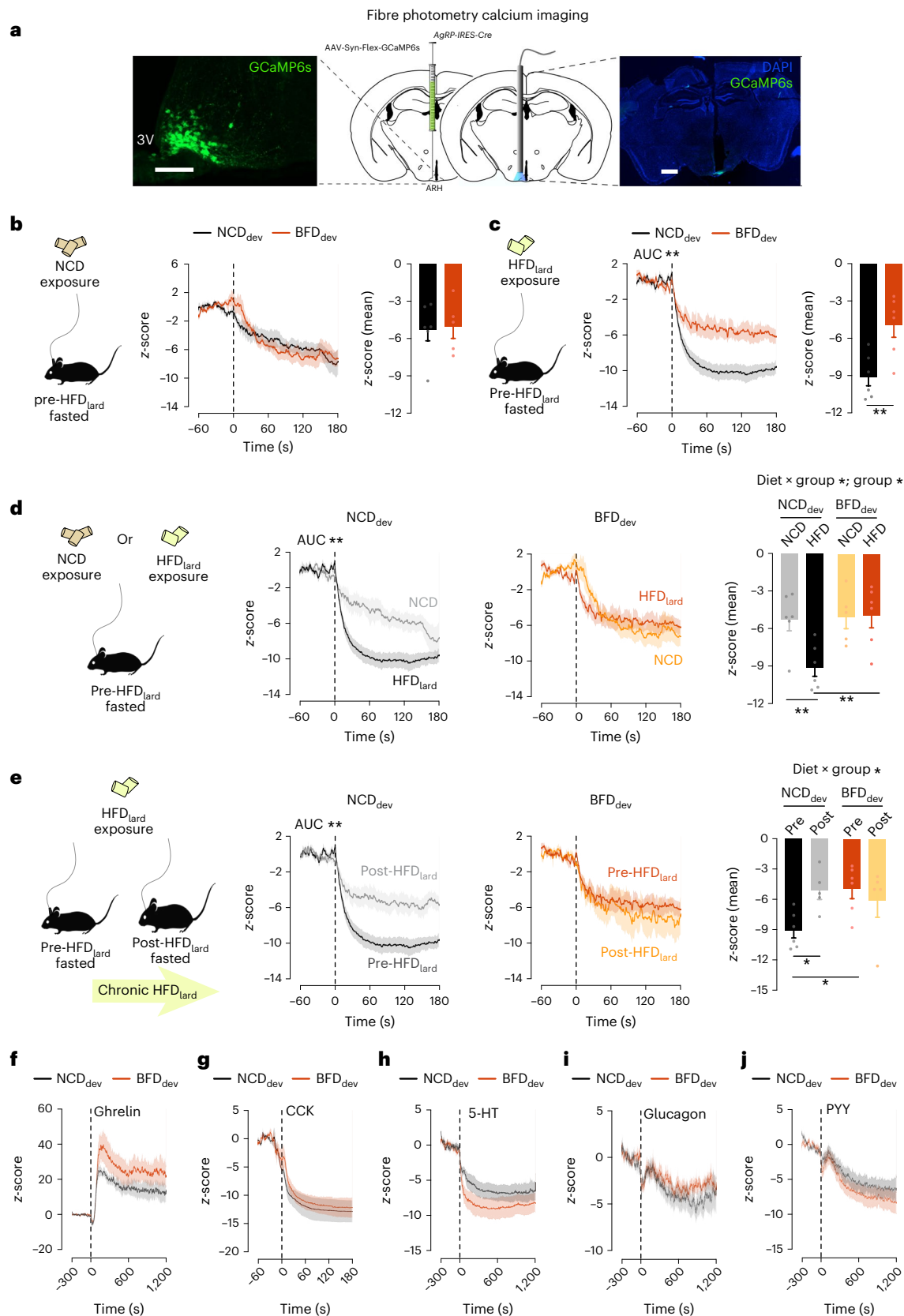
3 before assessing the resulting regulation of activity-dependent genes (Fig. 5g and Extended Data Fig. 10i). Expression of $Egr1$ and $Pcdh10$ increased upon light stimulation in OSN[ReaChR] pups, but not in light-stimulated Cre-negative littermates (OSN[WT]) or in OSN[ReaChR] non-light-stimulated pups (Fig. 5g and Extended Data Fig. 10i), demonstrating specific and selective light-induced activation of OSNs. Furthermore, light stimulation activated M71-expressing neurons in the MOE of ReaChR-expressing pups (M71[ReaChR]), as indicated by S6 phosphorylation, an effect not seen in Light OFF control animals (Fig. 5h). Thus, this model allows for acute, selective and non-invasive activation of olfactory circuits in neonates.

We first investigated the influence of this neonatal optogenetic activation of M71-expressing OSNs on the long-term acetophenone preference. Adult mice that underwent M71 optogenetic stimulation during early life (M71[ReaChR]) exhibited a preference for acetophenone as revealed by an increased investigation time of defined acetophenone concentrations (Fig. 5i). Furthermore, in an olfactory habituation-dishabituation test, M71[ReaChR] mice exhibited increased investigation time for a HFD flavoured with acetophenone (HFD[acetophenone]) (Extended Data Fig. 10j). To further assess the influence of M71 neonatal activation on feeding-related behaviour in adulthood, we exposed mice to NCD flavoured with acetophenone odour (AFD). Latency to eat AFD decreased in adult M71[ReaChR] compared with M71[WT] animals (Fig. 5j), demonstrating that neonatal optogenetic activation of M71-expressing OSNs is sufficient to programme odour preference in adulthood. Remarkably, M71[ReaChR] mice ate significantly more AFD (Fig. 5k), whereas intake of NCD was identical in both groups (Fig. 5l and Extended Data Fig. 10k). Further analysis of feeding behaviour revealed that increased AFD intake in M71[ReaChR] mice occurred only acutely (the first day) and that both groups ingested a similar quantity of AFD on the second day (Extended Data Fig. 10l). Thus, selective neonatal stimulation of olfactory circuits primes acute food preference similar to the HFD preference observed in BFD[dev] mice. Together, these findings reveal that activation of sensory circuits during development is sufficient to gate feeding preference in adulthood.

To evaluate whether neonatal optogenetic activation of a distinct sensory circuit can influence the onset of obesity in adulthood, adult M71[ReaChR] and Olfr51[WT] mice were fed HFD[acetophenone] (Fig. 5m).

Neonatal M71 optogenetic activation did not significantly influence diet-induced weight gain (Fig. 5n) or adiposity neither in males (Fig. 5o and Extended Data Fig. 10m) nor in females (Fig. 5p,q and Extended Data Fig. 10n). Thus, activation of sensory circuits alone programmes food and odour preference, but is not sufficient to exacerbate the obesogenic responses to HFD[acetophenone].

In contrast to our BFD-based model of developmental exposure to fat-related odours, optogenetic-based activation of sensory circuits is uncoupled from caloric intake. To investigate whether the sensory programming of metabolism relies on the association between sensory input and caloric intake, we paired neonatal M71 optogenetic activation with caloric ingestion. This sensory/caloric coupling was achieved by allowing the pups to lick the calorie-dense liquid diet Ensure during optogenetic stimulation (M71[ReaChR+Ensure] versus M71[WT+Ensure]) (Fig. 5r). Crucially, as pups consume only a small fraction of their daily caloric intake during the optogenetic procedure, this model enables sensory-caloric coupling without triggering neonatal overeating.

Coupling neonatal M71 optogenetic stimulation to caloric intake did not affect HFD[acetophenone]-induced weight gain (Fig. 5s) or adiposity (Fig. 5t and Extended Data Fig. 10o) in males. In contrast, M71[ReaChR+Ensure] females showed exacerbated weight gain (Fig. 5u; interaction sex × developmental diet × time, $P = 0.02$) and adiposity (Fig. 5v and Extended Data Fig. 10p; interaction sex x developmental diet: $P = 0.03$) compared with M71[WT+Ensure] control mice. Collectively, these results highlight that the sensory programming of metabolism is contingent on sensory/caloric association and further corroborate sexual dimorphism in these responses.

Discussion

Extensive research over the past three decades has established that maternal dietary habits can profoundly shape the health trajectories of their offspring. Yet, the primary focus has remained on the caloric and nutritional composition of the diet, while the role of food chemosensory cues has been neglected. Here, we demonstrate that exposure to the non-nutritive sensory components of HFD during development is sufficient to induce long-lasting metabolic dysregulation and prime obesity similar to the deleterious effects triggered by obese or HFD-fed dams[1–5]. We reveal that early life exposure to fat-related sensory cues is

Fig. 5 | The sensory programming of metabolism is contingent on sensory/ caloric association. a–e, Optogenetic activation of M71 glomeruli in M71-IRES-Cre:R26-LSL-ReaChR-mCitrine adult mice. Representative image of fibre placement above a M71 glomerulus in the olfactory bulb; scale bar, 300 μm (green, mCitrine (M71); blue, 4,6-diamidino-2-phenylindole (DAPI)) (**a**). Schematic of the experimental design to pair M71 photostimulation with a food reward in adult mice (**b**). The implantation of artificial memory was assessed using a two-chamber place preference test, with each chamber containing either acetophenone or a control odour (isoamyl acetate). Place preference test in C57BL/6NCrl mice ($n = 8$) (**c**). Odour preference in mice expressing ReaChR in M71 cells (M71[ReaChR, adult]) and control littermates (M71[WT, adult]). Odour preference test (two-way repeated-measures ANOVA; Sidak's post hoc; $n = 7, 8$; P group = 0.0151) (**d**) and average preference of M71[ReaChR, adult] and M71[WT, adult] mice (unpaired two-tailed t-test; $n = 7, 8$; P group = 0.015) (**e**). **f**, Paradigm of neonatal optogenetic activation of M71-expressing OSNs. **g**, Gene expression of OSN activity-dependent genes in P3 pups expressing ReaChR in OMP-expressing OSNs (OSN[ReaChR]) or WT OSNs (OSN[WT]) 60 min after optogenetic stimulation (multiple unpaired two-tailed t-test; $n = 5, 6$; P $Egr1$ = 0.0184; P $Pcdh10$ = 0.0337). **h**, Representative images of S6-phosphorylation (pS6) in the main olfactory epithelium in P5 pups expressing ReaChR in M71 OSNs (M71[ReaChR]) and control littermates (M71[WT]) (green, mCitrine (M71); red, pS6), scale bar, 20 μm. **i–v**, Behavioural and metabolic analysis of adult mice optogenetically stimulated during neonatal life. Investigation time of progressively increasing concentrations of acetophenone normalized to vehicle (two-way repeated-measures ANOVA; Sidak's post hoc; $n = 6, 5$; P concentration < 0.0001; P interaction = 0.0349) (**i**). Latency to eat AFD normalized to NCD following overnight fast (unpaired two-tailed t-test; $n = 8, 11$; $P = 0.0048$) (**j**). Cumulative food intake of AFD upon first exposure during the

dark cycle (time curve: two-way repeated-measures ANOVA; Sidak's post hoc; $n = 5, 5$; P group = 0.0364; P interaction = 0.0003) (total AFD intake, unpaired two-tailed t-test; $n = 5, 5$; P group = 0.0339) (**k**). Cumulative NCD intake (time curve, two-way repeated-measures ANOVA; $n = 5, 5$) (total NCD intake, unpaired two-tailed t-test; $n = 5, 5$) (**l**). Paradigm of neonatal optogenetic activation of M71-expressing OSNs and subsequent feeding of HFD[acetophenone] (**m**). Metabolic phenotyping of adult offspring optogenetically stimulated during the first week of life and fed a HFD[acetophenone] during adulthood. Body weight gain of male offspring on HFD[acetophenone] (two-way repeated-measures ANOVA; $n = 14, 12$) (**n**). Body composition of males following HFD[acetophenone] (two-tailed Wilcoxon rank-sum test; $n = 7, 9$) (**o**). Body weight gain of female offspring on HFD[acetophenone] (two-way repeated-measures ANOVA; $n = 8, 10$) (**p**). Body composition of females following HFD[acetophenone] (two-tailed Wilcoxon rank-sum test; $n = 7, 7$) (**q**). Schematic of the neonatal sensory/caloric coupling paradigm: light stimulation was coupled to the intake of high-calorie liquid diet Ensure in pups expressing ReaChR in M71-expressing OSNs (M71[ReaChR+Ensure]) and control littermates (M71[WT+Ensure]) (**r**). Metabolic phenotyping on HFD[acetophenone]. Body weight gain of male offspring on HFD[acetophenone] (mixed-effects model; $n = 10, 11$) (**s**). Body composition of males following HFD[acetophenone] (two-tailed Wilcoxon rank-sum test; $n = 9, 8$) (**t**). Body weight gain of female offspring on HFD[acetophenone] (mixed-effects model; Tukey's post hoc; $n = 9, 9$; P group = 0.0182; P interaction = 0.0036) (**u**). Body composition of females following HFD[acetophenone] (two-tailed Wilcoxon rank-sum test; $n = 8, 7$; $P = 0.056$) (**v**). Statistics are depicted as: for two-way ANOVA, group comparison and time x group interaction; for multiple unpaired t-test and Wilcoxon rank-sum test, horizontal bars represent group comparison. Bars represent mean value. Error bars represent s.e.m. *$P \leq 0.05$, **$P \leq 0.01$, ***$P \leq 0.001$.

sufficient to shift the responses of reward-related mesolimbic dopamin-ergic and homeostatic AgRP circuits towards response characteristics of obese animals. Altogether, we identify a novel pivotal mechanism through which maternal diet primes long-term metabolism and pro-grammes obesity in the offspring.

Our study provides evidence that maternal obesity per se and its associated adverse metabolic outcomes are not solely responsible for

the metabolic programming triggered by maternal HFD feeding. Our results are in line with previous work revealing that offspring of lean HFD-fed dams have an increased risk for metabolic dysregulation[1,3,4]. Notably, studies in non-human primates revealed that HFD consump-tion in diet-resistant lean mothers triggered metabolic alterations in the offspring[7,8]. Conversely, switching obese non-human primate moth-ers to a chow diet exclusively during pregnancy reversed peripheral
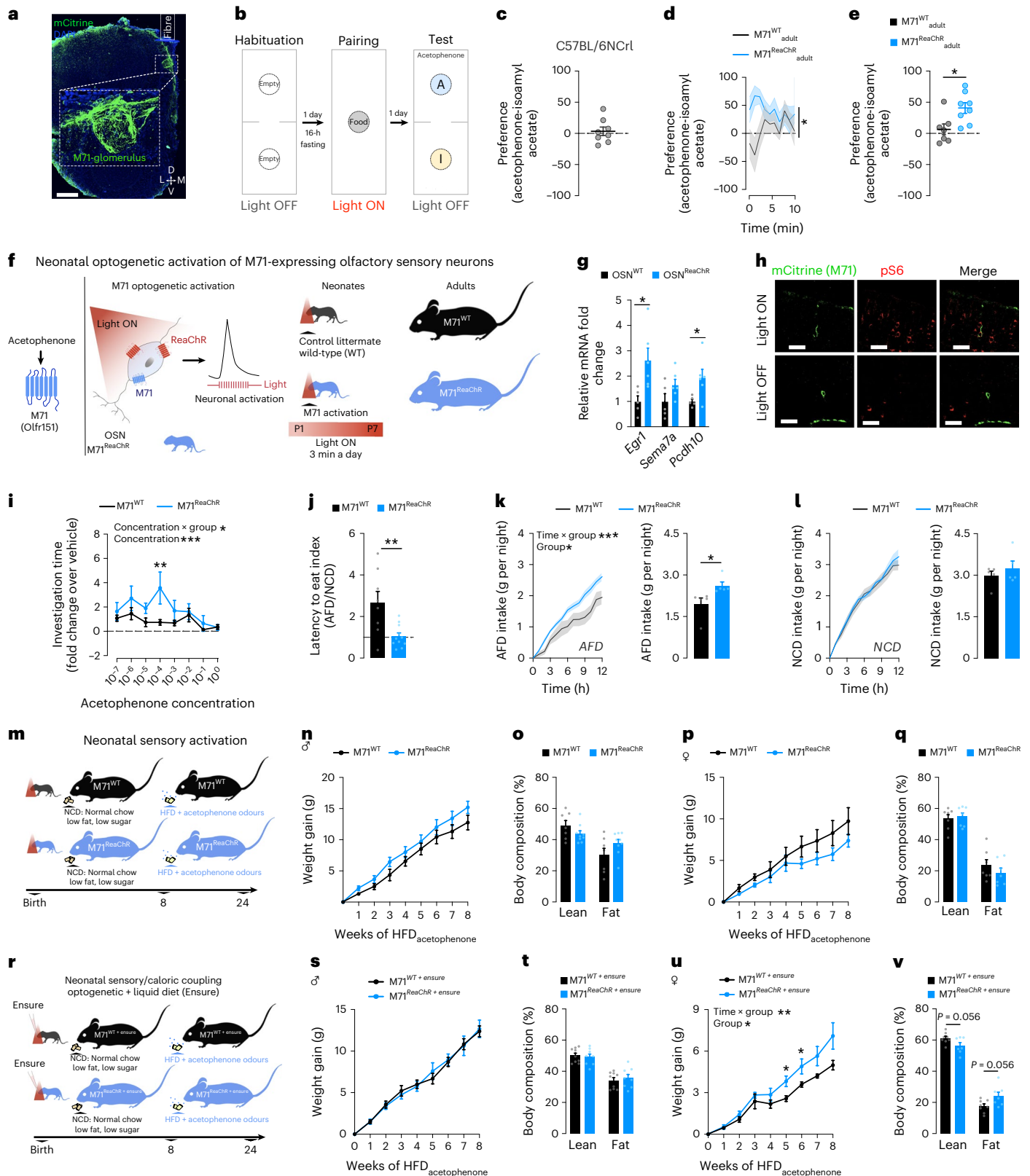
alterations in their offspring[7], further corroborating that diet itself plays a key programming role independent of maternal health status.

Maternal HFD consumption affects dopamine circuits and induces a preference for HFD in the offspring[41,55,56]. While the diet-induced remodelling of dopamine responses has been largely attributed to the hyperlipidaemic and hypercaloric aspects of palatable foods, our study alternatively reveals another pathway by demonstrating that non-nutritive sensory cues influence the mesolimbic reward pathway in adulthood. Critically, the blunted dopamine release observed in the LAcbSh and the shift in preference for HFD over a less palatable chow diet have recently been reported in adult HFD-fed mice[50]. The dampened dopamine response observed in BFD$_{dev}$ mice occurred in lean NCD-fed animals, suggesting that these alterations occur independently of metabolic changes. Consistent with our results, other studies have reported that altered dopamine responses to food and subsequent changes in feeding behaviour can occur in the absence of weight gain or metabolic alterations in adult animals fed HFD[50,57,58]. We show that the presence of fat-related sensory cues in the developmental diet not only durably altered dopamine responses to food, but also gated food discrimination and preference. Our neonatal M71 optogenetic model further emphasizes the importance of sensory circuit activation during development in shaping odour and food preference in adulthood. Although we attribute the results of the food preference test to a preference, they may also reflect reduced or absent neophobia (the reluctance to consume unfamiliar foods), which affects food choice, particularly in children[59]. Aligned with other studies[60], the preference for HFD$_{lard}$ occurs over the course of the first day of exposure in control animals, while mice exposed to BFD during development show an almost immediate preference for HFD$_{lard}$ over the control diet. Further supporting the involvement of neophobia, the effects on feeding preference were acute (≈24 h), indicating they arise from behavioural differences during initial encounters. Of note, while pups begin ingesting solid food in the second postnatal week, raising the possibility of pre-weaning BFD effects, our diet-independent neonatal optogenetic model rules out any major contribution of pup-driven BFD intake to the observed phenotypes.

In contrast to observations in adult obese mice[50,51], our model of developmental exposure to fat-related sensory cues shows that the diminished dopamine release in response to NCD was not accompanied by changes in AgRP neuronal activity. In fact, NCD exposure induced a rapid inhibition of AgRP neuronal activity in both groups, in line with the previously described sensory inhibition of these neurons[20,23–25,27]. This suggests that food sensory experiences in early life independently influence mesolimbic dopamine and AgRP hunger circuits to gate preference towards HFD and trigger metabolic alterations, respectively. Despite similar responses to NCD exposure, BFD$_{dev}$ mice exhibited AgRP neuronal desensitization to dietary fat, a phenomenon typically observed in mice chronically fed HFD[50,51]. Our findings align with previous studies demonstrating that genetic disruption of AgRP neuronal function leads to increased EE[61–65]. Similarly, neonatal ablation of AgRP neurons[66] as well as deletion of either the entire AgRP neuronal population or specific subpopulations[67,68] elevate EE, further emphasizing the critical role of AgRP neurocircuits in the regulation of energy metabolism and body weight control. Remarkably, early life sensory cues can outweigh the profound effects on AgRP neurons of diet-induced obesity during adulthood, which had no additional detrimental consequences on these neurons. While maternal HFD feeding has a well-known negative influence on the development of AgRP neurocircuits[1,39,42], the blunted responses to HFD did not seem to derive from general dysfunction of AgRP neurons, as they responded appropriately to NCD exposure and peripheral hormones. Consistent with the altered responses to HFD centrally and metabolically, reduced food cue-induced control of feeding behaviour is associated with overweight and obesity susceptibility in rodents and humans[69–73]. Considering the numerous central and peripheral pathways involved in the regulation of energy homeostasis, further studies will be required to define whether early life exposure to fat sensory cues

influences processes beyond those described in this study. Collectively, our findings demonstrate that fat sensory cues during development are sufficient to mimic the deleterious effects of HFD-induced obesity on AgRP neurons and resulting metabolic alterations.

Recent investigations of the regulation of AgRP neuronal activity dynamics revealed the critical importance of learning processes[20,23–25,60,74,75]. Consumption of a novel food in a single trial is sufficient to condition AgRP responses proportionally to the caloric content upon exposure to sensory food cues[20]. In adult mice, this learnt sensory regulation of AgRP neurons is dependent on food consumption and the subsequent activation of chemosensory pathways in the intestine[76,77]. Here, we provide evidence for the importance of learnt sensory/caloric coupling mechanisms during the developmental period, likely mirroring what is occurring during adulthood. Our study indicates that developmental exposure to fat sensory cues coupled with a NCD might pre-empt the learnt AgRP neuronal response to HFD$_{lard}$ during adulthood, resulting in maladaptive central and peripheral responses to an obesogenic diet. Furthermore, we demonstrate that the sensory programming of metabolism necessitates calorie ingestion. While real (caged food) and artificially implanted (neonatal optogenetics) food sensory memories during development did not influence diet-induced obesity when uncoupled from calorie intake, reintroducing calorie ingestion during neonatal M71 activation led to detrimental metabolic consequences. Remarkably, a short, daily artificial activation of M71 paired with caloric intake during the first days of life was sufficient to substantially exacerbate obesity and adiposity. In contrast, neonatal M71 activation, when uncoupled from caloric intake, did not induce metabolic alterations but was sufficient to influence odour and feeding preferences in adulthood. These findings suggest a model wherein food sensory cues during development gate feeding preferences independently of caloric intake, whereas the sensory programming of metabolism requires the coupling of sensory cues with calories. Given that both HFD and BFD emit a complex array of volatiles beyond acetophenone, our models of acetophenone exposure trough maternal diet and M71 neonatal activation serve as a proof of concept to validate the role of HFD-derived odorants in sensory modulation of metabolism, rather than delineating the primary molecular pathway mediating this effect. Future studies are required to dissect the intricate odour profile of fatty foods and elucidate the specific volatiles and olfactory receptors contributing to long-term obesogenic outcomes.

In mice, the acquisition of innate odour recognition is particularly influenced by sensory experience during early postnatal development[16,17,52]. Notably, OSN activity during this period regulates the expression of axon-sorting molecules, which in turn directly influence their development and life-long function[16,17,52]. Consistent with this, our optogenetic stimulation of M71 led to increased expression of axon-sorting molecules, including *Pcdh10*. Previous studies have demonstrated that OSN activity during this critical period, and the resulting modifications in the wiring of the glomerular map, have long-lasting effects on odour-evoked behaviours for odours encountered during development[16–19]. Accordingly, optogenetic stimulation of M71 olfactory circuits during the first week of life was sufficient to gate odour and feeding preference. Furthermore, neonatal M71 activation coupled with caloric intake and exposure to BFD during lactation triggered metabolic alterations only in females, highlighting that postnatal development may be a critical period for sensory programming of metabolism. This finding suggests that the sex-specific windows of sensitivity in models of maternal under- or over-nutrition also extend to the sensory programming of metabolism[78]. Although we did not observe sexual dimorphism in the sensory-induced programming of metabolism by bacon sensory cues when exposed throughout the developmental period, female mice exhibited heightened sensitivity to other paradigms of developmental food sensory manipulations. These sex-specific effects might arise from numerous factors, including sexual dimorphism in olfactory signalling[79] and the sex-specific expression

of distinct olfactory receptors in the main olfactory epithelium[80,81]. Further studies are required to clarify how sex shapes metabolic sensory programming, including effects on OSN activity and axon-sorting molecules. As experience drives sex differences in pheromone-sensing neurons of the vomeronasal organ[82], the main olfactory epithelium may exhibit similar sex-dependent responses to specific food-related odorants. In addition, given that each diet has a complex odour profile composed of a large variety of volatiles, the lack of metabolic alterations in males exposed to acetophenone suggests that other volatiles may play a more prominent role in mediating the effects in males. Critically, the finding that developmental exposure to a single HFD$_{lard}$-derived volatile sets the stage for obesity in adulthood further highlights the crucial importance of early food sensory experiences.

This study expands on previous work in human and animal models demonstrating that early chemosensory transmission through maternal diet can dictate feeding habits until adulthood towards a preference for the odours to which the embryos and neonates were exposed during development[12,15–19]. As the olfactory and gustatory systems are among the first senses to develop, food sensory experiences already begin in the amniotic environment in both humans and rodents. This early chemosensory transmission likely confers a notable evolutionary advantage by serving as teaching signals to guide individuals towards safe food choices while helping them avoid potentially toxic options. However, our study indicates that perinatal odour and flavour learning not only transmits food preferences to subsequent generations but can also have detrimental consequences for their metabolic health. In light of the large number of women consuming a HFD during pregnancy and lactation, these insights are important as they suggest that even a healthy weight mother, when exposed to an unhealthy fat-rich diet and despite apparent optimal health status, might put her offspring at higher obesity risk later in life. These findings might have far-reaching implications related to the long-term consequences of the consumption of flavouring agents during pregnancy and lactation. Given the rising prevalence of food additives in modern processed diets, our study raises the possibility that exposure to artificial flavours during development might create a mismatched association between food sensory signals and expected calorie content that might programme long-lasting inappropriate physiological and behavioural responses later in life. In this context, acetophenone, which we found to be sufficient to induce obesity in females when exposure occurs during development, is naturally present in foods, but is also an FDA-approved food flavouring agent widely used in industry. These findings, therefore, raise important questions about their translational relevance for human health and behaviour. In summary, our study reveals that the early life sensory environment exerts a long-lasting influence on the regulation of central responses to food cues and metabolic health and that an exacerbated response to an obesogenic diet can be primed by the mere exposure to fat-related sensory cues during development.

Methods

Animal care
Animal care, handling, and experimental procedures were conducted in compliance with protocols approved by local government authorities (Bezirksregierung Köln). Permission to maintain and breed mice was issued by the Department for Environment and Consumer Protection, Veterinary Section, Cologne, North Rhine-Westphalia, Germany. All mice were housed in individually ventilated cages at 22–24 °C at constant humidity (50–70%) with a 12-h light–dark cycle with ad libitum food and water unless otherwise stated for experimental conditions.

Mouse models
C57BL/6NCrl mice were purchased from Charles River. AgRP-IRES-Cre mice (JAX stock, #012899)[65], M71-IRES-Cre (JAX stock, #006677)[83], OMP-Cre (JAX stock, #006668)[83] and R26-LSL-ReaChR-mCitrine (JAX stock, #026294)[54] were originally obtained from The Jackson

Laboratory. Cre lines were maintained heterozygous through breeding to wild-type C57BL/6NCrl (Charles River), while R26-LSL-ReaChR-mCitrine mice were maintained as homozygous stock breeding at the Max Planck Institute for Metabolism Research.

Diets
All diets used were obtained from ssniff Spezialdiäten (ssniff). NCD (ssniff R/M-H-Phytoestrogenarm) was used as the control maintenance diet and contained 57% calories from carbohydrates, 34% from protein and 9% from fat. The BFD, the PB-FD and AFD are isonutritional diets to NCD, containing 0.15% artificial flavours (Elli's Aromen; bacon, AS10301; peanut butter, AS10312) or 1% acetophenone (AFD, used in behavioural tests). HFDs used in this study are: HFD$_{lard}$ (ssniff EF acc. D12492 (I) mod, which contains 21% calories from carbohydrates, 19% from protein and 60% from fat derived from pork lard); HFD$_{butter}$ (ssniff EF acc. D12492 (I) mod, which contains 21% calories from carbohydrates, 19% from protein and 60% from fat derived from butter) and HFD$_{acetophenone}$ containing 0.25% acetophenone in HFD (HFD$_{lard}$; ssniff EF acc. D12492 (I) mod). The peanut butter-based HFD (HFD$_{peanut-butter}$) containing 34.9% kcal from fat was produced in-house by mixing 40% organic peanut butter (Bio Erdnussmus, dm-Drogerie Markt) with 60% NCD (ssniff R/M-H-Phytoestrogenarm) previously ground using a Koenic food blender. Feeding preference tests were performed using control diet (CD; ssniff EF acc. E15748) containing 67% calories from carbohydrates, 20% of protein, and 13% of fat.

Paradigm of developmental exposure to fat-related sensory cues through the diet
C57BL/6NCrl mice were ordered from Charles River between 5 and 6 weeks old and allowed to acclimate in a group setting of 4–5 mice per cage for 2–3 weeks. To minimize the increased risks of pup mortality reported in primiparous C57BL/6N mice, experimental cohorts of animals were generated using pregnancy-experienced females that have already undergone one pregnancy at 8 weeks old. Mice were paired one male to one female for breeding (1:1 breeding) to generate experimental cohorts. Male breeders were C57BL/6NCrl or AgRP-IRES-Cre heterozygotes for photometry experiments. Males were removed upon first signs of visible pregnancy and single caged. Females taking longer than 19 days to show visible signs of pregnancy were excluded. At postnatal day 1 (P1; day of birth considered as P0) pups were removed from the cage and tissue collected. One week later, males were paired back with the same females in a 1:1 breeding scheme. The presence of a vaginal plug was checked each morning and used to time pregnancy. The presence of a vaginal plug was designated as gestational day (GD) 0.5 and female mice lacking vaginal plugs for 7 days were excluded. At GD 4.5, the males were removed from the breeding cage and the diet of the dam was switched as appropriate to either BFD, PB-FD, AFD or remained on NCD. Dams were maintained on their respective diets until weaning of the pups at postnatal day (P) 21. Litter size was adjusted to ensure adequate and standardized nutrition until weaning. Litters containing more than eight pups were culled down to eight pups at P1 and only these litters or those with six to eight pups naturally were used for future experiments. Offspring from a minimum of two separate litters per group were used for every experiment.

Paradigm of developmental exposure to BFD during gestation or lactation selectively
The exact same experimental paradigm as described above was followed with the differences that dams were either exposed exclusively to BFD from GD 4.5 until birth (BFD$_{ges}$; exposure during gestation only) or from birth (P0) until weaning (P21) (BFD$_{lac}$; exposure during lactation only).

Paradigm of developmental exposure to fat-related sensory cues ('caged BFD')
For caged food cohorts, the accessible diet remained NCD for the entire duration but a wire mesh containing 100 g of either NCD or

BFD was placed into the bottom of the food rack and replaced every other day. Breeding strategy and litter size controls were performed as detailed above.

Metabolic phenotyping: time line

Maternal metabolic phenotyping. Dams were weighed every 3 days during gestation and lactation. At weaning of the pups, body composition was analysed using micro-CT and mice were fasted overnight and blood was collected for HOMA-IR measurements. For LC–MS-based analysis of the hydrophobic (lipids fractions), 12 days after giving birth, milk was collected as described below as well as trunk blood upon killing.

Offspring metabolic phenotyping. Pups were weaned at P21 onto their respective diets and were weighed weekly throughout their lifespan. An insulin tolerance test (ITT) and body composition pre-HFD were performed at 6 and 8 weeks of age, respectively. At 8 weeks of age, animals from both groups were switched onto a HFD (post-HFD). At 12 weeks old (4 weeks on HFD), an ITT post-HFD was performed. At 16 weeks of age, resting blood glucose measurements were taken using a handheld glucometer from venous tail blood. At 18 weeks old, another micro-CT scan was performed for body composition analysis and body length measurements were taken from snout to anus using a ruler.

Offspring metabolic phenotyping (M71^{ReaChR}). Metabolic phenotyping of mice optogenetically stimulated during neonatal life was performed as described above but mice were fed an HFD enriched with acetophenone (0.25%).

Adult cohort metabolic phenotyping. Mice for adult cohorts were purchased from Charles River at 5–6 weeks old, housed four mice per cage and allowed to acclimate for 2–3 weeks in the animal facility. At 8 weeks old, mice were changed to BFD or maintained on NCD. Mice were then metabolically phenotyped according to a similar schedule to offspring mice. In short, at 16 weeks old, mice of both groups were switched onto HFD (HFD$_{lard}$, post-HFD$_{lard}$). TSE metabolic phenotyping cages were used during the change to HFD at 16 weeks old (pre- and post-HFD), an ITT post-HFD was performed at 20 weeks old, and resting blood glucose was taken at 24 weeks old.

Metabolic phenotyping: procedures

Insulin tolerance test. Each mouse underwent 1 week of habituation to daily handling and mock i.p. administration to minimize the stress induced by handling. Cages were changed the evening before the ITT to provide consistently clean cages and minimize leftover food spilling into the bedding. ITTs were performed in ad libitum-fed mice 2 h into the light cycle and food was withdrawn from the cage at the beginning of each test. Following determination of body weights and basal blood glucose concentrations, mice received an i.p. injection of 0.75 U kg^{-1} body weight of human insulin (Insuman Rapid, Sanofi Aventis) dissolved in room temperature 0.9% saline (Berlin Chemie). Blood glucose concentrations were measured from venous tail blood at baseline, 15, 30 and 60 min after injection using an automatic glucose monitor (Contour Ascensia, Bayer HealthCare).

Body composition analysis. Body composition analysis was performed using micro-computed tomography (micro-CT)-based imaging of mice under isoflurane anaesthesia. Data acquisition was performed in an IVIS Spectrum CT-scanner (Caliper LifeScience) using the IVIS LivingImage Software v.4.3.1. Quantification of fat and lean mass was performed with a modification of the Vinci software package v.4.61.038. Lean and fat mass were normalized to 100% before statistical analysis.

ELISA. Circulating leptin, CCK and PYY levels were measured in ad libitum-fed dams 5 h into the light phase. Circulating insulin levels were measured in overnight-fasted mice. For refeeding experiments,

circulating leptin, CCK and PYY levels were measured in 12 weeks old overnight-fasted female mice. To perform experiments in HFD$_{lard}$ non-naive mice, mice have received small pieces of HFD$_{lard}$ pellets at least three times before experiments. Blood was collected by decapitation 10 min after HFD feeding. The blood was then centrifuged for 10 min at 10,000g, and the serum fraction was collected and snap frozen in liquid nitrogen. Insulin ELISA (Crystal Chem, 90080), leptin ELISA (Crystal Chem, 90030), PYY ELISA (Crystal Chem, 81501) and CCK ELISA (RayBiotech, EIA-CCK) were performed according to the manufacturer's protocol.

HOMA-IR calculation. HOMA-IR was calculated as insulin (µIU ml^{-1}) multiplied per glucose (mmol l^{-1}) divided by 22.5.

Metabolic phenotyping cages. Measure of indirect calorimetry (EE and respiratory exchange ratio), locomotion and food intake were performed using the PhenoMaster System (TSE Systems). Mice were moved into training cages 3 days before data acquisition for acclimatation. Mice were maintained at 22 °C in sealed cages with ad libitum access to food and water. After 1 day in the PhenoMaster System to further acclimate, data acquisition was performed for 2 consecutive days starting 2 h into the light cycle on mice fed their respective diet (pre-HFD$_{lard}$). Following the 2 days of pre-HFD$_{lard}$ at 3 h into light cycle, mice were switched onto HFD$_{lard}$ and recordings continued uninterrupted (post-HFD$_{lard}$). All parameters were measured continuously and simultaneously. Data regarding EE were corrected for lean mass.

Milk collection

At 12 days after giving birth, lactating mothers were injected with 2IU oxytocin (Merck, O4375), anaesthetized under isoflurane (2–3%), and maintained at 37.0 ± 0.5 °C by a thermostatically controlled water heating system. Then, 5 min later the nipples were manually massaged to promote milk ejection, which was collected manually using a pipette. The milk was immediately snap frozen in liquid nitrogen for storage at −80 °C until analysis. Dams were killed after milk collection and tissue collected from offspring.

Amniotic fluid collection

Timed-pregnant dams carrying E15.5 fetuses fed NCD or BFD as described above were anaesthetized using 2% isoflurane and maintained on 2% isoflurane during the procedure. The abdominal skin was sterilized with Octenisept (Schülke) and an abdominal incision was made. The uterine horns were gently placed outside the abdominal cavity, sectioned and placed in phosphate-buffered saline (PBS) solution. Individual amniotic sacs were exposed and placed in a dry, sterile Petri dish. The amniotic membrane was carefully opened, allowing amniotic fluid to leak into the Petri dish, which was collected using a filtered micropipette and snap frozen in liquid nitrogen for storage at −80 °C until analysis. Following amniotic fluid collection, fetal and placental weight were recorded. Dams were killed after amniotic fluid collection and tissue collected from offspring.

Maternal behaviour

Maternal behaviour was assessed at P5. Dams were transported in their home cage to the test room 1 h before the experiment for acclimatization and remained in their home cage throughout the behavioural test. Trials were conducted between 4–7 h into the light phase. A camera (C920s HD Pro Webcam camera, Logitech) was mounted to capture a top-down view and connected to a laptop for recording. Each dam completed six trials, alternating between male and female pups (three males and three females). For each trial, one pup along with a small amount of bedding was placed on a heating pad. Once the dam returned to the nest, the pup was placed at the diagonally furthest point from the nest. Each trial lasted a maximum of 2 min. Analysis was conducted by measuring the time (in sec) required to retrieve the pup to the nest.

Gene expression analysis

Gene expression analysis. Samples were collected and snap frozen in liquid nitrogen. messenger RNA was extracted from the tissue using the mirVana miRNA Isolation kit (Ambion) and cDNA was produced by reverse transcription (High-capacity cDNA Reverse Transcription kit, Applied Biosciences). qPCR was performed using TaqMan Universal PCR Master Mix (Thermo Fisher) with Taqman probes (Thermo Fisher) listed below on a QuantStudio 7 Flex Real-Time PCR System (Applied Biosystems). *Gapdh* (Mm99999915_g1) was used as a housekeeping gene unless otherwise stated and data were analysed using the ΔCt method.

Dam hypothalamus. At weaning of the pups (P21) ad libitum-fed dams were killed by decapitation. Taqman probes used: *Agrp* (Mm00475829_g1), *Npy* (Mm00445771_m1), *Pomc* (Mm00435874_m1), *Cartpt* (Mm04210469_m1), *Sst* (Mm00436671_m1), *Hcrt* (Mm01964030_s1), *Crh* (Mm01293920_s1), *Trh* (Mm01182425_g1), *Prl* (Mm00599949_m1), *Oxt* (Mm01329577_g1) and *Gal* (Mm00439056_m1).

iBAT. Adult females' offspring ad libitum-fed were killed by decapitation after 1 week of HFD$_{lard}$ feeding. Taqman probes used were *Ucp1* (Mm01244861_m1), *Adrb3* (Mm00442669_m1), *Cidea* (Mm00432554_m1), *Pparg* (Mm01184322_m1) and *Ppargc1* (Mm01208835_m1).

Tongue. Adult offspring were killed by decapitation. Taqman probes used were *Cd36* (Mm00432403_m1), *Ffar4* (Mm00725193_m1) and *Plcb2* (Mm01338057_m1).

Gene expression analysis following neonatal optogenetic stimulation. Cre-negative and OMP-Cre-positive offspring heterozygous for ReaChR were light-stimulated or mock-stimulated once at P3 and returned to their home cage with their mother for 1 h until killing by decapitation. Taqman probes used were *Egr1* (Mm00656724_m1), *Sema7a* (Mm00441361_m1), *Pcdh10* (Mm00477987_s1), *Cnga4* (Mm01278645_m1), *Neurog1* (Mm00440466_s1), *Adcy3* (Mm00460371_m1) and *Omp* (Mm00448081_s1). *Omp* was used as a housekeeping gene.

HFD odour-induced hepatic p-mTOR

Olfactory exposure in freely behaving mice. Mice were split into cages containing two mice each 1 week before the experiment. A closed perforated metal tea ball was placed into their cages 3 days before to reduce the impact of a novel object during the experiment. Mice were acclimated to the experimental rooms and daily handling to minimize the effects of the odours related to the experimental room and the experimenter. After the acclimatization period, mice were fasted overnight and 2 h into the light cycle exposed to an empty tea ball (control, no odour) or to three pellets of HFD$_{lard}$ in a tea ball that allowed mice to smell HFD$_{lard}$ odours without physical access to the diet. Then, 30 min later, the mice were decapitated and the liver was quickly dissected and snap frozen in liquid nitrogen.

Protein isolation and western blotting. Approximately 50 mg liver tissue was transferred to a 2-ml tube containing 1 ml lysis buffer (containing Tris-HCl 25 mM, NaCl 25 mM, NP-40 1%, EDTA 1 mM, pH 7.4) with freshly added Halt Protease and Phosphatase Inhibitor Single-Use Cocktail (Thermo Fisher Scientific) and about 20 ZiO$_2$ beads (VWR, CAS 432-0356). Samples were shaken for 2 min or until the tissue was fully digested. Samples were then centrifuged for 20 min at 15,000*g* and supernatant taken for protein quantification using Pierce BCA assay (Thermo Fisher Scientific). The protein samples were diluted to 2 mg ml^{-1} and mixed 1:4 with Laemmli sample buffer containing 10% β-mercaptoethanol.

Protein samples were run on a precast gel from Bio-Rad (4–15%) with 26 wells. Gels were run with a constant current of 130 V for 80 min. Transfer of gels to PVDF membranes was performed using Trans-Blot Turbo System (Bio-Rad) at 2.5 A and 25 V for 13 min. Gels were run in running buffer containing 25 mM Tris-HCl, 190 mM glycine and 0.1% SDS. Blots were blocked in 5% Western Blocking Solution (Roche, 11829200) in TBS-T (20 mM Tris, 150 mM NaCl, 0.1% Tween-20, pH 7.4) for 1 h at room temperature. Blots were incubated in the same solution containing anti-phospho mTOR (S2448) (Cell Signalling, 2971S) overnight at 4 °C. The next morning, the membrane was washed 3 × 5 min in TBS-T and the secondary HRP-conjugated anti-rabbit IgG (Invitrogen, 31466) was incubated at 1:1,000 for 60 min. Proteins were imaged using the Fusion Solo Vilber Lourmat system. Afterwards, blots were stripped in stripping buffer (10% SDS, 0.5 M Tris, 3.5% β-mercaptoethanol, pH 6.8) for 30 min at 56 °C and membranes were washed with TBS-T for 3 × 10 min and re-blocked. Incubation with anti-mTOR (Cell Signalling, 2972S) and HRP-conjugated anti-rabbit IgG (Invitrogen, 31466) was repeated as before. Band density was measured with ImageJ (National Institutes of Health). Data are presented as p-mTOR/mTOR and normalized to the average ratio of the non-food-odour-exposed animals.

iBAT temperature

iBAT temperature upon food odour exposure. At 8 weeks old, an implantable electronic transponder with thermal couple (IPTT-300, Bio Medic Data Systems) was placed between the scapulae through a small incision under anaesthesia (2% isoflurane). The incision was allowed to heal for 1 week during which the animals were acclimated to handling and having temperature measurements taken with a wireless reader (DAS-8007C, Bio Medic Data Systems). The animals remained group housed. An empty tea ball was placed in the cages 3 days before the experimental day to eliminate effects of a novel object in the cage. On the day of experimentation, food was removed 2 h before the dark cycle. Baseline temperature measurements were taken every 20 min starting at the beginning of the dark cycle. Three readings for each mouse were averaged for the baseline value. A tea ball containing three pellets of HFD$_{lard}$ was then placed into the cage 1 h into dark cycle and temperature readings were taken 20 min later. All readings were recorded using DASHost 8000 software (Bio Medic Data Systems).

Longitudinal measurements of iBAT temperature. The 6–9-week-old mice were acclimatized to handling and thermal imaging procedure for approximately 2–3 weeks before experiments. Mice were carefully imaged using a thermal camera (FLIR E6, Teledyne FLIR LLC) by placing the camera at approximately 10 cm from the interscapular region. Temperature readings were taken weekly with an initial baseline measurement (pre-HFD; 9–12 weeks old), followed 1 week later by a diet change to HFD$_{lard}$ (1 h measurement) and 4-week follow-up measurements. Thermal images were analysed manually using thermal imaging software (FLIR Thermal Studio v.1.9.23.0).

Neonatal non-invasive optogenetic stimulation

OMP-Cre or M71-IRES-Cre were crossed to R26-LSL-ReaChR-mCitrine to allow for the expression of the optogenetic channelrhodopsin in all OSNs or only in OSNs expressing M71, respectively. The breeding strategy was similar to the one described above except that all dams were fed NCD. To optogenetically stimulate developing OSNs, a fibre optic cable (200 µm diameter, 0.48 NA, Doric Lenses) was held directly above but not in contact with the snout of the pup to deliver light at 625 nm (LEDFLS_625_625LED Fibre Light source, Doric Lenses). The stimulation paradigm was rectangular pulses of 100 ms ON/100 ms OFF for 3 s, 12 s OFF, repeated 12 times at 250 mA. This protocol has been previously demonstrated to replicate activity-dependent wiring of olfactory circuits and the glomerular map[52]. OMP^{ReaChR} mice and their Cre-negative control littermates were stimulated once at P3 for gene expression analysis. M71^{ReaChR} and their Cre-negative control littermates were stimulated daily from P1 to P7. To minimize the stress induced by the manipulation, the experimenter's gloves were rubbed with the bedding of the home cage to carry home cage and maternal

odorants, and neonatal optogenetic stimulation was performed on a warm heating pad.

Neonatal non-invasive optogenetic stimulation coupled with calorie ingestion

The same paradigm as described above for neonatal non-invasive optogenetic stimulation was followed, with the modification that the pups were fed an Ensure liquid diet (Abbott, 640587) during stimulation. The Ensure diet was freshly prepared each day and warmed to 37 °C before being offered to the pups. 100 µl of Ensure was placed on a heating pad and pups were gently placed and kept close to it during light stimulation. All pups consumed Ensure during the experiments.

Neonatal optogenetic activation induced pS6 activation

Mice were optogenetically stimulated following the same paradigm described above. Mice were stimulated at P5 and then returned to the cage with the dam. At 1 h later, P5 pups were killed by decapitation. Heads, were quickly rinsed with 0.1 M PBS, followed by fixation in 4% PFA for 24 h. Then, they were transferred into 20% sucrose in PBS for 48 h, followed by being embedded in tissue freezing medium (14020108926, Leica Biosystems). After being frozen they were cut at 30 µm on a cryostat (Leica). For the immunostaining, slides were blocked with 5% donkey serum (diluted in 0.3% Triton and 1× PBS) for 1 h at room temperature, and then incubated with the primary antibody anti-GFP (1:500 dilution, ab13970, Abcam) and anti-pS6 (Ser244, Ser247) (1:1,000 dilution, 44-923G, Thermo Fisher Scientific), followed by incubation in the secondary antibody anti-rabbit IgG (1:500 dilution, A11012, Thermo Fisher Scientific). Tissue was coverslipped with Vectashield mounting solution with DAPI (Biozol VEC-H-1200, Vector Laboratories). Images were acquired using a confocal microscope Leica STELLARIS (Leica Microsystems) with a ×40 objective.

Behavioural tests

Diet preference tests. *Adult C57BL/6NCrl cohorts.* The 7-week-old C57BL/6NCrl mice were single housed for 1 week and acclimated to two food hoppers (TSE Systems) for 4 days. Following the acclimation period, baseline food intake was measured for 3 days. The baseline food intake depicted in the figure represents the average daily food intake during these 3 days. The following day, mice were switched on HFD$_{lard}$ versus BFD or NCD versus BFD shortly before the onset of the dark cycle. Food intake was monitored for 5 days. For representation, baseline NCD intake is plotted as the average of the 3 days of NCD measurements.

NCD$_{dev}$ and BFD$_{dev}$ cohorts. At 8 weeks old, mice were single housed for 1 week and acclimated to two food hoppers allowing manual weighing of food intake. Following the acclimation period, on day 1, the diets in the food hoppers were changed to one food hopper containing HFD$_{lard}$ and the other containing CD, novel for both groups. For three consecutive days, food intake was recorded once per day after the onset of the light cycle and converted to calories of diet consumed. Data were calculated as percentage of calories consumed from HFD$_{lard}$ over the control diet.

Longitudinal food intake measurements. At 7 weeks old, mice were single housed for 1 week to acclimate to the food hopper and water bottle of the PhenoMaster System (TSE Systems). Mice had ad libitum access to food and water at all times. At 8 weeks old, mice were switched to HFD$_{lard}$ and food intake was measured until 20 weeks of age. Food intake was measured daily for the first 2 weeks on HFD and biweekly from week 2–10 on HFD.

Latency to eat. At 6 weeks old, the latency to eat was measured in overnight-fasted mice to determine relative attraction or aversion to AFD. Approximately 3 h into the light cycle, mice were placed individually into a clean cage and allowed to acclimate for 2 min. A single pellet of either NCD or AFD was then placed into the cage and the time it took for the mouse to approach and take the first bite of the pellet was measured. Mice were exposed to NCD or AFD in two consecutive weeks. The latency to eat AFD was normalized to the latency to eat NCD.

Odour investigation test. Approximately 3 h into the light cycle, ad libitum-fed mice were placed into a clean cage with a closed lid and allowed to acclimate for 2 min. Cotton swabs were dipped in solutions containing either vehicle (10% dimethylsulfoxide (DMSO) in water) or progressively increasing concentrations of acetophenone. The cotton swab was inserted through the hole for the water bottle spout to not open the cage between trials. The time spent sniffing each concentration, defined as head tilted up towards the cotton swab performing active sniffing motions, was measured over 2 min. The relative ratio of time spent sniffing each concentration of acetophenone normalized to time spent sniffing the vehicle was quantified for each group.

Habituation-dishabituation test. Approximately 3 h into the light cycle, ad libitum-fed adult female mice were moved into the experimental room and individually placed into a clean cage with a closed lid and allowed to acclimate for approximately 15 min. Mice were exposed to a sequential presentation of different odours presented in a perforated metal tea ball: empty tea ball (control), NCD, 1% AFD, 0.25% AFD and HFD$_{lard}$. Each odour is presented in three consecutive trials for a period of 2 min, with a 15–20-s intertrial time. The time spent sniffing each odour was defined as the head pointed up and active nose/whisker movement. Quantification was based on video analysis taken from the side view.

Stereotaxic surgery

Dopamine and calcium fibre photometry. All surgeries were performed in 8 weeks old mice. Mice were anaesthetized using 2% isoflurane and placed in a stereotaxic apparatus (Kopf Instruments). Before exposing the skull, the skin was sterilized with Octenisept (Schülke) and Anesderm (Pierre Fabre) was applied to the incision site. A small hole was drilled above target sites for viral delivery and fibre implantation. A 0.5-µl Neuros Hamilton Syringe (Hamilton 65450-03) was used to inject the virus at a rate of 100 nl min^{-1} and left in place for 5 min before being slowly withdrawn.

For photometry recordings, AAV9.Syn.Flex.GCaMP6s.WPRE.SV40 (400 nl, a gift from D. Kim & GENIE Project, Addgene viral prep #100845-AAV9) or AAV5-CAG-dLight1.1 (400 nl, a gift from L. Tian, Addgene viral prep #111067-AAV5) viruses were injected in the ARH and LAcbSh, respectively, using the following coordinates relative to bregma (in mm): ARH: −1.45 AP, 0.25 ML, −5.75 and −5.85 DV; LAcbSh: 1.0 AP, 1.75 ML, −4.6 and −4.7 DV. After virus delivery, an optical fibre (400 µm diameter, 0.48 NA, Doric Lenses) was implanted directly above the site of injection and secured using dental acrylic (Super-Bond C&B, Sun Medical). For postoperative care, mice were administered buprenorphine (0.1 mg kg^{-1}, i.p.) and meloxicam (5 mg kg^{-1}, subcutaneously) and received tramadol in the drinking water (1 mg ml^{-1}) for 2 days before and 3 days after surgery.

M71$^{ReaChR}_{adult}$ optogenetic stimulation. The 12-week-old M71-IRES-Cre:R26-LSL-ReaChR-mCitrine mice were anaesthetized, placed in the stereotaxic apparatus and subsequently implanted with an optical fibre (200 µm diameter, 0.48 NA, Doric Lenses) targeting the right M71 glomeruli in the olfactory bulb, using the following coordinates relative to bregma (in mm): 4.1 AP, 0.25 ML and 1.0 DV.

Dual-colour fibre photometry

Data collection. Data were acquired using a RZ5P lock-digital processor controlled by Synapse software (Tucker-Davis Technologies) as described previously[84].

Recording: dopamine sensor. Fibre photometry recording started 5 weeks after surgery to allow for mice recovery and optimal viral expression. Here, 2 weeks after surgery, mice were acclimated to the patch cord in the relevant behavioural setup for about 15 min each day. Mice were fasted overnight once during the fourth week post-surgery to reduce the future effects of first-time fasting. During the fifth week post-surgery, mice were fasted overnight and placed into a small experimental box 2–4 h into the light cycle. The experimental box (interior dimensions, 11.5 × 14 ×12 cm) is made in transparent plexiglass (wall thickness: 0.9 cm) with a circular cutout in the top corner (2 cm diameter) and a sliding lid containing a small hole to allow for the fibre optic cable to pass through. The experimental box was placed in a much larger arena with opaque black walls to block any view of the experimenter outside. A tube ran from outside the larger arena and through the circular cutout of the smaller box to allow for pellets to be delivered without interference from the experimenter. Food pellets were approximately ~20 mg each. After 10 min of acclimation, small pellets of BFD were provided to the mice at random intervals between 1 and 3 min to prevent anticipatory responses. An additional pellet was not given if the mouse had not eaten an already present pellet or if the mouse sat just below the delivery tube. In total, five pellets were delivered, as further pellets showed diminished responses during testing. Mice with no dopaminergic responses to refeeding on BFD were excluded from future experiments and analysis. This paradigm was repeated with 1 week in between for NCD and HFD$_{lard}$. Mice were provided with a small pellet of HFD$_{lard}$ a few days before the trial to eliminate artifacts related to the novelty-induced neophobia.

Recording: calcium recording of AgRP neurons. Fibre photometry recording started 4 weeks after surgery to allow for mouse recovery and optimal viral expression. Mice were kept on their respective diet (pre-HFD$_{lard}$) until 15 weeks of age and then both groups were switched to HFD$_{lard}$ (post-HFD$_{lard}$). Starting 2 weeks after surgery, mice were acclimated to the patch cord in the relevant behavioural setup for about 20 min each day. At 3–4 weeks post-surgery, mice were placed into a clean cage without bedding and allowed to acclimate for 10 min. Mice were then injected i.p. with ghrelin (50 μg; Tocris 1465) diluted in 0.9% saline and the signal was recorded for 5 min. Mice with no changes in 465 nm fluorescence signal in response to ghrelin were excluded from future studies.

AgRP neuronal response to diets. At 5 weeks post-surgery, mice were then fasted overnight and placed in the photometry recording setup at 2–4 h into the light cycle. Following a 10 min baseline recording, a pellet of either NCD or HFD$_{lard}$ was placed into the cage and signal was recorded for 5 min. At 7 weeks post-surgery (at 15 weeks old), mice were switched to HFD$_{lard}$ in their home cage (post-HFD$_{lard}$). At 3 weeks post-HFD$_{lard}$, mice were fasted and recordings were repeated with NCD exposure. 1 week later, overnight fasting was repeated and recording was performed during HFD$_{lard}$ exposure.

AgRP neuronal response to hormones. AgRP neuronal fibre photometry recordings started 4 weeks post-surgery (after 1 week of acclimatation to the cable and behavioural setup). For all recording of AgRP activity dynamics in response to hormones mice were tested every week following the same experimental design: mice were placed in the behavioural setup and allowed to acclimate for 10 min before i.p. injection of a hormone and the signal was recorded for 20 min. At 12 weeks (4 weeks post-surgery), mice were injected i.p. with ghrelin (2 mg kg^{-1} BW; Tocris 1465). At 13 weeks, mice were fasted overnight, placed in the recording setup and injected i.p. with PYY (0.1 mg kg^{-1} BW; R&D Systems). After the recording session, animals were returned to their home cages and given ad libitum access to food. At 14 and 15 weeks, mice were fasted overnight and tested as described above for serotonin hydrochloride (2 mg kg^{-1} BW; Sigma-Aldrich) and glucagon

(2 mg kg^{-1} BW; Bachem) respectively. All hormones were diluted in 0.9% saline and injected with a volume of 10 μl g^{-1} BW.

Viral expression and fibre placements. Virus expression and fibre placement were verified as described previously[85].

Fibre photometry data analysis
All fibre photometry data analyses were performed using a custom MATLAB script. In the event of technical issues encountered on a recording day, such as malfunctions with the photometry rig during the recording session, the animal was excluded from this experimental time point.

dLight analysis. The initial 10 s of recording (laser power-up) was discarded and the data were downsampled at 50 Hz. To correct for artifactual signal fluctuations, the 405 nm Ca^{2+}-independent isosbestic reference was aligned to the 465 nm signal using least-squares linear fit and then used as a baseline to compute the ΔF/F = (465 nm – scaled 405 nm)/(scaled 405 nm). The peri-event trace was extracted using a window spanning −30 s to +60 s around the moment of approach to the pellet manually identified from video recordings. Each trial was then z-scored using the −30 s to −20 s window as baseline to calculate the mean and s.d. All trials of a single animal and single diet were averaged, and the mean (z-scored) trace between 0 s to +5 s and +5 s to +10 s were taken to compare groups using unpaired t-test.

AgRP photometry analysis
The initial 10 s of recording was discarded and the data were smoothed using a 1-s moving-average window before being downsampled at 50 Hz. Peri-event traces were extracted from a window spanning −60 s to +180 s around the food pellet introduction or −120 s to +180 s around ghrelin injection. To avoid spurious influences of the stimulus administration, the baseline was defined as the window from −60 s to −20 s for food pellets and from −120 s to −60 s for CCK injection. For analysis of AgRP neuronal responses to ghrelin, PYY, 5-HT and glucagon, a similar approach was used with a smoothed using a 3-s moving-average window and downsampled at 50 Hz. Data were extracted from a window of −300 s to +1,200 s around the moment of injection. Baseline was defined from the window of −300 s to −60 s. The 465 nm signal was then z-scored, using this baseline to calculate the mean and s.d. Each trial was then z-scored using this baseline to calculate the mean and s.d. The mean (z-scored) trace between +15 s and +180 s was computed for each animal and then used to compare groups via unpaired t-tests.

M71 photostimulation-generated odour preference
The experiment followed the protocol for M72 photostimulation-generated odour preference described by Vetere et al.[86], with minor modifications.

Odorant preparation. An M71-activating odorant (acetophenone; A10701, Sigma-Aldrich) or a non-M71-activating odorant (isoamyl acetate; 101231, Merck) were diluted in mineral oil (330779, Sigma-Aldrich) achieving a 40% concentration. The mixtures were stored in light-protected vials. To use the odorants, 50 μl of an odorant was pipetted onto filter paper on an inverted Petri dish (60 × 15 mm) and covered with cage bedding.

M71-glomerulus photostimulation protocol. The delivery of light pulses (625 nm, 85 mA, 4 Hz, 100 ms ON, 150 ms OFF) was designed to approximately resemble mice's average natural duration of a sniff (100 ms) and breathing frequency (3–5 Hz)[87–92].

Behavioural paradigm. All mice were naive to HFD$_{lard}$, sucrose, acetophenone and isoamyl acetate before the experiment. The behavioural paradigm consisted of three phases: pre-exposure (day 1), optogenetic

conditioning (day 2) and odour preference test (day 3). The experiment took place in a custom-designed preference test chamber made of white Plexiglas (15 × 40 × 25 cm) divided into two identical compartments by removable walls. On the first day, mice were plugged to the patch cord and underwent a 25-min pre-exposure to the test chamber, with each chamber compartment containing a non-scented Petri dish filled with bedding material. Mice did not receive any photostimulation during this first day. Then, mice were fasted overnight (16 h). On the second day, mice were exposed to a 25-min conditioning period. After the removable walls of the Plexiglas chamber were taken out, fasted mice were plugged to the patch cord and exposed to a non-scented Petri dish located in the centre of the chamber. The bedding in this Petri dish contained small pieces of HFD_{lard} coated with 40% sucrose, which had been prepared the previous day. All mice engaged with the food pellets and ingested them. Simultaneously, mice received M71 photostimulation constantly during the 25 min of the conditioning, as described above. On the third day, the removable walls were re-inserted, and a Petri dish scented with either acetophenone or isoamyl acetate was placed into one of the chamber compartments, the location of which was randomly assigned. Mice were allowed to freely explore both compartments for 10 min without receiving any photostimulation. Mouse behaviour was continuously monitored with an overhead camera. These results reflect the whole 10-min observation period. Odour preference during the test day was calculated using the following formula: percentage of time spent in the acetophenone compartment − percentage of time spent in the isoamyl acetate compartment. After the experiments, mice were deeply anaesthetized with ketamine/xylazine and perfused transcardially with 0.1 M PBS followed by 4% PFA (pH 7.4) for future processing to verify fibre placements.

Histology
Tissue processing. For fibre photometry experiments, mice were deeply anaesthetized with ketamine/xylazine and transcardially perfused with 4% PFA in 0.1 M PBS, pH 7.4. Tissues were post-fixed overnight in the same PFA solution. Brain tissues from photometry experiments were cryoprotected in 20% sucrose in PBS and cut at 30 μm on a cryostat (Leica). Tissue was coverslipped with Vectashield mounting solution with DAPI (Biozol VEC-H-1200). Sections were imaged using only the endogenous fluorescence of GCaMP6s or dLight1.1. White adipose and liver tissues were post-fixed for 24 h, dehydrated in 30% sucrose and embedded in paraffin before cutting at 5 μm on a vibratome and directly mounted. Tissue was stained with hematoxylin (GHS132, Sigma-Aldrich) and eosin (HT110232, Sigma-Aldrich) after deparaffinization.

Microscopy. All tissue was imaged on a Zeiss Imager M2 microscope and AxioVision v.4.2 software (Carl Zeiss) at ×20 magnification.

Quantification. Adipocyte size was quantified using ImageJ software for a minimum of 500 adipocytes per mouse from five randomly selected areas.

Ribosome immunoprecipitations (ps6-ribotrap)
Tissue preparation and ribosome immunoprecipitation. Phosphorylated ribosome pulldown for the identification of olfactory receptor activation was adapted from previous protocols[31]. Experiments were performed on males C57Bl6/NCrl from 8–12 weeks old of age. Following 1 h of odour exposure, the olfactory epithelium was dissected on ice in buffer containing 1×HBSS (Gibco, with Ca^{2+} and Mg^{2+}), 2.5 mM HEPES (pH 7.4), 35 mM glucose, 100 μg ml⁻¹ cycloheximide, 5 mM sodium fluoride, 1 mM sodium orthovanadate, 1 mM sodium pyrophosphate and 1 mM β-glycerophosphate. Four epithelia were pooled and processed as described previously[85].

RNA sequencing. Due to the low amount of input material, RNA-seq libraries were prepared using the Ovation RNASeq System V2 and

Illumina Nextera XT protocol, as previously described[93], and sequenced on an Illumina HiSeq 4000 (2 × 75 bp). We applied the community-curated nfcore rnaseq analysis pipeline v.1.446. The gene-level quantification was carried out using Salmon v.0.14.147 using the reference genome GRCm38. To normalize the immuno-pulldown for each sample to its background, we divided the Salmon gene count per sample using the formula countpulldowncountinput. The differential gene expression analysis based on the normalized counts was carried out using the DESeq2 v.1.26. R package[94]. Gene Ontology term analysis was carried out using the clusterProfiler v.3.14.3 R package[95]. Olfactory receptors with a $P_{adj} < 0.001$ compared with no odour samples were defined as significantly activated, as defined by Jiang et al.[31].

Two-phase metabolite extraction of polar and lipophilic metabolites (dams milk, blood and food pellets)
For the extraction of total lipids, 50 μl milk/plasma were collected in 2-ml round bottom Eppendorf tubes. For the extraction of the snap frozen material, the milk/plasma samples were allowed to thaw on ice. Lipids were then extracted by adding 1 ml pre-cooled (−20 °C) extraction buffer containing internal standard as described previously[96].

LC–HRMS-based analysis of dams milk and blood lipids. The dried lipid extracts were resuspended in 200 μl UPLC-grade acetonitrile:isopropanol (70:30 (v:v)) before analysing them on a UPLC connected to a Tribrid Orbitrap HRMS as described previously[96].

The obtained Thermo .raw files were converted to .mzXML files using MSConvert from ProteoWizard software package (http://proteowizard.sourceforge.net)[97].

Data pre-processing for untargeted lipidomics analysis. Data pre-processing was performed with MZmine v.2.340 (http://mzmine.github.io/)[98]. Converted mzXML files were imported and extracted ione chromatograms were generated using the ADAP algorithm and peak picking was performed using the local minimum search algorithm. Isotopes were grouped and only peaks with at least one isotope were kept for further processing. Detailed parameters can be found in Supplementary Table 5. Finally, aligned peak lists were exported to CSV files for statistical analysis. Tables were corrected for solvent peaks by a blank subtraction. Features were removed when average peak area of samples was less than 2× average peak area of blanks.

Data evaluation. For data evaluation, CSV files were imported in Perseus (http://www.biochem.mpg.de/5111810/perseus)[99]. Data were further filtered for features that had a coverage of at least 70% valid data in at least one group. Filtered data were log_2 transformed and missing values were imputed from normal distribution using the default settings.

LC–MS analysis of lipid extracts from food pellets
Lipidomics of food pellets was performed using a Thermo Vanquish Flex with a quaternary pump (Thermo Fisher Scientific) coupled to a TimTOF Pro2 mass spectrometer equipped with a heated ESI source (VIP-HESI) (Bruker Daltonics). Dried lipid samples were resuspended in 500 μl of acetronitril:isopropanol (70:30 (v:v)). The resuspended samples were cleared by a 5 min centrifugation at 16,000g and the 200 μl of the supernatants were transferred to 2-ml glass vials with 300 μl glass inserts (Chromatography Zubehör Trott). Then, 1 μl was injected in the UHPLC system and separated as described above. Compounds were detected in the mass spectrometer using data-dependent parallel accumulation serial fragmentation (DDA-PASEF) acquisition mode. All analysis were run in positive ionization mode using SA capillary voltage set to 4,500 V with an end plate offset of 500 V. Nebulizer pressure was set to 2 bar, dry gas was running with 8 l min⁻¹ and a temperature of 230 °C. Sheet gas was running with 4 l min⁻¹ and a temperature of 400 °C. For MS2 experiments masses were isolated with a width of 2 mD and fragmentation was induced with a collision energy of 30 eV.

LC–HRMS-based analysis of polar and semi-polar compounds
The stored (−80 °C) polar and semi-polar extracts were resuspended in 100 µl of a UPLC-grade water: methanol (50:50 (v:v)). From each analytical sample a volume of 20 µl was taken and pooled together. These pools were used as instrumental and sample stability quality controls (QCs), which are run after every tenth analytical sample in the sample sequence or after each replicate group. All samples and pools were placed in an Vanquish flex UHPLC (Thermo Fisher Scientific), which was connected to a TimsTOF Pro 2 HRMS, (Bruker Daltonics). Of each sample 1 µl was injected onto a 100 × 2.1 mm HSS T3 UPLC column, packed with 1.7-µm particles (Waters). The flow rate of the UHPLC was set to 500 µl min⁻¹ and the buffer system consisted of buffer A (0.1% formic acid in UPLC-grade water) and buffer B (0.1% formic acid in UPLC-grade acetonitrile). The UHPLC gradient was as follows: 0–1 min 100% A (curve = 6), 1–11.5 min 100–0% A (curve = 7), 11.5–12 min 0% A, 12.0–12.1 min 0–100% A, 12.1–15 min 100% A. This leads to a total runtime of 15 min per sample. For better annotation some quality pool sample injections were run at the end of the sequence with a data-dependent parallel accumulation serial fragmentation (DDA-PASEF) acquisition mode with the same stepped mobility ramp to generate a MS2 spectra collection. Source parameters were as follows. Capillary voltage was set to 4,500 V with an end plate off set of 500 V. Nebulizer pressure was set to 2 bar, dry gas was running with 8 l min⁻¹ and a temperature of 230 °C. Sheet gas was running with 4 l min⁻¹ and a temperature of 400 °C. For MS2 experiments masses were isolated with a width of 2 mD and fragmentation was induced with a collision energy of 20 and 50 eV.

Feature extraction and data analysis. All samples were analysed in a randomized run-order after the column was conditioned with several blank and some QC sample injections. Before and after the set of samples pooled QC sample were injected. Lipidomics analysis and untargeted reversed phase analysis of food pellets were both performed with the following criteria: Raw data was further processed with MetaboScape (v.2024b) to generate an untargeted feature table. Detailed processing parameters can be found in Supplementary Table 3. Filtered feature table were normalized to the TIC median and further submitted to MetaboAnalyst (v.6.0). Missing values were replaced by LoDs (one-fifth of the minimum positive value of each variable). Remaining features (lipidomics 4084; untargeted RP 4020) were log-transformed and pareto scaled before further analysis.

Semi-targeted liquid chromatography-high-resolution mass spectrometry-based analysis of amine-containing metabolites
The LC–HRMS analysis of amine-containing compounds was performed using a QE-Plus high-resolution mass spectrometer coupled to a Vanquish UHPLC chromatography system (Thermo Fisher Scientific). Dried sample extracts were resuspended in 150 µl LC–MS-grade water for 10 min at 4 °C in a shaker at 1,500 rpm. After centrifugation, 50 µl of the extracts were mixed with 25 µl 100 mM sodium carbonate (Sigma), followed by the addition of 25 µl 2% (v/v) benzoylchloride (Sigma) in acetonitrile (UPC/MS-grade, Biosove), as reported previously. The derivatized samples were thoroughly mixed and kept at a temperature of 20 °C until LC–MS analysis[96].

The LC–MS data analysis was performed using the open-source software MZmine 2 using MSConvert (2) (v.3.0.22060, Proteowizard). Compounds were annotated with an in-house library with an *m/z* tolerance of <5 ppm.

VOC analysis
Analysis was performed in the laboratories of GC–ToFMS Sensenet (Odournet).

Sample preparation
Diets. Approximately 4 g of diet were introduced into an individual microchamber and heated to 30 °C. A thermodesorption tube (Tenax/

Carbocarph) was inserted in the microchamber to collect a total volume of 1,000 ml of headspace.

Milk and amniotic fluid. A total of 1 µl of milk or amniotic fluid was directly spiked in a desorption tube (Tenax). The milk and amniotic fluid samples used for the analyses consisted of a pool of 4–5 dams.

Analytical methods. Combined thermal-desorption gas chromatography and time-of-flight mass spectrometry TD-GC–ToFMS system was used to generate a full quantitative scan of VOCs from the previously collected samples. Analyses were performed using a thermal desorption unit (Unity, Markes International), a gas chromatographer (7890, Agilent), a time-of-flight mass spectrometer (BenchTOF-dx model, Almsco) and a mid-polar DB-624 column was used for chromatographic separation (60 m, 250 µm, 1.4 µm; Agilent). Desorption tubes were heated to 300 °C with a helium flow rate of 50 ml min l⁻¹ for 10 min (first desorption stage). Desorbed analytes were directed to a hydrophobic general purpose cold trap (10 °C, thermoelectric cooling), filled with Tenax TA and graphitized carbon. After flash-heating of the cold trap to 320 °C during 5 min (second desorption stage), analytes were injected into the chromatographic column for further separation, which took about 53 min. Molecules reaching the ToFMS detector were fragmented by electron impact ionization at 70 eV at a mass range of 28–330 amu. Deuterated toluene-d8 (Sigma-Aldrich) was used as an external standard for quantification. This compound was injected (10 ng) into an independent thermodesorption tube and was analysed by following strictly the same methodology as with the samples. Given the sensitivity of the method, two unused thermodesorption tubes were analysed as blanks, to exclude any potential contamination arising from these materials during the analysis. The deconvolution process for the chemical identification of the VOCs that were present in each analysed sample was carried out with the software TargetView v.3 (ALMSCO International). This algorithm identified the compounds of the chromatogram automatically based on an updated version of the NIST20 library. Chemical identifications were confirmed with at least 80% certainty. Results of each diet/sample were normalized as per cent for representation.

PET imaging
PET imaging was performed using an Inveon preclinical PET/CT system (Siemens) as previously described[100].

Olfactory exposure during PET imaging. Olfactory exposure was performed as described[85].

PET analysis. The kinetic model and statistical analysis was performed as previously described[85,100].

Statistical analysis
Statistical analysis was performed with GraphPad Prism 8 unless otherwise stated. Student's *t*-test, Wilcoxon test, multiple *t*-test, one-way analysis of variance (ANOVA), two-way ANOVA and three-way ANOVA were used when applicable. Data not representing a Gaussian distribution were analysed by nonparametric tests. Statistical data are represented in the figure legends. In brief, datasets comparing experiments in the same animal subjected to two different treatments were analysed for statistical significance using paired two-tailed Student's *t*-test. Datasets with only two independent groups were analysed for statistical significance using unpaired two-tailed Student's *t*-test. Datasets with more than two groups were analysed using a one-way ANOVA followed by a multiple-comparisons test. Datasets influenced by two independent factors were analysed using a two-way repeated-measures ANOVA, followed by Sidak's or Tukey's multiple-comparisons test or a mixed-effects model followed by a Tukey's multiple-comparisons test in cases where data were missing at certain time points. Datasets

subjected to two independent factors were analysed using two-way repeated-measures ANOVA followed by a Sidak's multiple-comparisons test in case of missing values at some time points. Three-way (type III) ANOVAs were performed in R v.4.3.0. For between-subject designs, we used linear models fitted with the stats package and analysed with the car package; for repeated measures, we implemented linear mixed-effect models using the lmerTest package and its built-in ANOVA function. No statistical methods were used to predetermine sample sizes but our sample sizes are similar to those reported in previous publications. Data distribution was assumed to be normal but this was not formally tested. Data collection and analysis were not performed blind to the conditions of the experiments. Alpha was defined as 0.05 and significance was depicted by $*P < 0.05$, $**P < 0.01$ and $***P < 0.001$. Code used for the analyses is available upon request.

Reporting summary

Further information on research design is available in the Nature Portfolio Reporting Summary linked to this article.

Data availability

The RNA-seq data conducted in this study have been deposited in Gene Expression Omnibus under accession code: GSE308362. Source data are provided with this paper.

References

1. Dearden, L. & Ozanne, S. E. Early life origins of metabolic disease: Developmental programming of hypothalamic pathways controlling energy homeostasis. *Front. Neuroendocrinol.* **39**, 3–16 (2015).
2. Chaves, W. F., Pinheiro, I. L., da Silva, J. M., Manhães-de-Castro, R. & da Silva Aragão, R. Repercussions of maternal exposure to high-fat diet on offspring feeding behavior and body composition: a systematic review. *J. Dev. Orig. Health Dis.* **12**, 220–228 (2021).
3. Ribaroff, G. A., Wastnedge, E., Drake, A. J., Sharpe, R. M. & Chambers, T. J. G. Animal models of maternal high fat diet exposure and effects on metabolism in offspring: a meta-regression analysis. *Obes. Rev.* **18**, 673–686 (2017).
4. Tellechea, M. L., Mensegue, M. F. & Pirola, C. J. The association between high fat diet around gestation and metabolic syndrome-related phenotypes in rats: a systematic review and meta-analysis. *Sci. Rep.* **7**, 5086 (2017).
5. Schoonejans, J. M. & Ozanne, S. E. Developmental programming by maternal obesity: Lessons from animal models. *Diabet. Med. J.* **38**, e14694 (2021).
6. Howie, G. J., Sloboda, D. M., Kamal, T. & Vickers, M. H. Maternal nutritional history predicts obesity in adult offspring independent of postnatal diet. *J. Physiol.* **587**, 905–915 (2009).
7. McCurdy, C. E. et al. Maternal high-fat diet triggers lipotoxicity in the fetal livers of nonhuman primates. *J. Clin. Invest.* **119**, 323–335 (2009).
8. Grayson, B. E. et al. Changes in melanocortin expression and inflammatory pathways in fetal offspring of nonhuman primates fed a high-fat diet. *Endocrinology* **151**, 1622–1632 (2010).
9. Buettner, A. A selective and sensitive approach to characterize odour-active and volatile constituents in small-scale human milk samples. *Flavour Fragr. J.* **22**, 465–473 (2007).
10. Sreng, L., Temime-Roussel, B., Wortham, H. & Mourre, C. Chemical identification of 'maternal signature odors' in rat. *Chem. Senses* **42**, 211–222 (2017).
11. Désage, M., Schaal, B., Soubeyrand, J., Orgeur, P. & Brazier, J. L. Gas chromatographic-mass spectrometric method to characterise the transfer of dietary odorous compounds into plasma and milk. *J. Chromatogr. B Biomed. Appl.* **678**, 205–210 (1996).
12. Schaal, B., Marlier, L. & Soussignan, R. Human foetuses learn odours from their pregnant mother's diet. *Chem. Senses* **25**, 729–737 (2000).
13. Spahn, J. M. et al. Influence of maternal diet on flavor transfer to amniotic fluid and breast milk and children's responses: a systematic review. *Am. J. Clin. Nutr.* **109**, 1003S–1026S (2019).
14. Schaal, B., Orgeur, P., Desage, M. & Brazier, J. L. Transfer of the aromas of the pregnant and lactating mothers diet to fetal and neonatal environment in the sheep. *Chem. Senses* **20**, 93–94 (1995).
15. Marlier, L., Schaal, B. & Soussignan, R. Bottle-fed neonates prefer an odor experienced in utero to an odor experienced postnatally in the feeding context. *Dev. Psychobiol.* **33**, 133–145 (1998).
16. Qiu, Q. et al. Acquisition of innate odor preference depends on spontaneous and experiential activities during critical period. *eLife* **10**, e60546 (2021).
17. Inoue, N. et al. The olfactory critical period is determined by activity-dependent Sema7A/PlxnC1 signaling within glomeruli. *eLife* **10**, e65078 (2021).
18. Liu, A., Savya, S. & Urban, N. N. Early odorant exposure increases the number of mitral and tufted cells associated with a single glomerulus. *J. Neurosci.* **36**, 11646–11653 (2016).
19. Todrank, J., Heth, G. & Restrepo, D. Effects of in utero odorant exposure on neuroanatomical development of the olfactory bulb and odour preferences. *Proc. Biol. Sci.* **278**, 1949–1955 (2011).
20. Su, Z., Alhadeff, A. L. & Betley, J. N. Nutritive, post-ingestive signals are the primary regulators of AgRP neuron activity. *Cell Rep.* **21**, 2724–2736 (2017).
21. Burke, L. K. et al. mTORC1 in AGRP neurons integrates exteroceptive and interoceptive food-related cues in the modulation of adaptive energy expenditure in mice. *eLife* **6**, e22848 (2017).
22. Brandt, C. et al. Food perception primes hepatic ER homeostasis via melanocortin-dependent control of mTOR activation. *Cell* **175**, 1321–1335.e20 (2018).
23. Chen, Y., Lin, Y.-C., Kuo, T.-W. & Knight, Z. A. Sensory detection of food rapidly modulates arcuate feeding circuits. *Cell* **160**, 829–841 (2015).
24. Betley, J. N. et al. Neurons for hunger and thirst transmit a negative-valence teaching signal. *Nature* **521**, 180–185 (2015).
25. Mandelblat-Cerf, Y. et al. Arcuate hypothalamic AgRP and putative POMC neurons show opposite changes in spiking across multiple timescales. *eLife* **4**, e07122 (2015).
26. Riera, C. E. et al. The sense of smell impacts metabolic health and obesity. *Cell Metab.* **26**, 198–211 (2017).
27. Beutler, L. R. et al. Dynamics of gut-brain communication underlying hunger. *Neuron* **96**, 461–475.e5 (2017).
28. Kolling, L. J. et al. Modulating the excitability of olfactory output neurons affects whole-body metabolism. *J. Neurosci.* **42**, 5966 (2022).
29. Tsuneki, H. et al. Food odor perception promotes systemic lipid utilization. *Nat. Metab.* **4**, 1514–1531 (2022).
30. Knight, Z. A. et al. Molecular profiling of activated neurons by phosphorylated ribosome capture. *Cell* **151**, 1126–1137 (2012).
31. Jiang, Y. et al. Molecular profiling of activated olfactory neurons identifies odorant receptors for odors in vivo. *Nat. Neurosci.* **18**, 1446–1454 (2015).
32. Vuong, H. E. et al. The maternal microbiome modulates fetal neurodevelopment in mice. *Nature* **586**, 281–286 (2020).
33. Ziętek, M., Celewicz, Z. & Szczuko, M. Short-chain fatty acids, maternal microbiota and metabolism in pregnancy. *Nutrients* **13**, 1244 (2021).
34. Zeng, Q., Dong, S.-Y., Sun, X.-N., Xie, J. & Cui, Y. Percent body fat is a better predictor of cardiovascular risk factors than body mass index. *Braz. J. Med. Biol. Res. Rev. Bras. Pesqui. Medicas E Biol.* **45**, 591–600 (2012).
35. Rubino, F. et al. Definition and diagnostic criteria of clinical obesity. *Lancet Diabetes Endocrinol.* **13**, 221–262 (2025).

36. St-Cyr, S. & McGowan, P. O. Programming of stress-related behavior and epigenetic neural gene regulation in mice offspring through maternal exposure to predator odor. *Front. Behav. Neurosci.* **9**, 145 (2015).

37. St-Cyr, S., Abuaish, S., Welch, K. C. J. & McGowan, P. O. Maternal predator odour exposure programs metabolic responses in adult offspring. *Sci. Rep.* **8**, 8077 (2018).

38. Li, X., Nie, Q., Liu, D. & Xu, Y. Changes in volatile organic compounds and lipid oxidation in traditional Chinese bacon during cold smoking. *Int. J. Food Eng.* **17**, 851–863 (2021).

39. Lippert, R. N. & Brüning, J. C. Maternal metabolic programming of the developing central nervous system: unified pathways to metabolic and psychiatric disorders. *Biol. Psychiatry* **91**, 898–906 (2021).

40. Fernandes, D. J. et al. Exposure to maternal high-fat diet induces extensive changes in the brain of adult offspring. *Transl. Psychiatry* **11**, 149 (2021).

41. Lippert, R. N. et al. Maternal high-fat diet during lactation reprograms the dopaminergic circuitry in mice. *J. Clin. Invest.* **130**, 3761–3776 (2020).

42. Bouret, S. G. Developmental programming of hypothalamic melanocortin circuits. *Exp. Mol. Med.* **54**, 403–413 (2022).

43. Tellez, L. A. et al. Separate circuitries encode the hedonic and nutritional values of sugar. *Nat. Neurosci.* **19**, 465–470 (2016).

44. Joshi, A. et al. Dopamine D1 receptor signalling in the lateral shell of the nucleus accumbens controls dietary fat intake in male rats. *Appetite* **167**, 105597 (2021).

45. Stice, E., Yokum, S., Blum, K. & Bohon, C. Weight gain is associated with reduced striatal response to palatable food. *J. Neurosci. J. Soc. Neurosci.* **30**, 13105–13109 (2010).

46. Patriarchi, T. et al. Ultrafast neuronal imaging of dopamine dynamics with designed genetically encoded sensors. *Science* **360**, eaat4422 (2018).

47. Gouveia, A., Oliveira Beleza, R. & Steculorum, S. M. AgRP neuronal activity across feeding-related behaviours. *Eur. J. Neurosci.* **54**, 7458–7475 (2021).

48. Deem, J. D., Faber, C. L. & Morton, G. J. AgRP neurons: Regulators of feeding, energy expenditure, and behavior. *FEBS J.* **289**, 2362–2381 (2022).

49. Jais, A. & Brüning, J. C. Arcuate nucleus-dependent regulation of metabolism—pathways to obesity and diabetes mellitus. *Endocr. Rev.* **43**, 314–328 (2021).

50. Mazzone, C. M. et al. High-fat food biases hypothalamic and mesolimbic expression of consummatory drives. *Nat. Neurosci.* **23**, 1253–1266 (2020).

51. Beutler, L. R. et al. Obesity causes selective and long-lasting desensitization of AgRP neurons to dietary fat. *eLife* **9**, e55909 (2020).

52. Nakashima, A. et al. Structured spike series specify gene expression patterns for olfactory circuit formation. *Science* **365**, eaaw5030 (2019).

53. Bozza, T., Feinstein, P., Zheng, C. & Mombaerts, P. Odorant receptor expression defines functional units in the mouse olfactory system. *J. Neurosci.* **22**, 3033–3043 (2002).

54. Lin, J. Y., Knutsen, P. M., Muller, A., Kleinfeld, D. & Tsien, R. Y. ReaChR: a red-shifted variant of channelrhodopsin enables deep transcranial optogenetic excitation. *Nat. Neurosci.* **16**, 1499–1508 (2013).

55. Bodden, C., Hannan, A. J. & Reichelt, A. C. Of 'junk food' and 'brain food': how parental diet influences offspring neurobiology and behaviour. *Trends Endocrinol. Metab.* **32**, 566–578 (2021).

56. Rivera, H. M. et al. Maternal high-fat diet and obesity impact palatable food intake and dopamine signaling in nonhuman primate offspring. *Obesity* **23**, 2157–2164 (2015).

57. Adams, W. K. et al. Long-term, calorie-restricted intake of a high-fat diet in rats reduces impulse control and ventral striatal D2 receptor signalling - two markers of addiction vulnerability. *Eur. J. Neurosci.* **42**, 3095–3104 (2015).

58. Tellez, L. A. et al. A gut lipid messenger links excess dietary fat to dopamine deficiency. *Science* **341**, 800–802 (2013).

59. Finistrella, V. et al. Neophobia, sensory experience and child's schemata contribute to food choices. *Eat. Weight Disord. Stud. Anorex. Bulim. Obes.* **29**, 25 (2024).

60. Sutton Hickey, A. K., Becker, J., Karolczak, E. O., Lutas, A. & Krashes, M. J. Dietary fat content and absorption shape standard diet devaluation through hunger circuits. *Mol. Metab.* **89**, 102021 (2024).

61. Deng, J. et al. Deletion of ATF4 in AgRP neurons promotes fat loss mainly via increasing energy expenditure. *Diabetes* **66**, 640–650 (2017).

62. Dodd, G. T. et al. Hypothalamic phosphatase switch coordinates energy expenditure with feeding. *Cell Metab.* **26**, 375–393 (2017).

63. Makimura, H., Mizuno, T. M., Mastaitis, J. W., Agami, R. & Mobbs, C. V. Reducing hypothalamic AGRP by RNA interference increases metabolic rate and decreases body weight without influencing food intake. *BMC Neurosci.* **3**, 18 (2002).

64. Reichenbach, A. et al. Metabolic sensing in AgRP neurons integrates homeostatic state with dopamine signalling in the striatum. *eLife* **11**, e72668 (2022).

65. Tong, Q., Ye, C.-P., Jones, J. E., Elmquist, J. K. & Lowell, B. B. Synaptic release of GABA by AgRP neurons is required for normal regulation of energy balance. *Nat. Neurosci.* **11**, 998–1000 (2008).

66. Joly-Amado, A. et al. Hypothalamic AgRP-neurons control peripheral substrate utilization and nutrient partitioning. *EMBO J.* **31**, 4276–4288 (2012).

67. Wortley, K. E. et al. Agouti-related protein-deficient mice display an age-related lean phenotype. *Cell Metab.* **2**, 421–427 (2005).

68. Han, Y. et al. Deciphering an AgRP-serotoninergic neural circuit in distinct control of energy metabolism from feeding. *Nat. Commun.* **12**, 3525 (2021).

69. Jansen, A. et al. Overweight children overeat after exposure to food cues. *Eat. Behav.* **4**, 197–209 (2003).

70. Robinson, M. J. F. et al. Individual differences in cue-induced motivation and striatal systems in rats susceptible to diet-induced obesity. *Neuropsychopharmacology* **40**, 2113–2123 (2015).

71. Belfort-DeAguiar, R. & Seo, D. Food cues and obesity: overpowering hormones and energy balance regulation. *Curr. Obes. Rep.* **7**, 122–129 (2018).

72. Ferriday, D. & Brunstrom, J. M. 'I just can't help myself': effects of food-cue exposure in overweight and lean individuals. *Int. J. Obes.* **35**, 142–149 (2011).

73. Sun, X. et al. Basolateral amygdala response to food cues in the absence of hunger is associated with weight gain susceptibility. *J. Neurosci.* **35**, 7964–7976 (2015).

74. Berrios, J. et al. Food cue regulation of AGRP hunger neurons guides learning. *Nature* **595**, 695–700 (2021).

75. Garfield, A. S. et al. Dynamic GABAergic afferent modulation of AgRP neurons. *Nat. Neurosci.* **19**, 1628–1635 (2016).

76. Bai, L. et al. Genetic identification of vagal sensory neurons that control feeding. *Cell* **179**, 1129–1143.e23 (2019).

77. Qu, T., Han, W., Niu, J., Tong, J. & de Araujo, I. E. On the roles of the duodenum and the vagus nerve in learned nutrient preferences. *Appetite* **139**, 145–151 (2019).

78. Dearden, L., Bouret, S. G. & Ozanne, S. E. Sex and gender differences in developmental programming of metabolism. *Mol. Metab.* **15**, 8–19 (2018).

79. Stowers, L. & Logan, D. W. Sexual dimorphism in olfactory signaling. *Curr. Opin. Neurobiol.* **20**, 770–775 (2010).

80. Vihani, A. et al. Semiochemical responsive olfactory sensory neurons are sexually dimorphic and plastic. *eLife* **9**, e54501 (2020).

81. Ibarra-Soria, X., Levitin, M. O., Saraiva, L. R. & Logan, D. W. The olfactory transcriptomes of mice. *PLoS Genet.* **10**, e1004593 (2014).

82. Xu, P. S., Lee, D. & Holy, T. E. Experience-dependent plasticity drives individual differences in pheromone-sensing neurons. *Neuron* **91**, 878–892 (2016).

83. Li, J., Ishii, T., Feinstein, P. & Mombaerts, P. Odorant receptor gene choice is reset by nuclear transfer from mouse olfactory sensory neurons. *Nature* **428**, 393–399 (2004).

84. Paß, T. et al. Preserved striatal innervation maintains motor function despite severe loss of nigral dopaminergic neurons. *Brain J. Neurol.* **147**, 3189–3203 (2024).

85. Bulk, J. et al. A food-sensitive olfactory circuit drives anticipatory satiety. *Nat. Metab.* **7**, 1246–1265 (2025).

86. Vetere, G. et al. Memory formation in the absence of experience. *Nat. Neurosci.* **22**, 933–940 (2019).

87. Carey, R. M. & Wachowiak, M. Effect of sniffing on the temporal structure of mitral/tufted cell output from the olfactory bulb. *J. Neurosci.* **31**, 10615 (2011).

88. Doucette, W. et al. Associative cortex features in the first olfactory brain relay station. *Neuron* **69**, 1176–1187 (2011).

89. Rojas-Líbano, D. & Kay, L. M. Interplay between sniffing and odorant sorptive properties in the rat. *J. Neurosci.* **32**, 15577 (2012).

90. Shusterman, R., Smear, M. C., Koulakov, A. A. & Rinberg, D. Precise olfactory responses tile the sniff cycle. *Nat. Neurosci.* **14**, 1039–1044 (2011).

91. Wesson, D. W., Donahou, T. N., Johnson, M. O. & Wachowiak, M. Sniffing behavior of mice during performance in odor-guided tasks. *Chem. Senses* **33**, 581–596 (2008).

92. Kepecs, A., Uchida, N. & Mainen, Z. F. The sniff as a unit of olfactory processing. *Chem. Senses* **31**, 167–179 (2006).

93. Jais, A. et al. PNOC(ARC) neurons promote hyperphagia and obesity upon high-fat-diet feeding. *Neuron* **106**, 1009–1025.e10 (2020).

94. Love, M. I., Huber, W. & Anders, S. Moderated estimation of fold change and dispersion for RNA-seq data with DESeq2. *Genome Biol.* **15**, 550 (2014).

95. Yu, G., Wang, L.-G., Han, Y. & He, Q.-Y. clusterProfiler: an R package for comparing biological themes among gene clusters. *Omics J. Integr. Biol.* **16**, 284–287 (2012).

96. Jiang, S. et al. Inhibition of mammalian mtDNA transcription acts paradoxically to reverse diet-induced hepatosteatosis and obesity. *Nat. Metab.* **6**, 1024–1035 (2024).

97. Chambers, M. C. et al. A cross-platform toolkit for mass spectrometry and proteomics. *Nat. Biotechnol.* **30**, 918–920 (2012).

98. Pluskal, T., Castillo, S., Villar-Briones, A. & Oresic, M. MZmine 2: modular framework for processing, visualizing, and analyzing mass spectrometry-based molecular profile data. *BMC Bioinform.* **11**, 395 (2010).

99. Tyanova, S. et al. The Perseus computational platform for comprehensive analysis of (prote)omics data. *Nat. Methods* **13**, 731–740 (2016).

100. Jais, A. et al. Myeloid-cell-derived VEGF maintains brain glucose uptake and limits cognitive impairment in obesity. *Cell* **165**, 882–895 (2016).

Acknowledgements

Author contributions

Conceptualization: L.C.R., A.G. and S.M.S. Methodology: L.C.R., A.G., A.C., C.G.A., F.D., Y.H., H.B., P.G. and S.M.S. Software: L.R., H.B. and P.K. Validation: L.C.R., A.G. and L.R. and A.L.C. Formal analysis: L.C.R., A.G., L.R., F.D., H.B., P.K., A.L.C., R.D.M.-S., J.N.S., M.E.M. and C.G.A. Investigation: L.C.R., A.G., A.C., C.G.A., F.D., Y.H., R.D.M.-S., J.N.S. and M.E.M. Resources: L.R., H.B. and P.G. Data curation: L.C.R., A.G., J.B., L.R., A.L.C., F.D., R.D.M.-S., J.N.S., M.E.M. and C.G.A. Visualization: L.C.R., A.G., L.R., F.D. and S.M.S. Funding acquisition: S.M.S. Project administration: S.M.S. Supervision: H.B., P.G. and S.M.S. Writing – original draft: A.G. and S.M.S. Writing – review and editing: A.G. and S.M.S. Writing – revised draft: S.M.S. Writing – revised review and editing: L.C.R. and S.M.S.

Funding

Competing interests

The authors declare no competing interests.

Additional information

Extended data is available for this paper at https://doi.org/10.1038/s42255-025-01405-8.

Supplementary information The online version contains supplementary material available at https://doi.org/10.1038/s42255-025-01405-8.

Correspondence and requests for materials should be addressed to Sophie M. Steculorum.
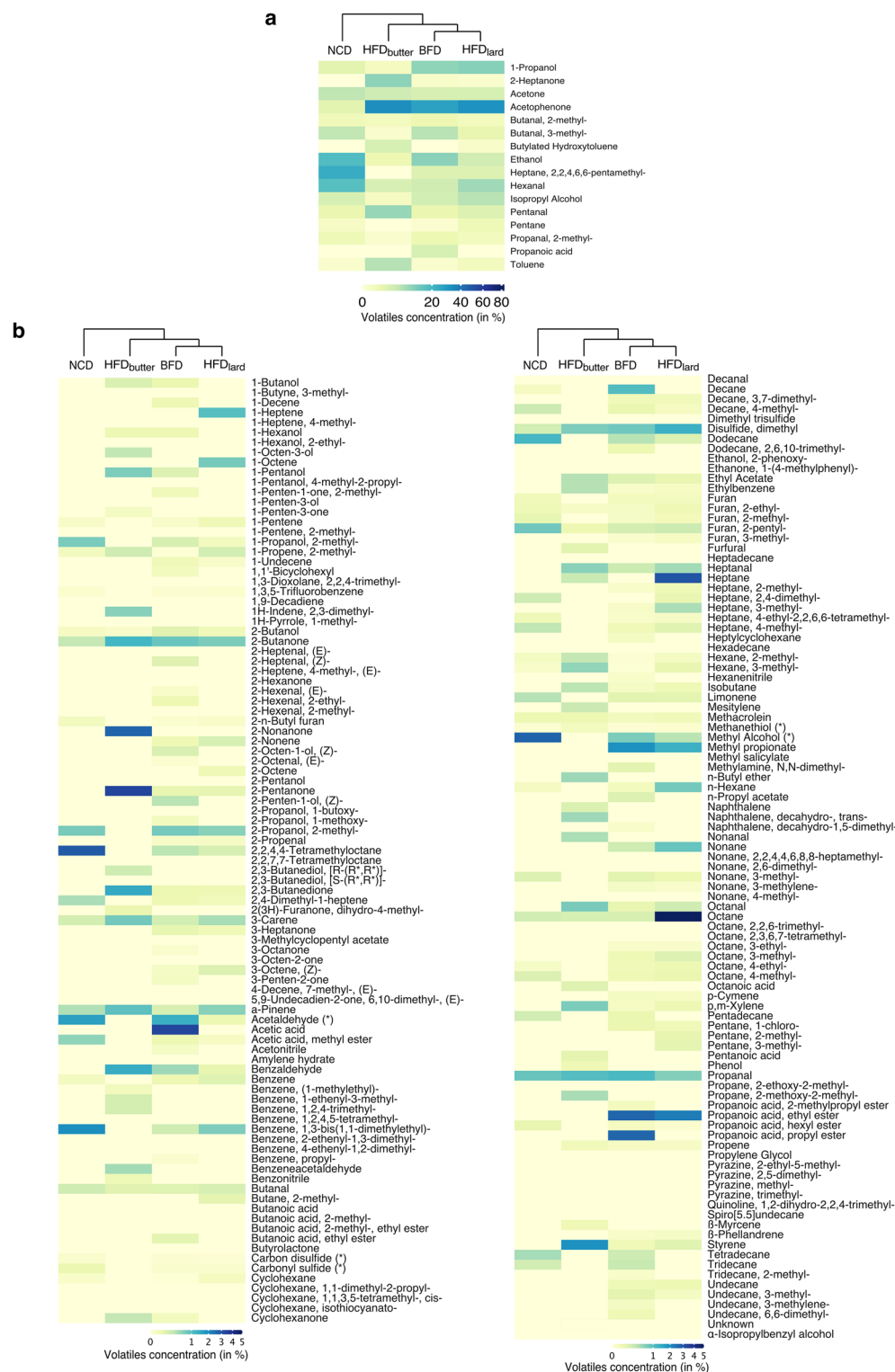
Peer review information *Nature Metabolism* thanks the anonymous reviewer(s) for their contribution to the peer review of this work. Primary Handling Editor: Christoph Schmitt, in collaboration with the *Nature Metabolism* team.

Reprints and permissions information is available at www.nature.com/reprints.

**Publisher's note** Springer Nature remains neutral with regard to jurisdictional claims in published maps and institutional affiliations.

Extended Data Fig. 1 | Diets' volatile profiles. (a-b) Hierarchical clustering of the volatile profiles of normal chow diet (NCD), bacon-flavoured diet (BFD), butter-based high-fat diet (HFD$_{butter}$) and lard-based HFD (HFD$_{lard}$). The colour scale represents the concentration of each volatile in percent. Volatiles with a concentration **(a)** > 5% and **(b)** < 5% in at least one of the diets.
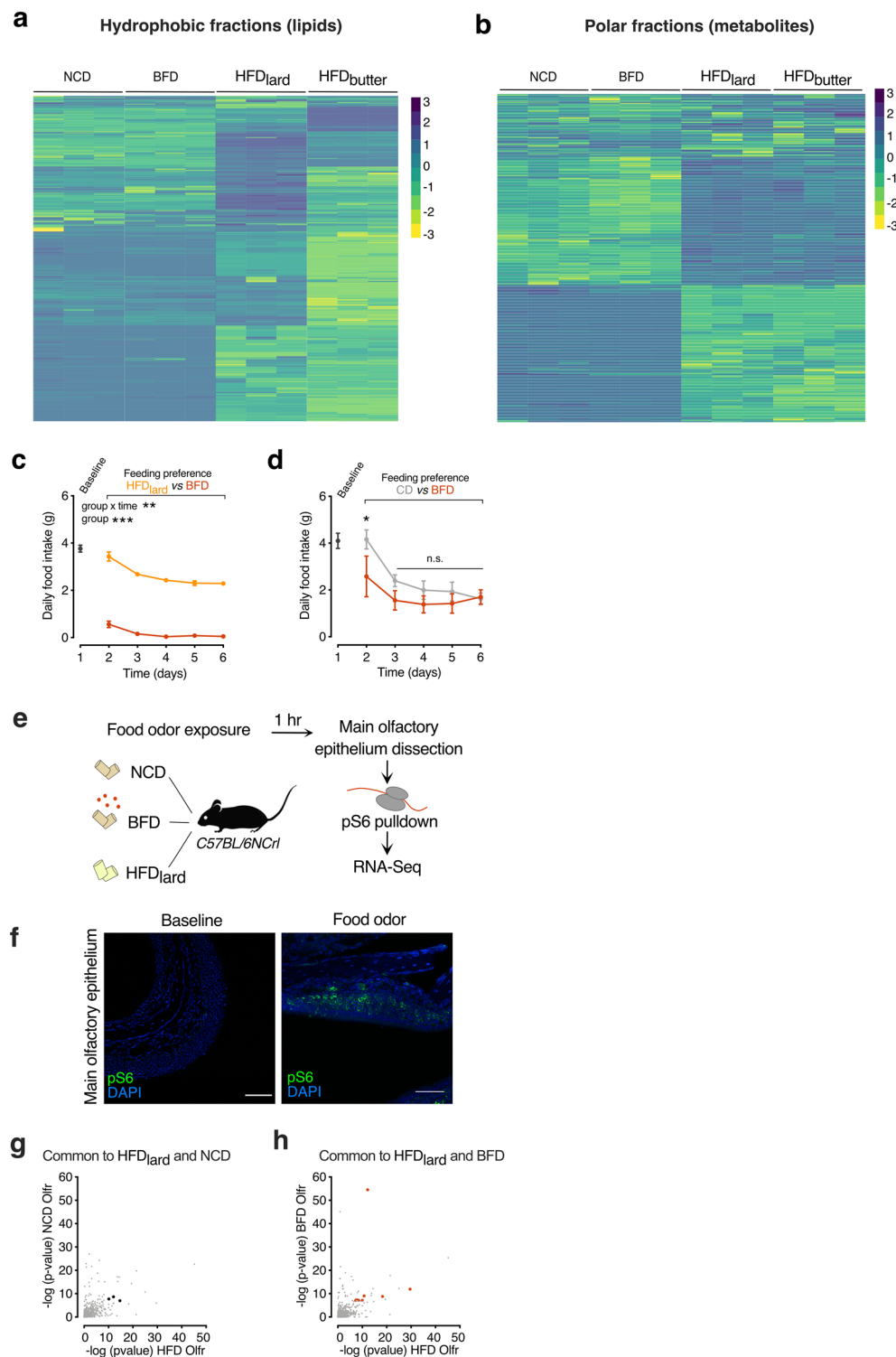
**Extended Data Fig. 2 | Characterization of the bacon-flavoured diet.**
(**a-b**) Diets' hydrophobic and polar fractions (lipid and metabolite components). Heatmap of normal chow diet (NCD), bacon-flavoured diet (BFD), HFD$_{lard}$ and HFD$_{butter}$. (**a**) Lipidomic and (**b**) metabolomic profile. The colour scale represents the log-transformed, pareto scaled, TIC median normalized raw peak areas. (**c-d**) Two-choice diet preference test in adult C57BL/6NCrl exposed to (**c**) lard-based HFD (HFD$_{lard}$) and bacon-flavoured diet (BFD) (two-way repeated measures ANOVA; uncorrected Fisher's LSD post hoc; n = 8; P group < 0.0001; P interaction = 0.0015) and (**d**) control diet (CD) and BFD [two-way repeated measures ANOVA; uncorrected Fisher's LSD post hoc; n = 7). (**e**) Paradigm of odour exposure and subsequent phosphorylated ribosome pulldown.

(**f**) Example olfactory epithelium following overnight fasting and food odour exposure or baseline stained for pS6 (green) and DAPI (blue), scale bar = 50 µm. (**g-h**) Volcano plot of fold change of HFD$_{lard}$-exposed olfactory receptors vs NCD or BFD. Highlighted olfactory receptors are significant for (**g**) only NCD and HFD$_{lard}$ or (**h**) only BFD and HFD$_{lard}$, but not the other food odour. [n = 5-6 per diet containing 4 main olfactory epithelia each; p-value ≤ 0.001 considered significant following multiplicity adjustment]. Statistics are depicted as: for two-way repeated measures ANOVA, group comparison and time x group interaction. Bars represent mean value. Error bars represent SEM. * $P ≤ 0.05$, ** $P ≤ 0.01$, *** $P ≤ 0.001$.
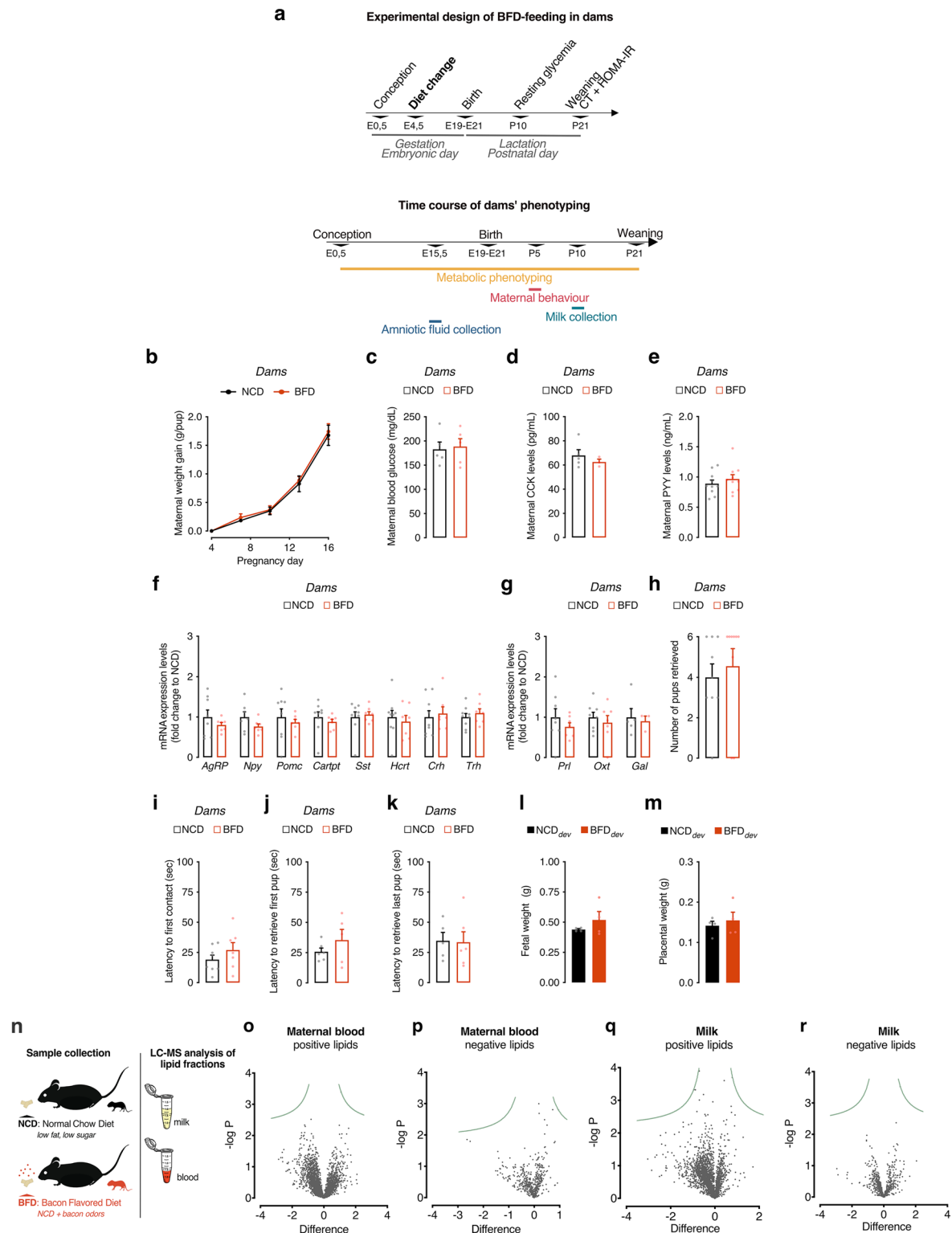
Extended Data Fig. 3 | Maternal BFD feeding does not alter maternal health and behaviour, nor blood and milk lipid profiles. (a) Overview of the timeline and different cohorts performed to phenotype dams fed normal chow diet (NCD) or bacon-flavoured diet (BFD). **(b)** Weight gain per pup through gestation [two-way repeated measures ANOVA; n = 5,6]. **(c)** Maternal ad libitum resting blood glucose [unpaired two-tailed t-test; n = 5,5]. **(d)** Maternal cholecystokinin (CCK) levels [unpaired two-tailed t-test; n = 5,3]. **(e)** Maternal peptide YY (PYY) levels [unpaired two-tailed t-test; n = 10,10]. **(f-g)** Hypothalamic gene expression of **(f)** energy homeostasis-related genes and **(g)** maternal behaviour-related genes [multiple unpaired two-tailed t-test; n = 9,7;8,7]. **(h-k)** Pup retrieval test [unpaired

two-tailed t-test]. **(h)** Total number of pups retrieved [n = 9,9]. **(i)** Latency to first contact [n = 8,7]. **(j-k)** Retrieval latencies to retrieve **(j)** the first [n = 6,5] and **(k)** the last pup [n = 5,6]. **(l)** Fetal [unpaired two-tailed t-test; n = 4,4] and **(m)** placental weight [unpaired two-tailed t-test; n = 4,4] at embryonic day 15.5 of offspring exposed to NCD (NCD$_{dev}$) and BFD (BFD$_{dev}$) through maternal diet. **(n)** Paradigm for milk and blood collection in dams fed normal chow diet (NCD) or bacon-flavoured diet (BFD). **(o-r)** Volcano plot for the lipidomic profiling of: **(o-p)** maternal blood and **(q-r)** milk. Green lines indicate multiplicity adjusted p = 0.05. Bars represent mean value. Error bars represent SEM.
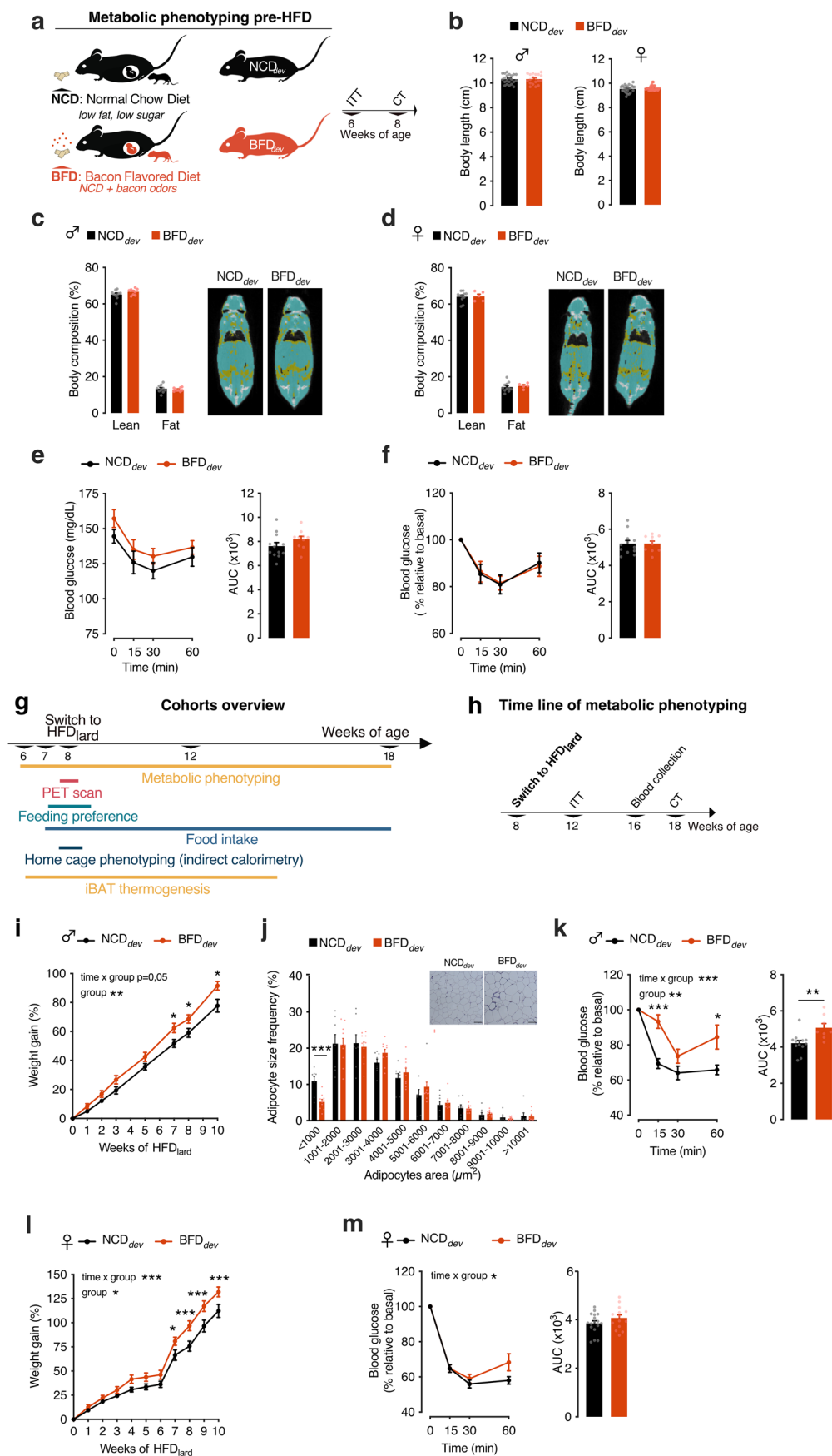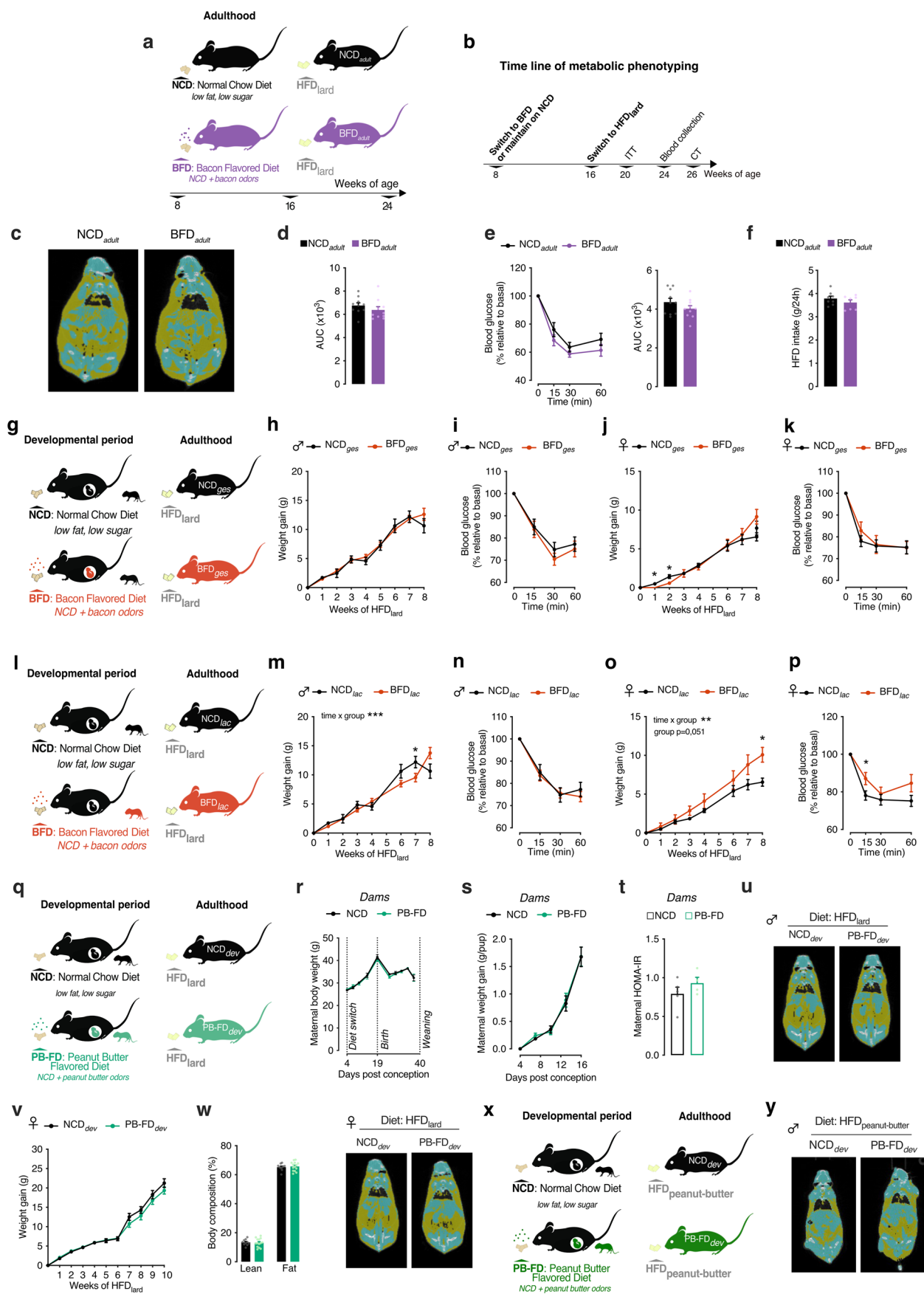
Extended Data Fig. 4 | See next page for caption.

Extended Data Fig. 4 | Developmental exposure to fat-related sensory cues does not alter adiposity and insulin sensitivity prior to HFD$_{lard}$ feeding. (a) Paradigm for the metabolic phenotyping before the switch to lard-based high-fat diet (HFD$_{lard}$) of offspring developmentally exposed to normal chow diet (NCD$_{dev}$) or bacon-flavoured diet (BFD$_{dev}$). **(b)** Body length of males [unpaired two-tailed t-test; n = 22,19] and females [unpaired two-tailed t-test; n = 25,29]. **(c-d)** Body composition and representative micro-CT images pre-HFD$_{lard}$ of **(c)** males [two-tailed Wilcoxon rank-sum test; n = 10,9] and **(d)** females [two-tailed Wilcoxon rank-sum test; n = 11,5]. **(e-f)** Insulin tolerance test (ITT) and associated area under the curve (AUC) pre-HFD$_{lard}$ males: **(e)** absolute glucose levels [time curve: two-way repeated measures ANOVA; n = 12,10] [AUC: unpaired two-tailed t-test; n = 12,10] and **(f)** relative to baseline [time curve: two-way repeated measures ANOVA; n = 12,10] [AUC: unpaired two-tailed t-test; n = 12,10]. **(g)** Overview of the timeline and different cohorts performed to phenotype NCD$_{dev}$ and BFD$_{dev}$ mice. **(h)** Timeline for post-HFD$_{lard}$ metabolic phenotyping of NCD$_{dev}$ or BFD$_{dev}$ mice. **(i)** Body weight gain of male offspring on HFD$_{lard}$ in percentage [two-way repeated measures ANOVA; Tukey's post hoc; n = 21,20; P group = 0.0029; P interaction = 0.0509]. **(j)** Size distribution of adipocytes in perigonadal white adipose tissue [two-way repeated measures ANOVA; Sidak's post hoc; n = 8,10; $P < 1000$ = 0.0006]. **(k)** Insulin tolerance test (ITT) and associated area under the curve (AUC) relative to baseline after 4 weeks of HFD$_{lard}$ in males [time curve: two-way repeated measures ANOVA; Tukey's post hoc; n = 13,8; P group = 0.0024; P interaction = 0.0002] [AUC: unpaired two-tailed t-test, n = 13,8; P = 0.0044]. **(l)** Body weight gain of female offspring on HFD$_{lard}$ in percentage [two-way repeated measures ANOVA; Tukey's post hoc; n = 25,27; P group = 0.0153; P interaction = 0.0002]. **(m)** ITT and associated AUC in females [time curve: two-way repeated measures ANOVA; n = 17,14; P interaction = 0.0375] [AUC: unpaired two-tailed t-test; n = 17,14]. Statistics are depicted as: for two-way repeated measures ANOVA or mixed-effects model, group comparison and time x group interaction. Bars represent mean value. Error bars represent SEM. * p ≤ 0.05, ** p ≤ 0.01, *** p ≤ 0.001.

Extended Data Fig. 5 | See next page for caption.

Extended Data Fig. 5 | Exposure to fat-related sensory cues during development, but not during adulthood, influences diet-induced obesity.
**(a)** Paradigm of adult exposure to NCD (NCD_{adult}) or BFD (BFD_{adult}) followed by lard-based high-fat diet (HFD_{lard}) feeding. **(b)** Overview of the metabolic phenotyping time line. **(c)** Representative micro-CT image (related to Fig. 1x) after 8 weeks of HFD_{lard}. **(d)** Area under the curve (AUC) of insulin tolerance test (ITT) in absolute glucose levels (related to Fig. 1y) after 4 weeks of HFD_{lard} [AUC: unpaired two-tailed t-test; n = 10,10]. **(e)** Insulin tolerance test (ITT) and associated AUC after 4 weeks of HFD_{lard} relative to baseline [time curve: two-way repeated measures ANOVA, n = 10,10] [AUC: unpaired two-tailed t-test; n = 10,10]. **(f)** Daily HFD_{lard} intake consumed during ad libitum access [unpaired two-tailed t-test; n = 8,7]. **(g)** Paradigm of developmental exposure to NCD and BFD during gestation exclusively (NCD_{ges} and BFD_{ges}) followed by HFD_{lard} feeding in adulthood. **(h)** Body weight gain of male offspring on HFD_{lard} [mixed-effects model; n = 15,13]. **(i)** ITT of male offspring on HFD_{lard} [two-way repeated measures ANOVA; n = 22,16]. **(j)** Body weight gain of female offspring on HFD_{lard} [mixed-effects model; Tukey's post hoc; n = 18,10]. **(k)** ITT of female offspring on HFD_{lard} [two-way repeated measures ANOVA; n = 30,15]. **(l)** Paradigm of developmental exposure to NCD and BFD during lactation exclusively (NCD_{lac} and BFD_{lac}) followed by HFD_{lard} feeding in adulthood. **(m)** Body weight gain of male offspring on HFD_{lard} [mixed-effects model; Tukey's post hoc; n = 15,20; P interaction = 0.0009]. **(n)** ITT of male offspring on HFD_{lard} [two-way repeated measures ANOVA; n = 22,24]. **(o)** Body weight gain of female offspring on HFD_{lard} [mixed-effects model; Tukey's post hoc; n = 18,10; P group = 0.0512; P interaction = 0.0026]. **(p)** ITT of female offspring on HFD_{lard} [two-way repeated measures ANOVA; Tukey's post hoc; n = 30,12]. **(q)** Paradigm of developmental exposure to fat-related sensory cues induced by normal chow diet (NCD) or isonutritional peanut butter-flavoured diet (PB-FD) feeding. **(r-u)** Metabolic phenotyping of dams fed either NCD or PB-FD. **(r)** Maternal weight across gestation and lactation [two-way repeated measures ANOVA; n = 8,7]. **(s)** Weight gain per pup through gestation of dams fed NCD or PB-FD [two-way repeated measures ANOVA; n = 5,4]. **(t)** Maternal insulin resistance defined by HOMA-IR [unpaired two-tailed t-test; n = 5,4]. **(u-y)** Metabolic phenotyping of offspring on HFD_{lard} exposed to NCD_{dev} or $PB-FD_{dev}$ **(u)** Representative micro-CT image of HFD_{lard}-fed males (related to Fig. 2j). **(v)** Body weight gain of female offspring on HFD_{lard} [two-way repeated measures ANOVA; n = 25,20]. **(w)** Body composition and representative micro-CT image of HFD_{lard}-fed females [two-tailed Wilcoxon rank-sum test; n = 10,14]. **(x)** Paradigm of developmental exposure to fat-related sensory cues induced by NCD or PB-FD feeding followed by peanut butter-based high-fat diet ($HFD_{peanut-butter}$) feeding in adulthood. **(y)** Representative micro-CT image of $HFD_{peanut-butter}$-fed males (related to Fig. 2l). Statistics are depicted as: for two-way ANOVA or mixed-effects model, group comparison and time x group interaction. Bars represent mean value. Error bars represent SEM. * p ≤ 0.05, *** p ≤ 0.001.

a Amniotic fluid volatiles' profile

b Milk volatiles' profile
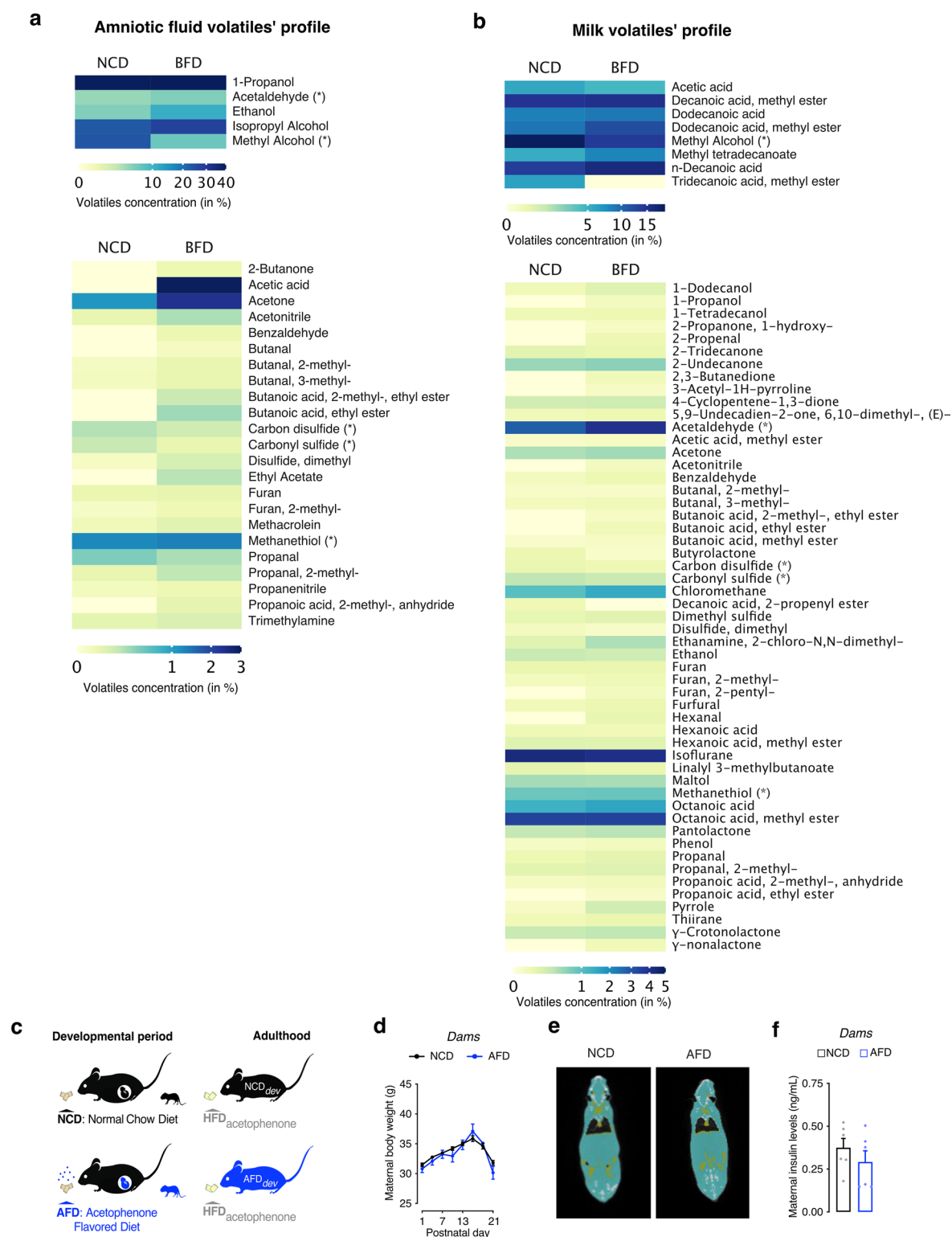
Extended Data Fig. 6 | BFD feeding in dams changes amniotic fluid and milk volatile profiles. (a-b) Volatile profiles of **(a)** amniotic fluid and **(b)** milk of dams fed normal chow diet (NCD) or bacon-flavoured diet (BFD). The colour scale represents the concentration of each volatile in percentage. Top and bottom heatmaps depict volatiles >5% and <5%, respectively. **(c)** Paradigm of developmental exposure to acetophenone-flavoured diet (AFD) feeding followed by acetophenone-flavoured HFD (HFD_acetophenone) feeding in adulthood. **(d)** Maternal weight during lactation [mixed-effects model; n = 20,6]. **(e)** Representative micro-CT image (related to Fig. 2o). **(f)** Maternal fasted insulin levels [unpaired two-tailed t-test; n = 6,6]. Bars represent mean value. Error bars represent SEM.
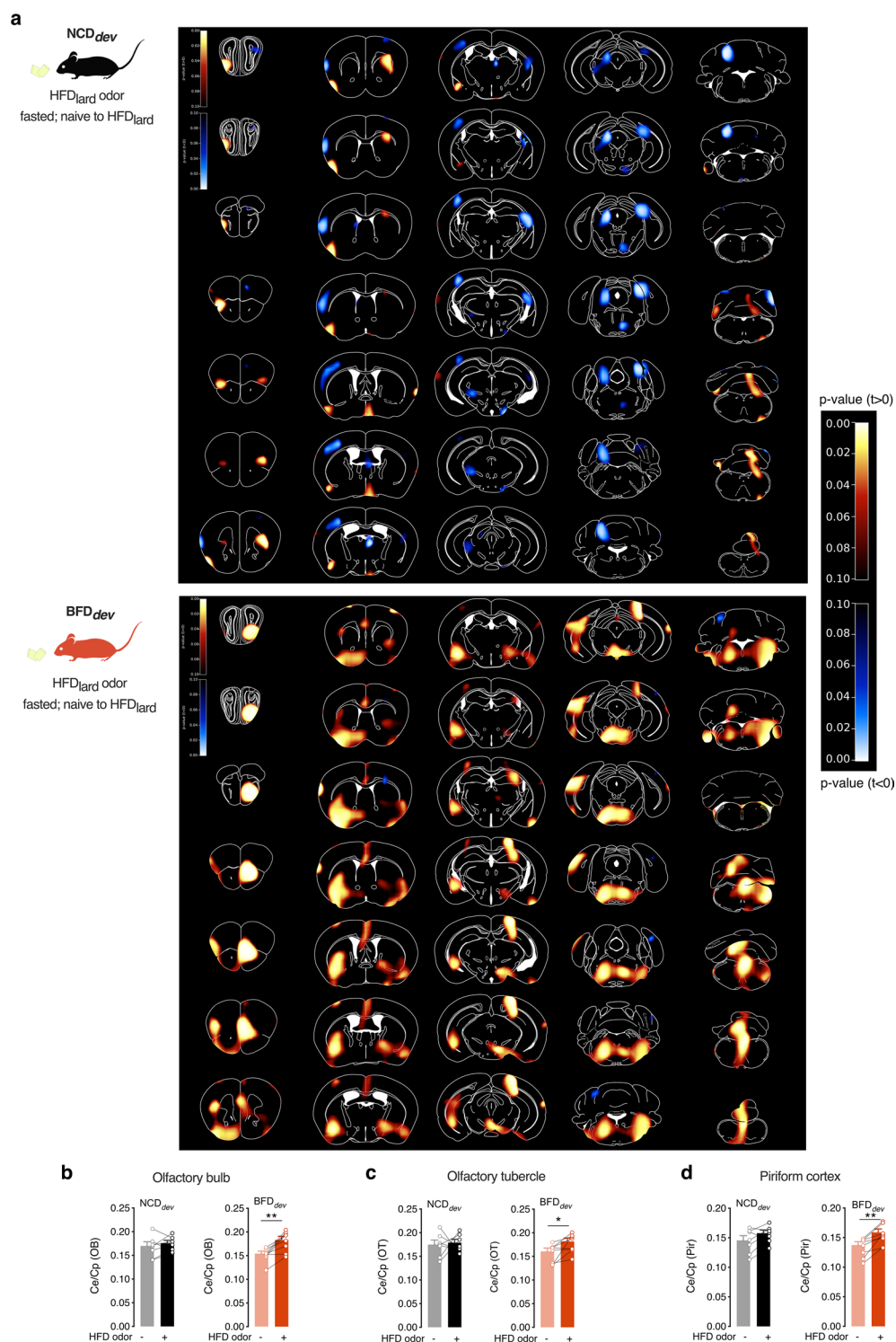
Extended Data Fig. 7 | Developmental exposure to fat-related sensory cues alters central responses to HFD_{lard} odour. (a) Positron emission tomography measurement of glucose transport based on fluorodeoxyglucose (^{18}FDG) kinetics in brains of NCD_{dev} or BFD_{dev} mice upon lard-based high-fat diet (HFD_{lard}) odour exposure. The colour code on the representative PET images depicts the paired t-test value for each voxel. Relative increases in glucose metabolism upon HFD_{lard} odour exposure are colour-coded in yellow to orange, whereas decreases are colour-coded in blue. **(b-c)** HFD_{lard} odour-induced differential glucose transport based on ^{18}FDG PET kinetics in: **(b)** the olfactory bulb (OB) [paired two-tailed t-test; n = 7,8; P = 0.0027], **(c)** the olfactory tubercle (OT) [paired two-tailed t-test; n = 7,8; P = 0.0253] and **(d)** the piriform cortex (Pir) [paired two-tailed t-test; n = 7,8; P = 0.0027]. Statistics are depicted as: paired t-tests. Bars represent mean value. Error bars represent SEM. * p ≤ 0.05, ** p ≤ 0.01.
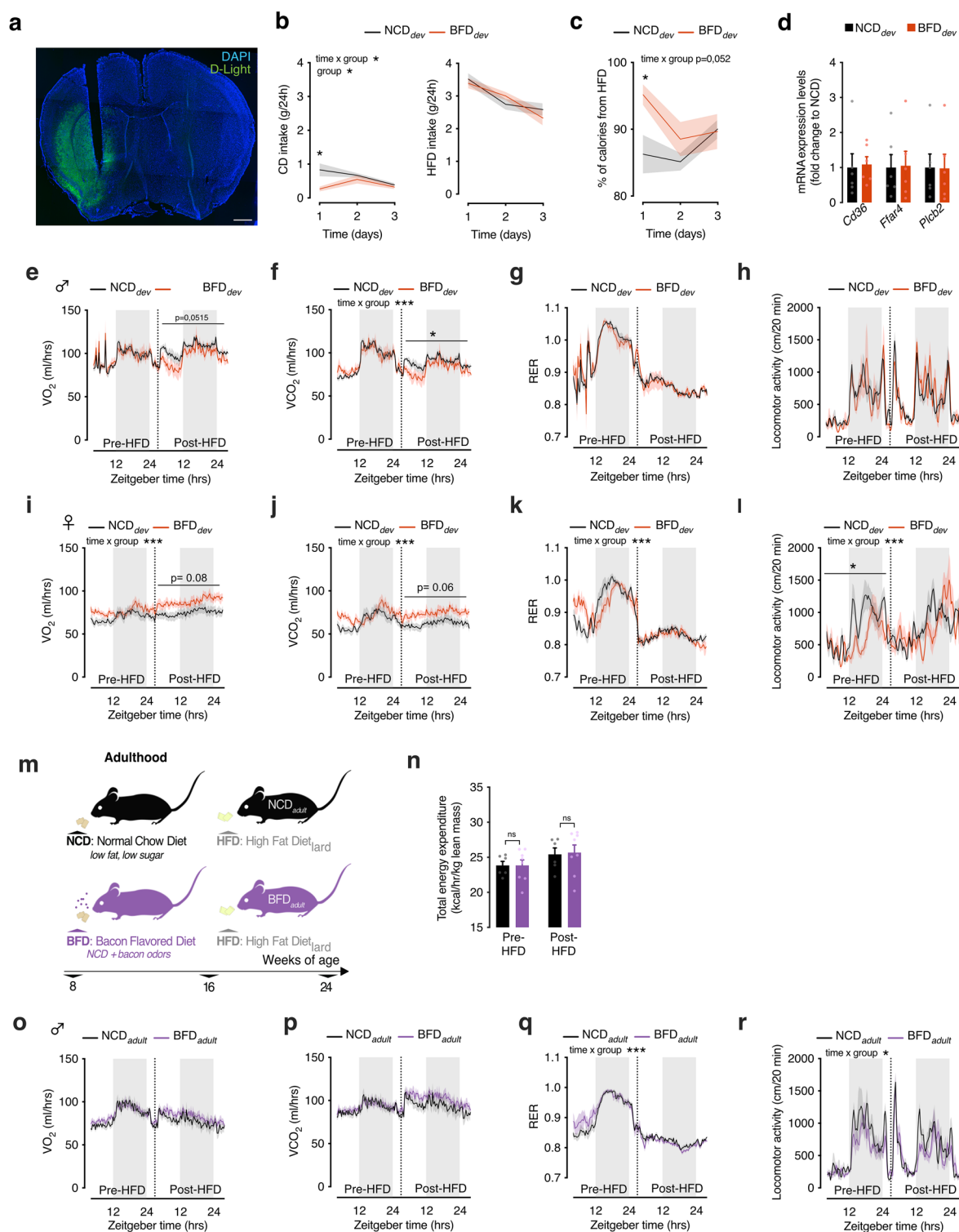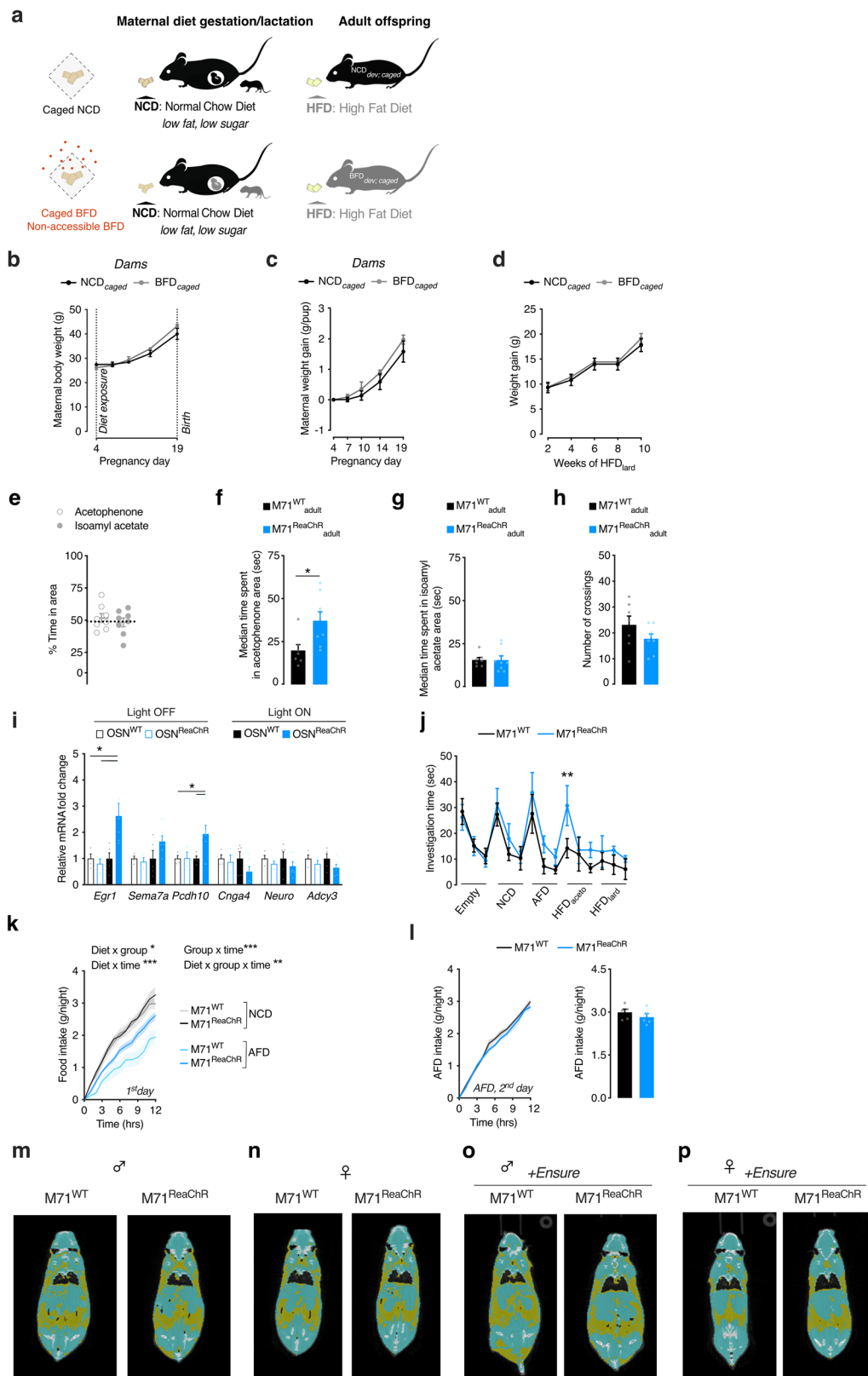
Extended Data Fig. 8 | See next page for caption.

Extended Data Fig. 8 | Exposure to fat-related sensory cues during adulthood does not influence diet-induced obesity. (a) Representative fibre placement and viral expression of dLight1.1, scale bar = 500 μm. **(b)** Intake of control diet (CD) or lard-based high-fat diet (HFD$_{lard}$) during a two-choice diet preference test in adult mice developmentally exposed to normal chow diet (NCD$_{dev}$) or bacon-flavoured diet (BFD$_{dev}$) [two-way repeated measures ANOVA; Tukey's post hoc; n = 13,10; P group = 0.0266; P interaction = 0.0354]. **(c)** Percentage of calories from HFD$_{lard}$ during 3 days of two-choice diet preference test [two-way repeated measures ANOVA; Tukey's post hoc; n = 13,10; P interaction = 0.0523]. **(d)** Relative expression of genes involved in fat-sensing in the tongue [Multiple unpaired two-tailed t-test; n = 6,6]. **(e-h)** Metabolic characterization upon the switch to HFD$_{lard}$, *that is* pre- and post-HFD$_{lard}$ feeding of NCD$_{dev}$ and BFD$_{dev}$ males: **(e)** VO$_2$, **(f)** VCO$_2$, **(g)** respiratory exchange ratio (RER), and **(h)** locomotor activity [two-way repeated measures ANOVA; n = 11,5; **(e)** Post-HFD

P group= 0.0515; **(f)** P interaction = 0.0002, Post-HFD P group = 0.0488]. **(i-l)** Metabolic characterization upon the switch to HFD$_{lard}$, *that is* pre- and post-HFD$_{lard}$ feeding in NCD$_{dev}$ and BFD$_{dev}$ females: **(i)** VO$_2$, **(j)** VCO$_2$, **(k)** RER, and **(l)** locomotor activity [two-way repeated measures ANOVA; n = 14,8; **(i)** P interaction < 0.0001, **(j)** P interaction < 0.0001, Post-HFD P group = 0.0647; **(k)** P interaction < 0.0001, **(l)** P interaction < 0.0001, Pre-HFD P group= 0.0201]. **(m-r)** Metabolic characterization upon the switch to HFD$_{lard}$, *that is* pre- and post-HFD$_{lard}$ feeding in NCD$_{adult}$ and BFD$_{adult}$ males: **(n)** total energy expenditure [linear mixed-effects models; Holm–Bonferroni post hoc; n = 6,8], **(o)** VO$_2$, **(p)** VCO$_2$, **(q)** RER, and **(r)** locomotor activity [two-way repeated measures ANOVA; n = 7,8]. Statistics are depicted as two-way repeated measures ANOVA for repeated t-test and t-test horizontal bar represents group comparison. Bars represent mean value. Error bars represent SEM. * p < 0.05, *** p < 0.001.
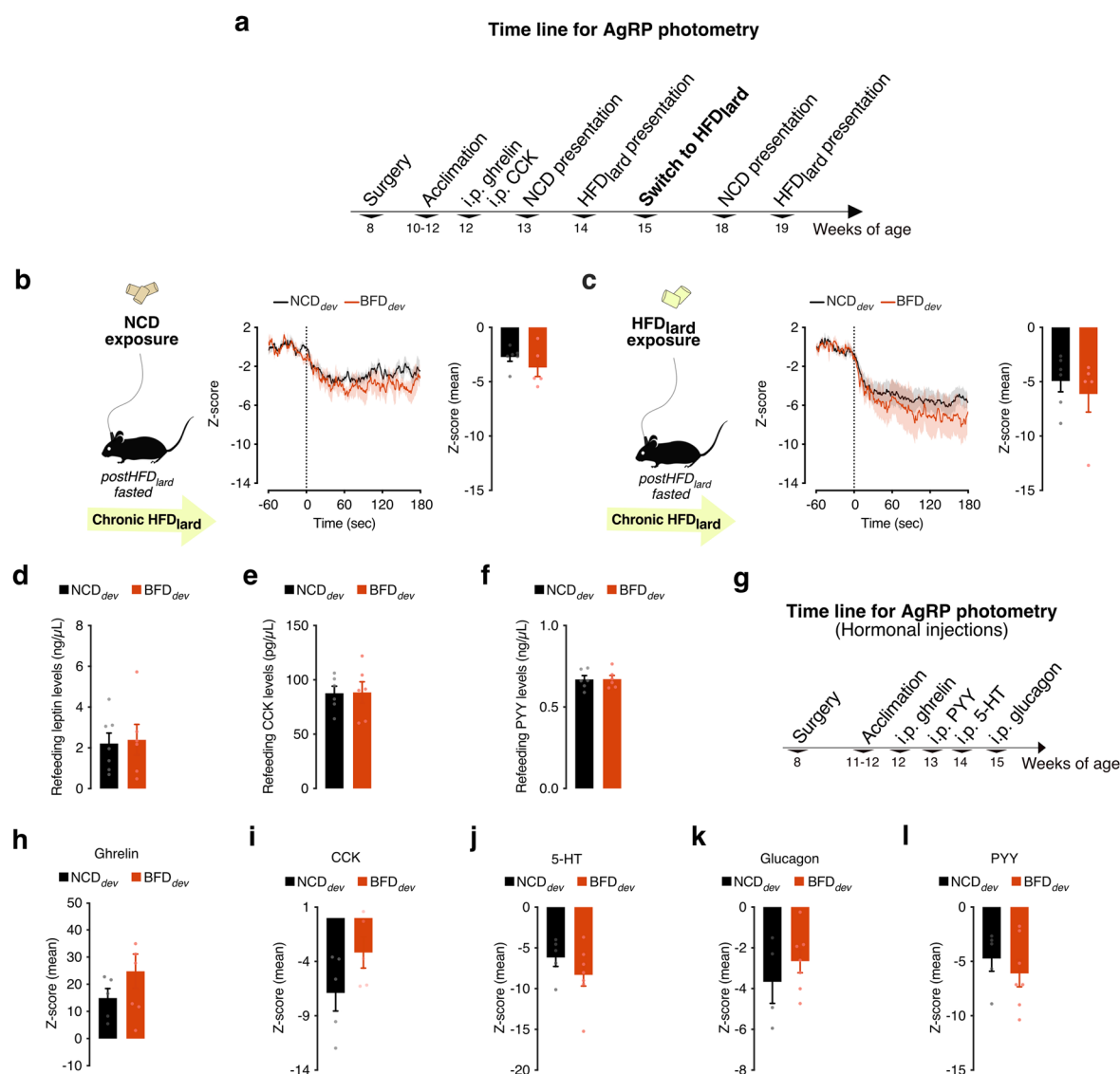
Extended Data Fig. 9 | Developmental exposure to fat-related sensory cues primes an obese-like AgRP neuronal response. (a) Overview of the time line for recording AgRP neuronal dynamics using fibre photometry. **(b-c)** AgRP calcium dynamics and average Z-score following 4 weeks of HFD_{lard} in response to: **(b)** NCD presentation [unpaired two-tailed t-test; n = 6,5], **(c)** HFD_{lard} presentation [unpaired two-tailed t-test; n = 6,5]. **(d-f)** Circulating levels upon refeeding of **(d)** leptin [unpaired two-tailed t-test; n = 7,6], **(e)** cholecystokinin (CCK) [unpaired two-tailed t-test; n = 6,6] and **(f)** peptide YY (PYY) [unpaired two-tailed t-test;

n = 6,6]. **(g)** Overview of the time line for recording AgRP neuronal dynamics upon intraperitoneal (i.p.) administration of hormones using fibre photometry. **(h-l)** Average Z-score of AgRP calcium dynamics in response to i.p. administration of **(h)** ghrelin [unpaired two-tailed t-test; n = 5,7], **(i)** cholecystokinin (CCK) [unpaired two-tailed t-test; n = 5,5], **(j)** serotonin (5-HT) [unpaired two-tailed t-test; n = 5,7], **(k)** glucagon [unpaired two-tailed t-test; n = 4,7] and **(l)** peptide YY (PYY) [unpaired two-tailed t-test; n = 5,7]. Statistics are depicted as: t-test. Bars represent mean value. Error bars represent SEM.

Extended Data Fig. 10 | See next page for caption.

Extended Data Fig. 10 | The sensory programming of metabolism is contingent on sensory/caloric association. (a) Paradigm of developmental exposure to odour cues in their home cage from inaccessible NCD (NCD$_{dev;caged}$) or BFD (BFD$_{dev;caged}$) feeding followed by lard-based high-fat diet feeding (HFD$_{lard}$) during adulthood. **(b)** Maternal weight across gestation [two-way repeated measures ANOVA; n = 4,3]. **(c)** Maternal weight across gestation [two-way repeated measures ANOVA; n = 4,3]. **(d)** Body weight gain of male NCD$_{dev;caged}$ or BFD$_{dev;caged}$ offspring on HFD$_{lard}$ [mixed-effects model; n = 16,15]. **(e)** Percentage of time spent in each area in C57BL/6NCrl mice [unpaired two-tailed t-test; n = 8,8]. **(f-h)** Two-chamber place preference test in adult mice expressing ReaChR in M71-expressing cells (M71$^{ReaChR}_{adult}$) and control littermates (M71$^{WT}_{adult}$) that underwent an optostimulation/food reward pairing protocol [unpaired two-tailed t-test; n = 7,8]. Median time spent **(f)** in acetophenone [$P = 0.0186$]. and **(g)** in isoamyl acetate area. **(h)** Number of crossings between the two areas of the experimental box. **(i)** Relative expression of olfactory sensory neuron (OSN) activity-dependent genes in P3 pups expressing ReaChR in OMP-expressing OSNs (OSN^{ReaChR}) or wildtype OSNs (OSN^{WT}) 60 min after optogenetic stimulation [two-way ANOVA; Tukey's post hoc; n light off = 4,3; n light on = 5,6;

P Egr1 < 0.0001; P Pcdh10 = 0.0196]. **(j)** Habituation-dishabituation test in adult mice with neonatal optogenetic activation of M71-expressing OSNs (M71^{ReaChR}) and control littermates (M71^{WT}). Mice are consecutively exposed to control (empty tea ball) and odours of normal chow diet (NCD), acetophenone-flavoured diet (AFD), high-fat diet flavoured with acetophenone (HFD$_{aceto}$) and lard-based high-fat diet (HFD$_{lard}$) placed in tea balls [two-way repeated measures ANOVA; Tukey's post hoc; n = 5,4]. **(k)** Cumulative food intake of NCD and AFD upon first exposure during the dark cycle [three-way repeated measures ANOVA; n = 5,5; P diet:group = 0.0135; P diet:time < 0.001; P group:time < 0.001; P group:time:diet = 0.0014]. **(l)** Cumulative food intake of AFD upon first exposure during the second dark cycle of exposure [unpaired two-tailed t-test; n = 5,5]. **(m-p)** Representative CT images of **(m)** male and **(n)** female M71^{ReaChR} mice and control littermates M71^{WT} fed HFD$_{acetophenone}$ during adulthood (related to Fig. 5o and q). **(o)** Male and **(p)** female M71$^{ReaChR+Ensure}$ mice and control littermates M71$^{WT+Ensure}$ fed HFD$_{acetophenone}$ during adulthood (related to Fig. 5t and v). Statistics are depicted as two-way repeated measures ANOVA or mixed-effects model, group comparison. Bars represent mean value. Error bars represent SEM. * p ≤ 0.05, ** p ≤ 0.01, *** p ≤ 0.001.

nature portfolio

Corresponding author(s): Dr. Sophie Steculorum

Last updated by author(s): 30/04/2025

Reporting Summary

Nature Portfolio wishes to improve the reproducibility of the work that we publish. This form provides structure for consistency and transparency in reporting. For further information on Nature Portfolio policies, see our Editorial Policies and the Editorial Policy Checklist.

Statistics

For all statistical analyses, confirm that the following items are present in the figure legend, table legend, main text, or Methods section.

n/a	Confirmed	
☐	☒	The exact sample size (*n*) for each experimental group/condition, given as a discrete number and unit of measurement
☐	☒	A statement on whether measurements were taken from distinct samples or whether the same sample was measured repeatedly
☐	☒	The statistical test(s) used AND whether they are one- or two-sided *Only common tests should be described solely by name; describe more complex techniques in the Methods section.*
☒	☐	A description of all covariates tested
☐	☒	A description of any assumptions or corrections, such as tests of normality and adjustment for multiple comparisons
☐	☒	A full description of the statistical parameters including central tendency (e.g. means) or other basic estimates (e.g. regression coefficient) AND variation (e.g. standard deviation) or associated estimates of uncertainty (e.g. confidence intervals)
☐	☒	For null hypothesis testing, the test statistic (e.g. *F*, *t*, *r*) with confidence intervals, effect sizes, degrees of freedom and *P* value noted *Give P values as exact values whenever suitable.*
☒	☐	For Bayesian analysis, information on the choice of priors and Markov chain Monte Carlo settings
☒	☐	For hierarchical and complex designs, identification of the appropriate level for tests and full reporting of outcomes
☒	☐	Estimates of effect sizes (e.g. Cohen's *d*, Pearson's *r*), indicating how they were calculated

Our web collection on statistics for biologists contains articles on many of the points above.

Software and code

Policy information about availability of computer code

Data collection
- Indirect calorimetry and food intake data acquisition were carried out using TSE Phenomaster versions 6.2.5 and above.
- Body composition was measured using an IVIS Spectrum CT scanner (Caliper LifeScience, USA) using the IVIS LivingImage Software V4.3.1.
- Imaging of western blots was performed with FusionCapt Advance software (Vilber).
- Quantitative PCR was performed on a QuantStudio 7 Flex Real-Time PCR System using the QuantStudio Real-Time PCR Software v1.3 (Life Technologies).
- For ELISA, the optical density was determined using a FilterMax F5 Multi-Mode microplate reader and SoftMax Pro 6.3 software (Molecular Devices).
- For measurement of interscapular temperature, temperature measurements were taken using a wireless reader (Biomedic data systems DAS-8007C) or thermal camera (FLIR E6, Teledyne FLIR LLC)
- Liquid Chromatography-High Resolution Mass Spectrometry-based (LC-HRMS) analysis of lipids was performed using Thermo Fisher Q-Exactive GC Orbitrap GC-MS/MS with EI or CI source.
- PET imaging was performed using an Inveon preclinical PET/CT system (Siemens).
- Photometry recordings were performed using a RZ5P lock-digital processor controlled by Synapse software (Tucker-Davis Technologies, TDT, USA).
- Tissue was imaged on a Zeiss Imager M2 microscope and AxioVision 4.2 software (Carl Zeiss) or a Leica STELLARIS (Leica Microsystems)
- RNA-sequencing has been performed using Applied Biosystems 7900HT Sequence Detection and sequenced on an Illumina HiSeq 4000 sequencing instrument.
- Volatiles analyses were performed on a time-of-flight mass spectrometer (BenchTOF-dx model, Almsco,

Data analysis

Data analysis

- Data analysis was performed using Graphpad Prism (version 8.0; Graphpad Software Inc., La Jolla, CA, USA), unless otherwise stated below.
- All fiber photometry data analyses were performed using a custom Matlab script (version R2021a).
Three-way (type III) ANOVAs were performed in R 4.3.0. For between-subjects designs, we used linear models fitted with the stats package and analyzed with the car package; for repeated measures, we implemented linear mixed effect models using the lmerTest package and its built-in anova function.

- Analysis of PET Imaging was performed using the Vinci software.
- RNA-sequencing analysis was performed using Salmon 0.14.147 using the reference genome GRCm38. Analysis were performed using the DESeq2 1.26. R and the 3.14.3 R packages.
- Results of quantitative PCR experiments were calculated using Microsoft Excel.

- Densitometric analysis of protein bands was performed by FIJI (NIH, version 2.0.0-rc-41/1.50d).
- Quantification of fat mass (IVIS Spectrum CT scanner) was determined with a modification of the Vinci software package 4.61.038.
- The deconvolution process for the chemical identification of the VOCs that were present in each analyzed sample was carried out with the software TargetView v3 (ALMSCO International, Germany)
- Readings of interscapular temperature measurement were performed using DASHost 8000 software (Biomedic data systems).
- Analysis of LC-HRMS data was performed on Thermo RAW files were converted to mzXML files by MSConvert from Proteowizard 40. Further analysis were performed using MZmine 2.340 and Perseus.

For manuscripts utilizing custom algorithms or software that are central to the research but not yet described in published literature, software must be made available to editors and reviewers. We strongly encourage code deposition in a community repository (e.g. GitHub). See the Nature Portfolio guidelines for submitting code & software for further information.

Data

Policy information about availability of data

All manuscripts must include a data availability statement. This statement should provide the following information, where applicable:
- Accession codes, unique identifiers, or web links for publicly available datasets
- A description of any restrictions on data availability
- For clinical datasets or third party data, please ensure that the statement adheres to our policy

All raw data has been made available

Human research participants

Policy information about studies involving human research participants and Sex and Gender in Research.

Reporting on sex and gender

Use the terms sex (biological attribute) and gender (shaped by social and cultural circumstances) carefully in order to avoid confusing both terms. Indicate if findings apply to only one sex or gender; describe whether sex and gender were considered in study design whether sex and/or gender was determined based on self-reporting or assigned and methods used. Provide in the source data disaggregated sex and gender data where this information has been collected, and consent has been obtained for sharing of individual-level data; provide overall numbers in this Reporting Summary. Please state if this information has not been collected. Report sex- and gender-based analyses where performed, justify reasons for lack of sex- and gender-based analysis.

Population characteristics

Describe the covariate-relevant population characteristics of the human research participants (e.g. age, genotypic information, past and current diagnosis and treatment categories). If you filled out the behavioural & social sciences study design questions and have nothing to add here, write "See above."

Recruitment

Describe how participants were recruited. Outline any potential self-selection bias or other biases that may be present and how these are likely to impact results.

Ethics oversight

Identify the organization(s) that approved the study protocol.

Note that full information on the approval of the study protocol must also be provided in the manuscript.

Field-specific reporting

Please select the one below that is the best fit for your research. If you are not sure, read the appropriate sections before making your selection.

☒ Life sciences ☐ Behavioural & social sciences ☐ Ecological, evolutionary & environmental sciences

For a reference copy of the document with all sections, see nature.com/documents/nr-reporting-summary-flat.pdf

Life sciences study design

All studies must disclose on these points even when the disclosure is negative.

Sample size	No statistical methods were used to pre-determine sample sizes. Sample sizes in the study were chosen based on previous similar experiments performed in the laboratory or in the literature.
Data exclusions	For breeding paradigm, strict exclusion criteria were based on time to pregnancy and litter size (6-8 pups). For the photometry analyses, mice showing no viable fluorescent signals were excluded. All exclusion criterion were pre-established.
Replication	Every mouse represents a replicate (n) and the number of replicates is mentioned for each experiment. Experiments were performed in cohorts generated in different time periods.
Randomization	Mice have been assigned randomly to each group and experiment.
Blinding	Investigators were not blinded during group allocation or analysis due to the nature of the experiments and the presence of different diets in the cage.

Reporting for specific materials, systems and methods

We require information from authors about some types of materials, experimental systems and methods used in many studies. Here, indicate whether each material, system or method listed is relevant to your study. If you are not sure if a list item applies to your research, read the appropriate section before selecting a response.

Materials & experimental systems

n/a	Involved in the study
☐	☒ Antibodies
☒	☐ Eukaryotic cell lines
☒	☐ Palaeontology and archaeology
☐	☒ Animals and other organisms
☒	☐ Clinical data
☒	☐ Dual use research of concern

Methods

n/a	Involved in the study
☒	☐ ChIP-seq
☒	☐ Flow cytometry
☒	☐ MRI-based neuroimaging

Antibodies

Antibodies used	- anti-GFP (1:500, ab13970, abcam) - anti-pS6 (Ser244, Ser247) (1:1000, # 44-923G, Thermo Fisher Scientific). - anti-mTOR (1:1000, 2972S, Cell Signaling) - HRP-conjugated anti-rabbit IgG (1:1000, 31466, Invitrogen) - anti-phospho mTOR (S2448) (1:1000, 2971S, Cell Signaling) - goat anti-rabbit IgG (1:500, A11012, Thermo Fisher)
Validation	anti-GFP (1:500, ab13970, abcam): (3612 publications) https://www.abcam.com/en-us/products/primary-antibodies/gfp-antibody-ab13970?srsltid=AfmBOorEamv23bU538PiV3vJ6gZAKgcLJE6xvTpRw5_pE71yIQvnffpu anti-pS6 (Ser244, Ser247) (1:1000, # 44-923G, Thermo Fisher Scientific): (22 references) https://www.thermofisher.com/antibody/product/Phospho-S6-Ser244-Ser247-Antibody-Polyclonal/44-923G anti-mTOR (Cell Signaling 2972S): (2033 citations) https://www.cellsignal.com/products/primary-antibodies/mtor-antibody/2972?srsltid=AfmBOopsHWtMgccOe55zJ00E9w5lPAWvEV1yC56o6aQApD6pv_5fCorP HRP-conjugated anti-rabbit IgG (Invitrogen 31466): (171 references) https://www.thermofisher.com/antibody/product/Goat-anti-Rabbit-IgG-H-L-Secondary-Antibody-Polyclonal/31466 anti-phospho mTOR (S2448) (Cell Signaling 2971S): (2280 citations) https://www.cellsignal.com/products/primary-antibodies/phospho-mtor-ser2448-antibody/2971?srsltid=AfmBOopP0UQY3ncFBofR4RTfAmMY86s6eqafoqPuktHdHTziXkiYbV9P secondary HRP-conjugated anti-rabbit IgG (Thermo Fisher A11012): (3598 reference) https://www.thermofisher.com/antibody/product/Goat-anti-Rabbit-IgG-H-L-Cross-Adsorbed-Secondary-Antibody-Polyclonal/A-11012

Animals and other research organisms

Policy information about [studies involving animals](#); [ARRIVE guidelines](#) recommended for reporting animal research, and [Sex and Gender in Research](#)

Laboratory animals	C57BL/6N mice were purchased from Charles River (Germany). AgRP-IRES-Cre mice (JAX stock #012899), M71-IRES-Cre (JAX stock #006677), OMP-Cre (JAX stock #006668), and R26-LSL-ReaChR-mCitrine (JAX stock #026294) were originally obtained from The Jackson Laboratory. Cre lines were maintained heterozygous through breeding to wildtype C57BL/6N (Charles River, Germany), while R26-LSL-ReaChR-mCitrine mice were maintained as homozygous stock breeding at the Max Planck Institute for Metabolism Research, Cologne, Germany. All mice were housed in individually ventilated cages at 22-24°C at constant humidity (50-70%) with a 12/12-h light/dark cycle with ad libitum food and water unless otherwise stated for experimental conditions.
Wild animals	*Provide details on animals observed in or captured in the field; report species and age where possible. Describe how animals were caught and transported and what happened to captive animals after the study (if killed, explain why and describe method; if released, say where and when) OR state that the study did not involve wild animals.*
Reporting on sex	Metabolic phenotyping data in offspring exposed to BFD, PBFD and acetophenone during development have been generated in both genders. Hormonal release upon refeeding, iBAT thermogenesis and habituation-dishabituation tests have been performed in females only. Other experiments reported in the manuscript have been performed in male mice.
Field-collected samples	We did not use field-collected samples in this study.
Ethics oversight	Permission to maintain and breed mice was issued by the Department for Environment and Consumer Protection - Veterinary Section, Cologne, North Rhine-Westphalia, Germany.

Note that full information on the approval of the study protocol must also be provided in the manuscript.